UNIVERSIDADE DE SÃO PAULO
DEPARTAMENTO DE FÍSICA - FACULDADE DE FILOSOFIA, CIÊNCIAS E LETRAS DE RIBEIRÃO PRETO

NATÁLIA APARECIDA FONTANA

Golgi Reassembly and Stacking Protein: biophysical properties and their functional implications

Ribeirão Preto
2021

Natália Aparecida Fontana

Proteína de Reorganização e Empilhamento do Golgi*:* propriedades biofísicas e suas implicações funcionais

(Versão Corrigida)

Tese apresentada ao Departamento de Física da FFCLRP-USP como parte das exigências para obtenção do título de doutora em ciências

Área de concentração: Física Aplicada à Medicina e Biologia
Orientador: Prof. Dr. Antonio José da Costa Filho

Ribeirão Preto
2021

Ficha catalográfica

Fontana, Natália Aparecida
Proteína de Reorganização e Empilhamento do Golgi: propriedades biofísicas e suas implicações funcionais. Ribeirão Preto, 2021. 148 p.

Tese de Doutorado, apresentada à Faculdade de Filosofia Ciências e Letras de Ribeirão Preto/USP. Área de concentração: Física Aplicada à Medicina e Biologia.
Orientador: Costa-Filho, Antonio José

1. GRASP 2. Secreção não convencional de proteínas 3. Fibras amiloides 4. Proteínas intrinsecamente desordenadas 5. Espectroscopia

Janus

Universidade de São Paulo

ATA DE DEFESA

Ata de defesa de Tese do(a) Senhor(a) Natália Aparecida Fontana no Programa: Física Aplicada à Medicina e Biologia, do(a) Faculdade de Filosofia, Ciências e Letras de Ribeirão Preto da Universidade de São Paulo.

Aos 09 dias do mês de junho de 2021, no(a) Auditório da Física realizou-se a Defesa da Tese do(a) Senhor(a) Natália Aparecida Fontana, apresentada para a obtenção do título de Doutora intitulada:

"Proteína de reorganização e empilhamento do Golgi: propriedades biofísicas e suas implicações funcionais"

Após declarada aberta a sessão, o(a) Sr(a) Presidente passa a palavra ao candidato para exposição e a seguir aos examinadores para as devidas arguições que se desenvolvem nos termos regimentais. Em seguida, a Comissão Julgadora proclama o resultado:

Nome dos Participantes da Banca	Função	Sigla da CPG	Resultado
Antônio José da Costa Filho	Presidente	FFCLRP - USP	Não Votante
Richard Charles Garratt	Titular	IFSC - USP	APROVADA
Paulo Mascarello Bisch	Titular	UFRJ - Externo	APROVADA
Luis Lamberti Pinto da Silva	Titular	FMRP - USP	APROVADA
Luciano Bachmann	Titular	FFCLRP - USP	APROVADA
Jerson Lima da Silva	Titular	UFRJ - Externo	APROVADA

Resultado Final: APROVADA

Parecer da Comissão Julgadora *

A defesa ocorreu de forma remota e não houve problemas técnicos. A banca destacou a grande qualidade do trabalho e competência da aluna.

Eu, Cesar Pereira Brites _____, lavrei a presente ata, que assino juntamente com os(as) Senhores(as). Ribeirão Preto, aos 09 dias do mês de junho de 2021.

p/ Richard Charles Garratt

p/ Paulo Mascarello Bisch

p/ Luis Lamberti Pinto da Silva

p/ Luciano Bachmann

p/ Jerson Lima da Silva

Antônio José da Costa Filho
Presidente da Comissão Julgadora

* Obs: Se o candidato for reprovado por algum dos membros, o preenchimento do parecer é obrigatório.

A defesa foi homologada pela Comissão de Pós-Graduação em _____ e, portanto, o(a) aluno(a) _____ jus ao título de Doutora em Ciências obtido no Programa Física Aplicada à Medicina e Biologia.

_____
Presidente da Comissão de Pós-Graduação

This thesis is dedicated to my parents.
I love you.
Deeply.

ACKNOWLEDGEMENTS

I am still not convinced of the existence of a supreme force that guides us, and I am not sure being thankful for being privileged is a good thing, but I think is important to acknowledge that. There is a good chance I wouldn't be here, finishing this thesis now, have I not had the privilege of being born in a family that always prioritized education and had the means to keep me in school. That is not saying I didn't have to sacrifice things or this path was easy, but I had the choice to pursue it, and for that I am very grateful.

As I write this section I am just coming out of one of the scariest moments of my life, and I cannot express how much support I have received from my family. "Thank you" is not enough, but unfortunately I am not good with words. So, thank you for all the love and care, thank you for always being there, thank you for understanding my absence and my quiet nature. Thank you for rooting for me and encouraging my plans even if that means I will be physically distant. I love you so, so much.

I'm deeply indebted to my supervisor, Jabah, for receiving me in his group and sharing his knowledge. I have grown a lot during these 6 years, and your light and fun way of dealing with things is a great balance to all the anxiety I have. Thank you for supporting my crazy ideas and being enthusiastic about them. Thank you for worrying and looking after me.

I'm extremely grateful to all the LBM members and also the colleagues of the Physics department. I am very grateful for your company, for the experience shared, for the discussions, for the beers and wine and caipirinhas and cocktails we have had.

I am also grateful to prof. Anthony Watts for receiving me in his lab. I cannot express how important this experience was to me. Thanks should also go to prof. Paulo Sérgio Coelho, who has been so kind and helpful.

Special thanks to Dany and Iara, my Mosketeers, for being in my life and coloring life in the lab. Thank you for all the care, all the meals, all the moments we have spent together.

Thanks should also go to my babies, Ariane and Murilo, who showed me another side of science. I hope you have learned from me as much as I've had from you. Thank you for sharing the frustration of unsuccessful experiments and the joy of the successful ones. Above all, thank you for your friendship.

Many thanks to my dear friends at the inn. I am very lucky to have met you all. Your company made it possible to stand this crazy pandemic situation. I will miss our rolês.

Thanks should also go to my friends from Caeté, Belo Horizonte, Ribeirão Preto and all over the world. Life is better because I have you.

I am very grateful to FAPESP for its financial support over the years (grants nº 2016/23863-2 and 2018/18717-2). CAPES and CNPq were too fundamental for the execution of this project.

“But nature is always more subtle, more intricate, more elegant than what we are able to imagine.”

(Carl Sagan (2011). “Demon-Haunted World: Science as a Candle in the Dark”, p.422, Ballantine Books)

“Anyone whose goal is 'something higher' must expect someday to suffer vertigo.”

(Milan Kundera (1984). “The unbearable lightness of being”, p. 59, Harper & Row)

Resumo

GRASPs (de Golgi ReAssembly and Stacking Proteins) são proteínas inicialmente envolvidas na organização e manutenção do complexo de Golgi. Enquanto este papel vem sendo questionado nos últimos anos, muitas outras funções vem sendo a elas atribuídas. Em especial, destacamos a participação no ancoramento de vesículas de secreção que precisam atravessar o Golgi e processos de secreção não convencional. Estruturalmente, GRASPs podem ser divididas em um domínio N-terminal chamado GRASP e um domínio C-terminal que é altamente desordenado e não conservado, chamado SPR. Informação estrutural sobre GRASPs, até agora, tem sido muito escassa, o que motivou o início deste trabalho. Para estudar GRASPs, usamos a única GRASP da levedura *Saccharomyces cereviseae* (Grh1), um organismo modelo. Demonstramos que Grh1 possui regiões de desordem intrínseca também no domínio GRASP, sendo considerada uma proteína do tipo *molten globule*. Além disso, Grh1 é capaz de formar fibras do tipo amiloide quando em condições específicas *in vitro*, como baixo pH e temperatura levemente elevada. No objetivo de investigar uma possível correlação entre a formação de fibras e a função desempenhada por Grh1 em processos de secreção não convencional, parte desse trabalho foi realizada *in vivo*, e foi possível mostrar que a GRASP de levedura fibrila em condições específicas de privação de nutrientes e choque térmico. Aqui, discutimos o uso da microscopia do tempo de vida de fluorescência como uma técnica válida para auxiliar na detecção de formação de fibras *in cell*, e também as possíveis implicações da formação de fibras por GRASPs para formação de Compartimentos para Secreção Não Convencional (do inglês CUPS). Esse trabalho também contém experimentos iniciais que apontam para uma separação de fase líquido-líquido sofrida poe Grh1, o que estaria em consonância com os achados de desordem intrínseca e a recente proposta de que o Golgi seria, na verdade, uma organela em fase separada do citosol. No final deste trabalho, apresentamos ainda experimentos iniciais de caracterização de Bug1, a golgina parceira de Grh1. Não existem dados estruturais disponíveis para nenhuma golgina em solução, e sua purificação sempre se mostrou um obstáculo. Descrevemos aqui um protocolo através do qual foi possível se purificar Bug1 em grandes quantidades, abrindo caminho assim para que muitas outras descobertas sejam feitas no que diz respeito à secreção de proteínas e separação de fase líquido-líquido.

Palavras-chave

1. GRASP 2. Secreção não convencional de proteínas 3. Fibras amiloides
4. Proteínasintrinsecamente desordenadas 5. Espectroscopia

Abstract

GRASPs (from Golgi ReAssembly and Stacking Proteins) are proteins involved in the organization and maintenance of the Golgi complex. While the extension of this role has been questioned in the past few years, many other functions have been assigned to them. In particular, we highlight the participation in tethering vesicles that need to move along the Golgi and processes of unconventional protein secretion. Structurally, GRASPs can be divided in an N-terminal domain called GRASP and a non-conserved, highly disordered C-terminal domain, termed SPR. Structural information, hitherto, has been scarce, which motivated the beginning of this project. To study GRASPs, we used the only GRASP (called Grh1) of a model organism: the yeast *Saccharomyces cereviseae*. We showed that Grh1 contains regions of intrinsic disorder also in its GRASP domain, being classified as a molten globule. Besides, Grh1 is capable of forming amyloid-like fibrils when in specific conditions *in vitro*, such as low pH and moderately elevated temperature. With the aim of investigating a possible relationship between fibril formation and the role played by Grh1 in unconventional protein secretion, part of the present thesis was done *in vivo*, and it was possible to demonstrate that the yeast GRASP fibrillates in starvation and heat-shock conditions. Here, we discuss the use of Fluorescence Lifetime Imaging Microscopy as a valid technique to help detect fibril formation *in cell* and also the possible implications of fibrillation for the formation of the Compartments for Unconventional Protein Secretion (CUPS). This work also contains initial experiments that point to a liquid-liquid phase separation of Grh1, an observation in consonance with the findings of intrinsic disorder and the recent proposition that the Golgi is actually an organelle phase separated from the cytosol. Finally, we present initial experiments of the characterization of Bug1, the golgin partner of Grh1. There are no structural data available on golgins in solution yet and their purification always presented an obstacle on obtaining them. We describe here a protocol capable of purifying Bug1 in high quantities, therefore paving the way for many other discoveries in the fields of protein secretion and liquid-liquid phase separation.

Key words

1. GRASP 2. Unconventional protein secretion 3. Amyloid fibrils
4. Intrinsicallydisordered proteins 5. Spectroscopy

List of Figures

D). DiSpi is a web-crawler that aggregate the results from a set of commonly used predictors of intrinsic disorder, such as PONDR® VLXT [*168*], PONDR® VL3 [*167*], PONDR® VLS2B [*245*], PONDR® FIT [*92*], IUPred2 (Short) and IUPred2 (Long) [*164*,*246*, *247*], and enables the rapid generation of disorder profile plots for individual polypeptides as well as arrays of polypeptides. On the other hand, D2P2 (http://d2p2.pro/, accessed in 2020) is a database of predicted disorder for a large library of proteins from completely sequenced genomes [*162*] that in addition to using the outputs of IUPred [*164*,*246*], PONDR® VLXT [*168*], PrDOS [*166*], PONDR® VSL2B [*167*,*245*], PV2 [*162*], and ESpritz [*163*] represents several disorder-based functional annotations, such as location of various posttranslational modifications and predicted disorder-based protein binding sites, known as molecular recognition features, MoRFs. It is known that many disorder-based binding regions are characterized by the presence of less disordered sub-regions, which are not capable of folding on their own, but can undergo binding-induced folding at interaction with its binding protein partner. In disorder profiles, such regions are typically manifested as local “dips” within the regions with high disorder score [*248*,*249*]. In D2P2, the presence of MoRFs is evaluated by ANCHOR algorithm [*250*,*251*]. 111

List of Tables

List of Supplementary Figures

Summary

1 Introduction

1.1 The conventional secretory pathway

Membrane and soluble vacuolar/lysosomal proteins and proteins to be secreted pass through the conventional secretory pathway that involves the Endoplasmic Reticulum (ER) and the Golgi complex (GC). These proteins possess signal sequences that act as markers for them to enter the ER once they are produced by the ribosome [*1*,*2*]. Once in the ER various chaperones assist the newly-synthesized protein to ensure correct folding. Post-translational modifications, such as glycosylation, also take place prior to the protein transport by coated vesicles [*1*].

In between the ER and GC there is the ER-Golgi intermediate compartment (ERGIC). The nature of this compartment (whether it is an extension of the ER or not) is still unclear, but it is accepted as a sorting station of retrograde and anterograde movement [*1*]. Retrograde flow is the movement toward the endoplasmic reticulum, whereas anterograde movement refers to the classical flow starting at the ER [*1*].

1.1.1 The Golgi complex

The Golgi complex was first reported by Camilo Golgi (hence the name) in 1888 by the observation with the use of silver chromate staining of reticular structures in the cytoplasm of many cell types [*3*]. It is an organelle formed by several stacked cisterns. In protozoan, plants, invertebrates and many fungi, these cisterns are dispersed in the cytoplasm, being located somewhat close to the exit of the ER. In other unicellular organisms, like the yeast *Saccharomyces cereviseae*, the Golgi membranes are isolated cisterns, randomly distributed in the cytoplasm [*4*]. In most vertebrates, though, they are laterally connected, forming a tunnel with multiple layers that are adjacent to the nucleus and act as an extension of the endoplasmic reticulum [*5*].

The Golgi complex is polarized, being divided in *cis*, *medial* and *trans* parts. The former is the connection of the organelle with the endoplasmic reticulum; the latter faces the plasma membrane and is the exit point of the vesicles [*4*]. The Golgi is the site of post-translational modification of the proteins that come from the endoplasmic reticulum, and is responsible for their packaging into carriers and addressing to membranes or the

extracellular medium [*6*]. The *cis*-Golgi is the site for the first steps of mannose 6-phosphate signal attachment and O-glycosylation [*7*,*8*]. The *medial*-Golgi contains a transferase involved in N-glycosilation that is a marker for this region [*9*]. The *trans*-Golgi is the site for sialylation and tyrosine sulfation, two of the last steps before a protein exits the organelle [*10*].

In *S. cereviseae*, unlike mammalian and many fungi cells, the Golgi is not stacked, but rather presents itself as individual cisterns scattered throughout the cell that only occasionally associate with one another [*11*]. Despite this different organization, once proteins leave the ER they undergo a series of processing steps that are very similar to those happening in mammalian cells [*11*]. Because of that, *S. cereviseae* is used as a model in the study of Golgi components and functioning.

1.1.2 Moving through the secretory pathway

Conventionally, the transport to and from the Golgi happens via vesicles formed by cytosolic coat proteins (COPs) in which the protein to be transported is engulfed. There are three different types of COPs: COPI, COPII and clathrins [*1*]. As a general mechanism, these complexes move and anchor at specific sites in the acceptor membrane, where they fuse and release the cargo protein.

First, proteins that have gone through the necessary post-translational modifications and quality control in the ER are packed in COPII-coated vesicles [*12*]. COPII transports the cargo to the ERGIC and there the transported protein is engulfed by COPI-coated vesicles, responsible for the transport to the *cis*-Golgi. Retrograde vesicle traffic is also performed by COPI [*12*].

Clathrins are formed in the *Trans*-Golgi network (TGN), a portion of the Golgi beyond the *trans*-face. The primary function of the TGN is cargo sorting, and clathrins cooperate to transport cargoes from the Golgi to endosomes [*13*]. Figure 1 illustrates the currently accepted model of vesicular transport along the secretory pathway, evidencing the role of COPs and clathrins. From the endosome, the cargo can be transported to the plasma membrane or incorporated into lysosomes.

While the vesicle model had been widely accepted for many years, it cannot explain the complexity of the Golgi apparatus. Today, the cisternal maturation model (and the variations that came from it) is the most debated [*1*]. According to this model, instead of having the vesicle travel along the Golgi complex, the Golgi cisternae is formed continuously, maturing progressively into TGN cisternae. During this process the cargo, i.e. the protein to

be secreted, is moved along the organelle [*1*].

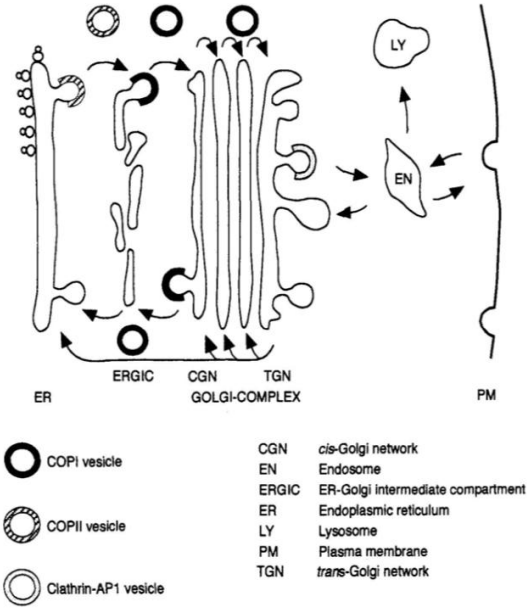

Figure 1: Model of transport along the classical secretory pathway in a mammalian cell. COPII-coated vesicles ensure the export from the ER to the ERGIC. From there to the *cis*-side of the Golgi and through the complex, the transport is mediated by COPI-coated vesicles. These are also involved in retrograde vesicle movement (from the Golgi to the ER). Sorting at the *trans*-Golgi network can be mediated by clathrin-coated vesicles. Adapted from reference [1].

1.1.3 GRASP

Golgi Reassembly and Stacking Proteins (GRASPs) comprise a family of proteins peripherally associated with the Golgi membranes that are involved in the organization and formation of its multiple stacks [*5*]. Mammals have 2 GRASPs (GRASP55 and 65). GRASP55 is found in the *trans*-Golgi, while GRASP65 resides in the medial (the intersection between cis and trans faces) and the *cis*-Golgi [*5*]. Most organisms possess only one GRASP ortholog, while plants have none (at least it is not known to this date) [*14*].

The first GRASPs to be identified were the previously mentioned GRASP65 and GRASP55. Initially, it was suggested that through *trans*-oligomerization and anchoring in the Golgi membranes they would help keeping the peculiar organization of the many stacks. However, the extension of their importance in the organization and maintenance of the Golgi apparatus has been questioned [*5*]. Experiments studying the effect of depletion of GRASP65 showed that there is no effect on the Golgi stacks, although part of the tubular structure is lost [*15*]. Similar effect has been observed for GRASP55 [*16*]. These studies suggest that GRASPs are actually laterally linking the Golgi stacks, probably with GRASP65 and 55 linking *cis-cis* and *medial-medial* faces, respectively [*17*,*18*].

Recently, Grond *et al*. [*19*] generated a mouse knocked out for both GRASP65 and 55. The result was Golgi cisterns still stacked, but not laterally connected and with a cross-sectional diameter reduced in comparison with the normal mouse. Tie *et al*. [*20*] showed that GRASPs are concentrated at the rim of the cisterns That can explain why knocking out both GRASPs would lead to disturbance in the area. Absence of GRASP55 and 65 leads to hypervesiculation, which is translated into an intact but smaller Golgi complex [*19*]. Genome sequencing made it possible to identify GRASP ortho and homologues in all animal species, with the exception of plants [*21*], whose Golgi nonetheless presents the usual organization of stacked cisterns. Some of these homologues even showed diverse localization, being also found in ERES and in the ER itself [*22*]. It is speculated that in these other sites GRASPs play a role in the anterograde movement [*22*].

Of particular interest to this thesis, the budding yeast *Saccharomyces cereviseae* has one GRASP, Grh1, homologue of GRASP65. In this case one might wonder about the role in Golgi structure, given the fact that only 40% of the Saccaromyces GC is organized in stacks [*23*]. Present also in tER, Grh1 binds to COPII vesicles and is involved in unconventional protein secretion processes (discussed later in this introduction).

Both mammalian GRASPs are myristoylated at the N-terminus, a feature that together with binding to other partners ensure tight association to the membrane, even though these proteins lack a membrane-spanning region [*24*]. Myristoylation happens at the Glycine in position 2, a conserved residue among species, with the exception of budding yeast and one variant of Plasmodium [*23*,*25*]. The N-terminal half of GRASPs is called GRASP domain (from now on referred to as DGRASP) and is conserved among species. It is composed by two PDZ subdomains [*21*]. A PDZ is a globular domain very often involved in supporting interactions among proteins, being responsible for addressing of target proteins and forming protein complexes [*26*]. Some structures of DGRASPs have been solved: Human GRASP55 [*27*, see Figure **2**]; GRASP55 and 65 homologues of *Rattus norvegicus* [*28*].

The GRASP domain spans residues 1 to 201 (except in yeast) and is responsible for dimerization. The overall organization of the PDZs is more similar to that seen in prokaryotes than eukaryotes. The dimerization is believed to occur via a protuberance in PDZ2 (conserved motif IGYGYL) inserting in a binding pocket in the PDZ1 of the juxtaposed GRASP [*28*]. Given the way the PDZs are organized, dimer formation is achieved in a *trans* manner [*28*]. However, the structural arrangement of the GRASP dimer has been a matter of extensive debate over the years with more complicated models also suggested [*29*].

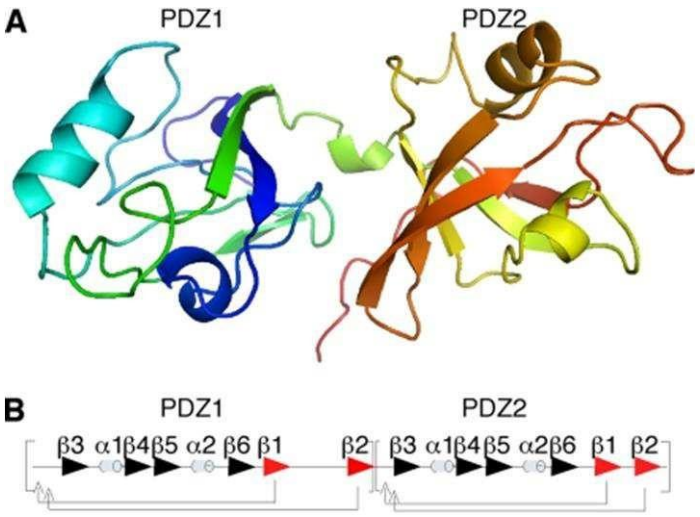

Figure 2: (A) Crystallographic Structure of the GRASP domain of GRASP55 evidencing the presence of the two PDZ subdomains. (B) Schematic representation of the arrangement of secondary structural elements within PDZ1 and PDZ2 of GRASP55. Adapted from reference [28].

The C-terminal domain of GRASPs is enriched in serine and proline residues, and for that reason is called SPR domain. It has variable lengths across different GRASPs and is the subject of phosphorylation by mitotic kinases. The N-terminal DGRASP can still *trans*-oligomerize in the absence of the SPR domain, but the mitotic Golgi of cells expressing this GRASP construct are bigger, suggesting the mitotic regulation done via SPR is important for the overall structure of the organelle [*24*].

Wang et al [*24*] demonstrated that GRASP65 forms more stable oligomers when the SPR is not present. During mitosis, it is necessary to breakdown GRASP65 dimers, but direct phosphorylation is prevented by the way the GRASP domains are arranged, so it is suggested that indirect regulation, i. e., phosphorylation of SPR sites could be the key [*30*]. Besides that, the SPR domain contains caspase cleavage sites necessary for Golgi fragmentation during apoptosis [*31*] and other phosphorylation sites important for Golgi reorientation to the leading edge of migratory cells [*32*]. These data evidence the important role of the SPR as a regulatory domain.

Given its sequence, with a high content of charged/polar residues and low content of hydrophobic ones, intrinsic disorder of the SPR domain was predicted [*33*]. In fact, Mendes *et al* have shown that the SPR domain is highly flexible and fully disordered, a pattern that is conserved among GRASPs, even though they have different sizes and amino acid sequences [*34*]. This high flexibility can be the reason why very few studies have been devoted to explore SPR structural features.

1.1.3.1 The Yeast GRASP

The yeast *Saccharomyces cereviseae* contains only one GRASP, Grh1. It associates peripherally with secretion vesicles, and although not essential, it can participate in the movement of vesicles at the interface of the ER and the GC [*21*]. Since the *S. cereviseae* Golgi is dispersed in the cytoplasm rather than organized in stacks, the participation of Grh1 in keeping the Golgi together in this organism has not been investigated [*27*].

Unlike mammalians GRASPs, Grh1 interacts with proteins in the inner layer of membranes coated with COPII [*23*,*35*] that are localized in the transitional Endoplasmic Reticulum (tER) and not in the Golgi [*23*,*36*]. So Grh1 is at the beginning of the secretory pathway and does not seem to be involved in the organization of the Golgi. Since GRASP65 is found at the *cis*-portion of the GC and also in the vesicles that exit the ER [*37*], Grh1 is considered a homologue of GRASP65 [*23*]. Another difference is the fact that instead of myristoylation, Grh1 is acetylated by the NatC complex and possesses an amphipathic helix that is needed to target it to early Golgi membranes [*23*].

Akin to other GRASPs, Grh1 associates with a Golgin, Bug1. Being 342 residues long, Bug1 has a basic N-terminal and a potential coiled-coil domain that is necessary for the recruitment of Grh1 to membranes *in vivo* [*23*]. Grh1 binds to the C-terminal region of Bug1, and is thought that its role in membrane trafficking is related to this protein complex [*23*].

1.1.4 Golgins

Another class of proteins that participate in the structuration of the GC is the Golgins. They are extended coiled-coil proteins that have been firstly identified using antibodies derived from patients suffering from a variety of autoimmune conditions [*38*,*39*,*40*]. They are Golgi-localized and either peripherally associated with the cytoplasmic face of the membrane or, less frequently, tail-anchored [*41*]. Just like GRASPs, different Golgins also localize to

different parts of the Golgi. The first one to be discovered, GM130, is present in the *cis*-part of the GC [*41*], while golgin-245 can be found only in the *trans* region [*38*]. Their different localizations suggest they perform different roles, and are indeed involved in various processes [*5*]. However, that is out of the scope of the thesis, so we are going to focus only on their GRASP-related functions.

The coiled-coil nature of the Golgin structure makes them ideal for membrane-tethering/linking, since they can span over relatively large distances [*42*]. Waters and Pfeffer proposed the tethering hypothesis that would explain how the vesicles are transported through the secretory pathway and how adjacent membranes are linked together [*42*]. Taking the *cis*-face of the Golgi as an example, another protein, p115, is recruited on to COPII vesicles that arrive in the anterograde movement. p115 then interacts with GM130 and GRASP65, making the connection between the vesicles and the *cis*-Golgi. Once tethered is expected that the vesicle fuses with the target membrane, but other events along the way can change that [*43*]. Figure 3 presents a scheme of tethering events. The tethering hypothesis is rather simple and further studies are necessary to paint a complete picture of the transport of vesicles. Nonetheless the main events and functions assigned to each protein remain valid.

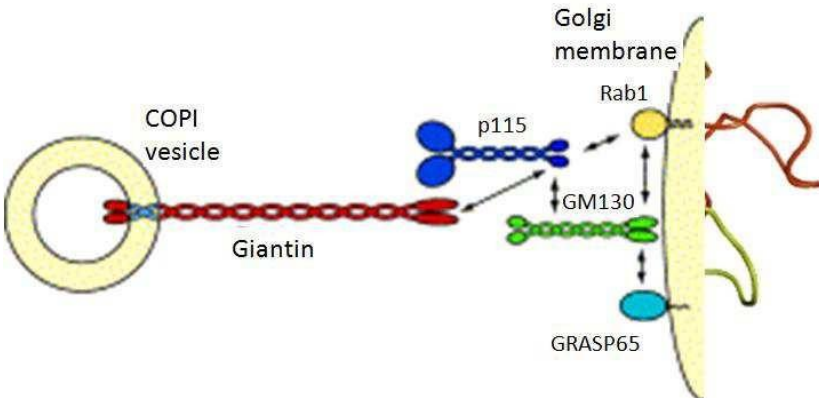

Figure 3: Schematic representation of the interaction between Golgi proteins that have been proposed to tether COPI-coated vesicles to the Golgi membrane. The protein Giantin, present on the surface of the COPI vesicle, binds to GM130 via p115. GM130 is localized to the *cis*-Golgi via its interaction with GRASP65, which is in turn attached to the membrane via an N-terminal anchor. Adapted from reference [43].

1.2 Unconventional Protein Secretion

Most proteins produced by cells that need to be secreted or have their function in the plasma membrane follow the classical route starting at the endoplasmic reticulum and

passing through the Golgi, where they are addressed to the plasma membrane or the extracellular medium as described above [*44*].

Some proteins, though, are capable of leaving the cell by other routes that are collectively called Unconventional Protein Secretion (UPS) pathways. There are two categories of cargos secreted in UPS: the first involves “leaderless” proteins that are active in the extracellular medium despite the fact that they do not have a signal peptide. They may have other signals to direct their secretion, but will not be addressed to the ER during their synthesis in the ribosome [*44*]. The second involves proteins that do enter the ER but whose secretion proceed without traversing the Golgi in a so-called Golgi-bypass [*45*].

The leaderless soluble proteins can be secreted via different mechanisms that have been classified in three main types of UPS pathways: Type I involves the formation of pores in the plasma membrane, through where cytoplasmic proteins reach the extracellular space. This type of UPS can be either self-sustained or activated by inflammation, such as in the case of IL-1β [*44*]. Type II or ATP-binding cassette (ABC) transporter-based secretion is very poorly understood so far, despite being described in the literature for the first time in 1989 [*46*]. It seems to be used to secrete lipidated proteins and peptides [*45*]. Because the mechanism is very similar to Type I UPS (leaderless proteins passing through a channel in the plasma membrane), they are often considered together in review articles [*47*].

UPS Types III and IV have GRASPs as a player in common [*48*] and therefore will be considered in more detail. A schematic summary of mechanisms of unconventional protein secretion is presented in Figure 4.

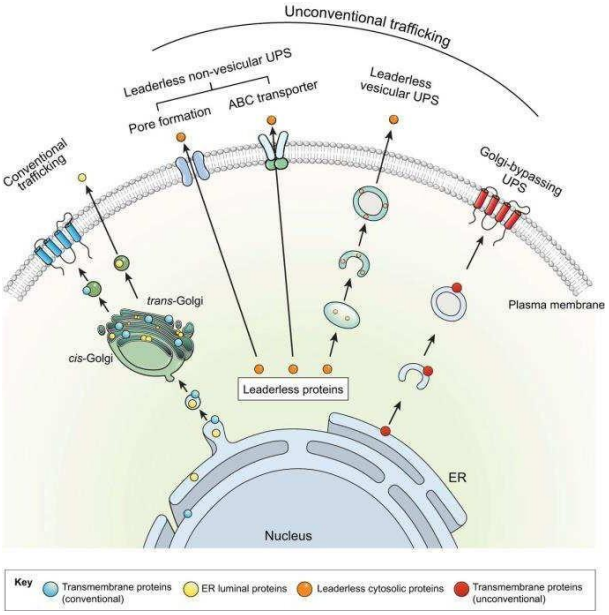

Figure 4: Protein trafficking pathways. The so-called conventional secretory pathway refers to the transport of proteins (blue and yellow circles) through the ER and GC. A number of alternative routes have been discovered and are collectively called Unconventional Protein Secretion (UPS) pathways. Some leaderless cytosolic proteins (orange circles) can be secreted via a membrane pore (Type I) or the ABC transporter (Type II). These are leaderless non-vesicular UPS. Others need autophagy-associated vesicles, like CUPS (Type III UPS). Transmembrane proteins (red circles) con also be secreted unconventionally, using a route that requires the ER but the GC, and for this reason is called Golgi-bypass (Type IV). Adapted from reference [49].

1.2.1 Type III UPS

This UPS route differs from the first two in the fact that leaderless proteins are transported in what is believed to be membrane-bound compartments. These can be multivesicular bodies or lysosomes, autophagosomes or autophagy derived structures, and microvesicles derived from the plasma membrane [*50*].

GRASPs have been shown to participate in UPS Type III by Kinseth *et al* [*21*]. Silencing of GRASP in *Dictyostelium discoideum* led to the accumulation of acyl-coA binding protein (ACBP) inside the cell and defects in sporulation under cell stress. The same was also observed in *Cryptoccoccus neoformans* [*51*]. ACBP is secreted under stress conditions such as starvation, and goes through proteolytic cleavage that generates a 34 amino acid peptide required for rapid encapsulation of the prespore cells [*52*].

Besides GRASP participation, another common feature observed in those initial studies was the triggering of UPS by stress. For example, once the cell enters starvation, a series of events begins to ensure survival. A constant supply of energy is necessary in order to keep key parameters for the cell survival, such as pH, osmotic pressure and ion

concentration [*45*]. If the cell is faced with nutrient starvation and can no longer maintain the energy levels, these parameters are affected. One of the first changes observed is a pH drop (from 7.4 to about 5.7 in yeast) [*53*].

Studies with yeast under nutrient starvation led to the discovery of a Compartment for Unconventional Protein Secretion (CUPS) [*54*]. Their formation requires autophagy genes and MVB components [*55*], but they are not canonical autophagosomes or MVBs. In the absence of glucose, ER, Golgi and endosomal membranes are remodeled to make up the CUPS [*56*].

The marker of CUPS formation is Grh1 (the yeast GRASP). Within 30 minutes of starvation, Grh1 leaves the Golgi and relocates to the cytoplasm where several foci CUPS are found [*54*,*56*]. CUPs were characterized as a spheroidal organelle with ~200 nm in diameter [*57*]. Initially CUPS are comprised of tubules and small vesicles. They mature into ACBP-positive stable tubular structures engulfed by ESCRT-III-coated saccules [*57*]. The exact mechanism by which ACBP reaches the extracellular medium is still unknown, but it has been suggested that ACBP translocates into the ESCRT-III-coated saccules, which then fuse with the plasma membrane [*57*]. Figure 5 represents the steps of unconventional secretion of ACBP, starting from Grh1 membranes.

Participation of GRASPs in a different UPS Type III mechanism was recently discovered. GRASP55 was seen to be involved in the “unfolded protein response” that controls Interleukin-1β aggregation and secretion [*58*]. Interleukin-1β uses an autophagy-based secretion pathway to reach the extracellular medium. Autophagy is involved in secretion during both normal and pathological situations. Its malfunction can, for example, favor tumor growth, because cancer cells have an up-regulated autophagy system, which leads to increased secretion of IL-1β, a known cancer-promoting factor [*59*].

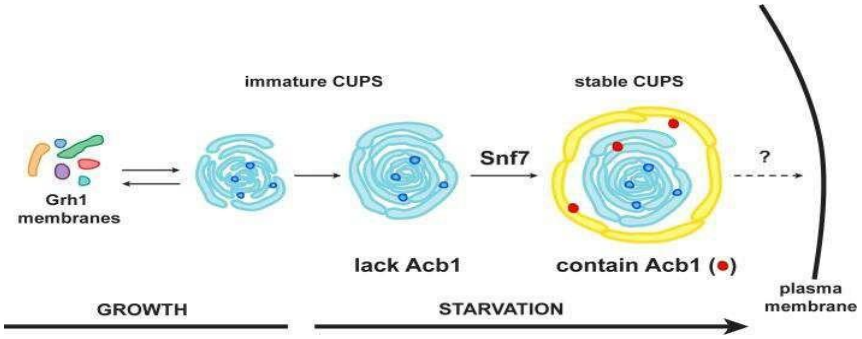

Figure 5: A schematic representation of steps in CUPS maturation. Grh1 containing membranes are formed and consumed constitutively during growth (immature CUPS). When the cells are faced with starvation, these immature CUPS become enclosed by a saccule (yellow membrane). These new compartments are the “mature CUPS” and contain the Acb1 molecules for secretion. Adapted from reference [57].

1.2.2 Type IV UPS

In Type IV UPS, proteins that do enter the ER are transported directly to the plasma membrane without passing through the Golgi. That is why this secretion mechanism is also called Golgi-bypass. Some transmembrane proteins, such as the integrin subunit αPS1, use this route at specific stages of Drosophila development [*60*]. GRASPs have been suggested to be involved in the process when it was seen that DGRASP is needed for αPS1 to leave the ER in those same stages. Furthermore, DGRASP mRNA is enriched near the plasma membrane domains where the αPS1-containing vesicles are tethering [*60*].

Akin to Type III, a correlation between stress and UPS has been also established for Type IV. The Golgi bypass of αPS1 was determined after the observation that the targeted enrichment of GRASP mRNA is triggered by mechanical stress [*61*,*62*]. In mammalian cells, GRASPs have been shown to mediate Type IV UPS of the mutated form of CFTR (cystic fibrosis transmembrane conductance regulator), ΔF508 [*63*].

1.3 Liquid-liquid Phase Separation (LLPS) in the Golgi context

In 2019, Rebane et al. [*64*] showed that the Golgin GM130, one of the partners of GRASP65, is capable of separating into dynamic liquid droplets both when purified and placed in buffers with composition close to physiological, and when overexpressed in HeLa cells. They suggested that the protein can act then not only as a tether, but also participates in the organization of the Golgi [*64*]. A few months later, the group generalized the finding for the family of Golgins, demonstrating that the remaining *cis* e *trans* Golgins could also form

condensates inside the cells when overexpressed [*65*]. The analysis of GM130 condensates in the same report shows that the proteins assemble into flexible sheets 1-2 molecules thick.

These observations and the position of Golgins in the Golgi led James Rothman (2013 Nobel Laureate in Medicine and Physiology) to challenge the current understanding of the Golgi organization [*66*]. To him, while Golgins do have a tethering function, they perform a far more essential role in the Golgi, that is, to help in the phase-separation of the organelle. In his view, the Golgi complex would not be a flattened membrane sandwich but rather a liquid-crystal formed by cytosol-derived proteins and Golgi-membranes [*66*]. The idea is open for debate and further data regarding LLPS of Golgi-related proteins are needed to rest the case.

Even though the phenomenon of phase separation is well known in the fields of physics and chemistry since the decade of 1940 [*67*, *68*], it was only in 2009 that the idea has expanded to explain biological phenomena. At that time, it was observed that pellets of RNA and proteins called P granules formed in worm embryos were liquid droplets [*69*]. In 2011 the same group showed that the nucleolus is also a phase separated within the nucleus [*70*], andmany other reports of such behavior *in vitro* and *in vivo* followed [*71*,*72*,*73*].

Phase separation can be a way to explain phenomena that require concentrating and/or excluding specific molecules within the crowded cellular environment. The implications on cellular compartmentalization are enormous and it is not surprising that the scientific community is on a quest to understand more of the so-called membrane-less organelles and their triggering and controlling mechanisms of LLPS [*74*].

While there is still much to be discovered about LLPS in cell biology, many *in vitro* and *in vivo* studies allowed for the observation that the phenomenon usually involves protein with a high degree of flexibility, e. g., proteins containing intrinsically disordered regions [*75*,*76*]. The lack of a well-defined 3D structure along with a high promiscuity seem to be crucial for phase separation and membrane-less organelle formation [*76*,*77*].

The interplay between LLPS and amyloid formation has also been observed in cases of proteins related to neurodegenerative diseases, such as TDP-43 [*78*]. Aberrant phase separation has been suggested as a trigger for amyloid formation, which would then put LLPS as an essential event in the causative process of many disorders, like Alzheimer's [*79*].

The presence of IDRs in GRASP sequences, the amyloidogenic behavior seen for some GRASPs, the involvement of Golgins, the hypothesis of the Golgi being a phase separated organelle were ideas that led us throughout the development of our Ph. D. project,

and whose results constitute the thesis here presented. We aimed to characterize Grh1 using biophysical and biochemical methods. The experiments resulted in interesting findings that led us into an unexpected journey. Chapter 2 brings the paper published in 2018, in Scientific Reports, with our initial findings of intrinsic disorder and fibrillation *in vitro*. Chapter 3 contains the second paper submitted for publication, in which we present the data regarding the findings of fibrillation *in vivo* under stress conditions and discuss the implications of that for UPS and HSR. Chapter 4 contains exploratory experiments regarding phase separation of Grh1. Chapter 5 brings initial experiments with Bug1, the Golgin partner of Grh1. Chapter 6 is the review about GRASPs published in the International Journal of Biological Macromolecules, for which I shared first authorship with Dr Luis Felipe Santos Mendes and Dr Thirupathi Reddy Soudherpally. Chapter 7 is a brief conclusion with future perspectives.

2 The yeast GRASP Grh1 displays a high polypeptide backbone mobility along with an amyloidogenic behavior

Abstract

GRASPs are proteins involved in cell processes that seem paradoxical: responsible for shaping the Golgi cisternae and involved in unconventional secretion mechanisms that bypass the Golgi. Despite its involvement in several relevant cell processes, there is still a considerable lack of studies on full-length GRASPs. Our group has previously reported an unexpected behavior of the full-length GRASP from the fungus *C. neoformans*: its intrinsically-disordered characteristic. Here, we generalize this finding by showing that is also observed in the GRASP from the yeast *S. cerevisae* (Grh1), which strongly suggests it may be a general property within the GRASP family. Furthermore, Grh1 is also able to form amyloid fibrils either upon heating or when submitted to changes in the dielectric constant of its surroundings, a condition that is experienced by the protein when in close contact with membranes of cell compartments, such as the Golgi apparatus. Intrinsic disorder and amyloid fibril formation can thus be two structural properties exploited by GRASP during its functional cycle.

Based on the manuscript published in Scientific Reports, 2018

Fontana NA*, Fonseca-Maldonado R*, Mendes LFS, Meleiro LP, Costa-Filho AJ. The yeast GRASP Grh1 displays a high polypeptide backbone mobility along with an amyloidogenic behavior. Sci Rep. 2018 Oct 24;8(1):15690

* These authors contributed equally to this work.

DOI: 10.1038/s41598-018-33955-1

2.1 Introduction

The Golgi complex is composed of a series of cisternal membranes opposed to one another to form stacks [*80*]. In mammalian cells, the stacks are linked at their edges by tubules to form a ribbon-like structure [*17*,*81*]. An assay that blocks cisternal stacking in postmitotic events was the basis for the discovery of the two proteins known as Golgi Reassembly and Stacking Proteins (GRASP65 and GRASP55) [*81*,*18*]. Furthermore, other functions of GRASPs have already been reported, such as chaperoning and transport of some proteins, participation in cell apoptosis, Golgi reorientation during cell migration, unconventional protein secretion, and, during mitosis, as a possible G2/M checkpoint [*27*].

GRASP structure is divided in two regions: an N-terminal half, called GRASP domain, which contains two PDZ domains [*21*] and the second half (the C-terminal region), rich in proline, serine, glutamine and asparagine residues, also known as SPR domain [*29*,*28*,*24*]. The formation of the Golgi ribbon-like structure requires membrane bridging by the dimeric state of the GRASP domain [*29*,*28*]. In mammalian and Drosophila, GRASPs are tightly associated with the Golgi membranes via an N-myristoylation of the residue Gly2[*17*,*22*] and, in yeasts, via an acetylated amphipathic helix [*23*]. The association of GRASP65 also depends on a Golgi receptor, identified as the coiled-coil protein called GM130 [*17*]. The dual membrane association is important for the correct *trans* dimerization, a necessary step in the stack formation [*82*,*83*].

Details of the involvement of GRASPs in membrane trafficking and other functions in mammalian cells have been reported by researchers using model organisms, such as the yeast *Saccharomyces cerevisiae*. Although *Saccharomyces cerevisiae* has the basic organization of its Golgi cisternae, only 40% of the cisternae are in stacks and the stacks are never found linked to each other [*27*]. This budding yeast contains a single GRASP65 homolog, known as Grh1, which localizes in compartments of the early secretory pathway [*84*]. Grh1 is analog to GRASP65 and forms a complex with a coiled-coil protein, Bug1, that shares structural features with GM130. The Grh1-Bug1 complex is involved in membrane trafficking, contributes to the formation of the cis-Golgi [*23*] and, although dispensable for conventional secretion, is essential for the unconventional secretion of ACBP1 [*48*]. Furthermore, Grh1 interacts with the dimer formed by Sec. 23 and Sec. 24, protein components of the COPII coat, an event necessary for the fusion of vesicles derived from ER with Golgi membranes [*23*].

Here, we present the first structural characterization of the yeast GRASP Grh1. We investigated the biophysical and biochemical features of Grh1 and the isolated GRASP

domain (called here DGRASP) by circular dichroism (CD), fluorescence and optical spectroscopies, differential scanning calorimetry (DSC), computational predictions and established that Grh1 is a molten globule-like protein, making it a member of the collapsed intrinsically disordered protein (IDP) family. IDPs are proteins involved in a large set of functions and characterized by regions of high polypeptide mobility, and without a well-defined 3D structure [*85, 86*]. These proteins have been grouped into two broad structural classes: (1) collapsed (molten globule-like) and (2) extended (coil-like and pre-molten globule-like) [*87*]. The structural flexibility of IDPs allows a broad functional repertoire and a number of interaction partners [*88*] to act and to influence protein function in different processes, such as transcriptional regulation, translation, cellular signal transduction, and storage of small molecules [*89*].

Alongside with its disorder, Grh1 also shows an unexpected feature. We report here our findings on the amyloidogenic behavior of this GRASP. They are derived from CD, fluorescence using a specific dye, and Congo Red absorbance experiments. The results obtained from this wide range of techniques led us to the conclusion that Grh1 can form amyloid-like structures in conditions that could be reasonably found in the cell. Moreover, we showed that the DGRASP, which is the most conserved region along GRASP family, is sufficient for the fiber formation. Our results suggest that this could be a general feature of GRASPs.

2.2 Materials and Methods

2.2.1 Bioinformatics Tools

The aggregation prediction was done in the AGGRESCAN server [*90*], using a 5-residue window. The disorder prediction was done using the DisEMBL [*91*] and the PONDR-FIT [*92*] servers.

2.2.2 Protein expression and purification

Genomic DNA of a strain of *Saccharomyces cerevisiae* was used as the template for PCR amplification of the gene encoding Grh1 (Gene ID: 852129) using primers Grh1F (5′-CCCGGATCCTTTAGAATAGCTAAAAACCTCGTACGG-3′) and Grh1R (5′-GGGTTCGAATTAATCAGAGGATGACTGTTTTTGTGGT-3′). The PCR reaction was carried at 94 °C for 3 min, followed by 30 cycles of 94 °C for 1 min, 50 °C for 1 min, 72 °C for 1 min and final incubation at 72 °C for 10 min. The PCR product was digested with BamHI and HindII

(recognition sites underlined in the oligonucleotide sequences) and cloned into the plasmid pETSUMO. The resulting construct (pETSUMO-Grh1) was transformed into DH5α *Escherichia coli*, and the plasmid DNA was purified and sequenced. *E. coli* Rosetta (DE3) cells (Novagen, Darmstadt, Germany) transformed with pETSUMO-Grh1 were grown at 37 °C and 200 rpm agitation until reaching an OD 600 nm of 0.6 in 2 L shake flasks containing 1 L LB medium supplemented with 40 $\mu g.mL^{-1}$ kanamycin and 34 $\mu g.mL^{-1}$ chloramphenicol. The expression was carried out for 21 h and induced with 0.5 mM IPTG at 18 °C and 200 rpm agitation. The cells were harvested and transferred to 20 mL of lysis buffer (40 $mmol.L^{-1}$ HEPES pH 8.0, 300 $mmol.\ L^{-1}$ NaCl, and 10% Glycerol). After disruption by sonication, cell debris were removed by centrifugation, and the supernatant was applied to a nickel affinity column (Promega – Madison, USA). The column was washed with buffer containing 40 $mmol.L^{-1}$ HEPES pH 8.0, 300 $mmol.L^{-1}$ NaCl, 10% Glycerol supplemented with 25 $mmol.\ L^{-1}$ imidazole and was eluted in the same buffer with 300 $mmol.L^{-1}$ imidazole. The imidazole was removed by extensive washing using centrifugation in a Vivaspin column (GE Healthcare, Buckinghamshire, United Kingdom) and the sample was incubated for 3 h with recombinant ULP-1 protease followed by incubation in a nickel affinity chromatographic column to remove the SUMO protein and ULP-1 protease. The remaining contaminants were removed by size exclusion chromatography onto a Superdex 200 10/300 GL gel filtration column (GE Healthcare, Buckinghamshire, United Kingdom) in 40 $mmol.L^{-1}$ HEPES pH 8.0, 300 $mmol.L^{-1}$ NaCl, 10% Glycerol buffer. The purification of the GRASP domain (DGRASP) followed the same protocol, using a different reverse primer, with a stop codon at the end of the GRASP domain to exclude the SPR domain.

2.2.3 Circular Dichroism (CD)

Far-UV (190–260 nm) CD experiments were carried out in a Jasco J-815 CD Spectrometer (JASCO Corporation, Japan) equipped with a Peltier temperature control and using a quartz cell with a path length of 1 mm. Grh1 was in 10 mM sodium phosphate buffer, pH 8.0 and at final concentration of 5 µM. All far-UV CD spectra were recorded with a scan speed of 50 nm/min and at time response of 1 s. Chemical stability experiments were performed in the same buffer and increasing urea concentration (0–8.0 M). To investigate the effects of solvents Grh1 was incubated in aqueous methanol (MeOH) and acetonitrile (ACN) over a range of 0–50% solvent. The spectra were averaged, baseline-corrected and smoothed with a Savitsky-Golay filter using CDTools software [*93*]. The processed spectra were deconvoluted by using the software Continll [*94*] with database 7 [*95*] available in the DichroWeb analysis server [*96*]. The normalized root-mean-square deviation (NRMSD)

goodness-of-fit parameter was always less than 0.15, suggesting that the calculated spectra are in agreement with the experimental data [*97*].

2.2.4 Steady-State Fluorescence Spectroscopy

Intrinsic and extrinsic fluorescence were monitored using a Hitachi F-7000 fluorimeter equipped with a 150 W xenon arc lamp. The excitation and emission monochroma- tors were set at 2.5 nm slit width in all experiments. The protein concentration was 5 μM for Grh1 and 7 μM for DGRASP in 40 mM Hepes, 150 mM NaCl, 10% glycerol. For tryptophan fluorescence experiments, the selective tryptophan excitation wavelength was set at 295 nm and the emission spectrum was monitored from 300 up to 400 nm. The fluorescence of tryptophan across chemical denaturation was measured in increasing concentrations of urea (0–7.5 M). For the ThT experiments, 15 μM of the dye solution was used along with the protein, excited at 440 nm. For the ANS experiments, a 250 μM solution was used, with excitation at 355 nm. For the intrinsic fluorescence experiment the samples were excited at 357 nm, both at room temperature and 50 °C. The emission was monitored at 470 nm, with a 3 minutes interval between measurements.

2.2.5 Congo Red Assay

The absorbance spectrum of Congo Red (CR) was monitored in the presence and in the absence of the protein, between 400 and 700 nm, with a Beckman DU 640 Uv-Vis Spectrometer. CR was in a buffer solution as reported elsewhere [*98*].

2.2.6 Fluorescence Lifetime Imaging Microscopy (FLIM)

The FLIM experiments were performed in a PicoQuant MT 200 microscope. We set three different conditions: control, heating for 30 and for 90 minutes. 15 μM samples in each condition were analyzed with an excitation in 378 nm and the fluorescence lifetimes were obtained at 440 nm.

2.3 Results and Discussion

2.3.1 Sequence and structure prediction

Grh1 is composed of 372 amino acids and the analysis of the protein family database using the Pfam program [*99*] predicted that the GRASP domain, including the two PDZ sub-domains, comprises residues 1 to 280, and the SPR domain extends from residue 281 to

372. In addition, the sequence-based prediction of disordered regions (Figure 6) showed that the C-terminal domain and the central region of the PDZ subdomains (spanning 55% of the protein sequence) have high probability of being intrinsically disordered, a tendency already observed for the SPR and the PDZ subdomains within the GRASP family [*34*].

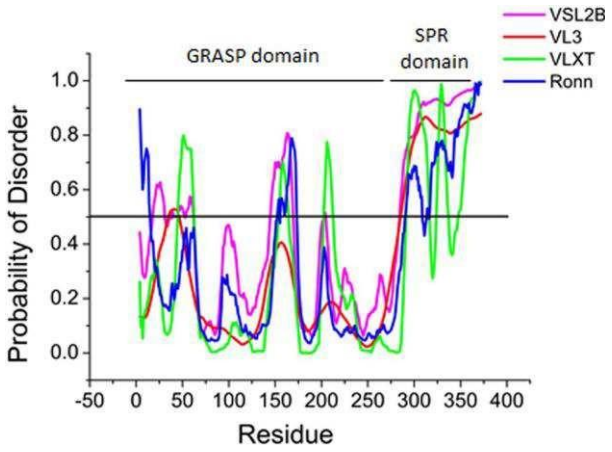

Figure 6: Predictions of intrinsically disordered regions in the Grh1 sequence using VSL2B (Magenta), VL3 (Red) VLXT, (Green) and Ronn (Blue). The black line indicates the threshold to be considered as a disordered region.

2.3.2 Structural Behavior in Solution

Unlike GRASP55 and GRASP65 [*29*,*28*], full-length Grh1 was successfully expressed as a soluble, monodisperse protein in *E. coli* (Figure 7). The theoretical molecular mass of the recombinant Grh1 is 41,119 Da, but SDS-PAGE analysis (Figure 7A) resulted in an apparent molecular mass of ca. 45,000 Da. This suggests that the amount of hydrophobic aminoacids that compose Grh1 is smaller than expected for well-structured proteins, a phenomenon similar to what was previously observed for other IDPs [*100*]. Size exclusion chromatography of the soluble protein on Superdex-200 column, whose result is shown in Figure 7B, indicates an apparent molecular mass of 45,200 Da. The differences between the expected molecular mass of Grh1 and the values determined from hydrodynamic methods is likely a consequence of the not-fully globular conformation of Grh1 in solution, which has been observed for other proteins rich in disordered regions [*101*], including the GRASP homologue in *C. neoformans* [*34*]. The chromatogram for the GRASP domain (DGRASP) is also presented in Figure 7B. We can see that it is eluted slightly after the full-length Grh1, which is expected since DGRASP lacks the SPR domain. Based on an elution curve calibrated with molecular mass standards (Supplementary Figure 1), we conclude that Grh1 and its GRASP domain behave predominantly as a monomer in solution. This is different from the observed dimers in mammalian and rat GRASPs, which may be due to the lack, in Grh1's primary

sequence, of the residues involved in dimerization [*29*] and trans-oligomerization [*27*] of GRASPs in mammalian and rat.

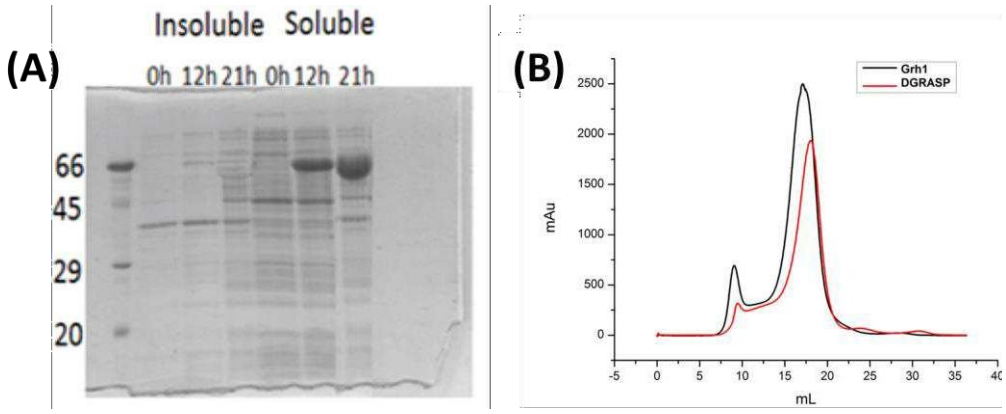

Figure 7: (A) SDS-PAGE monitoring the time course of Grh1 recombinant expression. Insoluble and soluble samples at specific times (0 h, 12 h 21 h) after IPTG induction. **(B)** Size exclusion chromatography of Grh1 and DGRASP. The first peak represents aggregates of at least 45 molecules of Grh1 and the second peak, the elution of the monomeric Grh1 and DGRASP. The pattern for the GRASP domain construct is the same observed for Grh1 (data not shown here).

The CD spectrum of Grh1 in aqueous solution (Figure 8) has a minimum around 204 nm and a poorly resolved and lower intensity peak at 222 nm, which are features typical of CD spectra of proteins with a high content of unordered structures [*88*]. However, the negative peak at 222 nm is an indication of some ordered elements. Although the intensity ratio of the peaks at 222 nm ([−4,264 deg.cm^2.dmol^{-1}) and 200 nm (−6,904 deg.cm^2.dmol^{-1}) in the CD spectrum of Grh1 is similar to values observed for other proteins in the pre-molten-globule-like state, according to the "double wavelength" plot, $[\theta]_{222}$ vs. $[\theta]$[88], Grh1 does not fit perfectly as a natively unfolded protein based on the estimation of its secondary structure content (11.5% α-helix, 22.1% β-sheet, 17.4% turns, and 49.8% random coil). Comparing these results with those from the GRASP domain only, we observe that here the spectrum also presents a minimum around 200 nm and a low (even lower than for the whole protein) intensity peak at 222 nm, which suggests decreased ordering of the protein structure (Figure 8). In fact, when we subtract the DGRASP spectrum from that of Grh1, we have a spectrum that resembles that of a Poly(Pro)II conformation [*102*], which is expected based on the high content of prolines in the SPR domain.

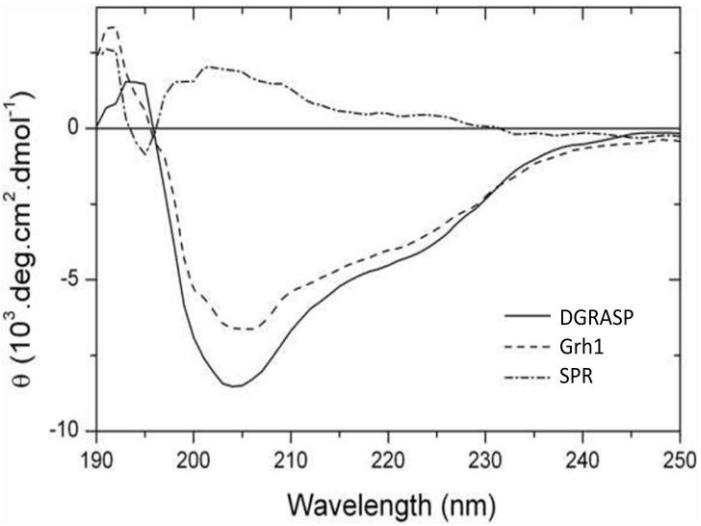

Figure 8: Far UV CD spectra of Grh1 (solid line), DGRASP (dotted line) and the SPR domain (dash line – Grh1 subtracted of DGRASP).

2.3.3 Effects of Strong Denaturants

The urea-induced unfolding of Grh1 and DGRASP were analyzed by CD and fluorescence spectroscopies. The unfolding monitored by CD spectroscopy (Figure 9) is a low cooperative transition as seen in the gradual change of the denatured fraction of the protein (fd) calculated from the molar ellipticity at 222 nm. The sigmoid-like transition is not as abrupt as expected for well-structured proteins of similar size [*88*]. The low steepness of the transition curve is typical of native molten globules or native coiled proteins and is due to the low percentage of secondary structure [*88*,*34*]. We also obtained a low cooperative unfolding pattern for DGRASP, suggesting that the pattern observed for Grh1 does not come only from contributions of the SPR domain, but also from the GRASP domain (see below).

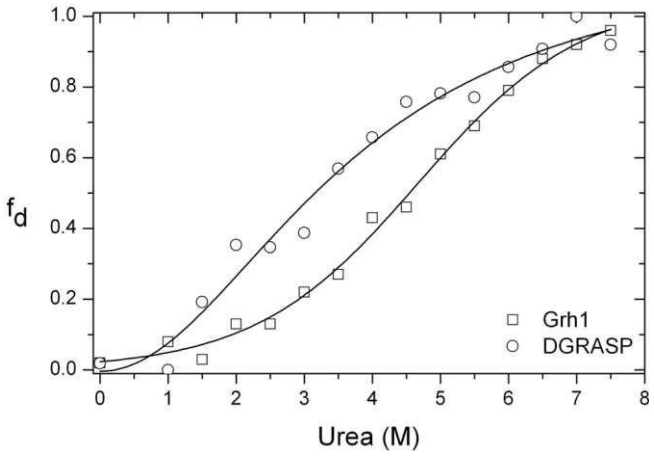

Figure 9: The unfolding fraction (fd) of Grh1 and DGRASP obtained from the CD intensity at 222 nm upon increasing concentrations of the denaturant. The solid lines are fits of a Boltzmann model to the experimental data.

The urea-induced unfolding was also monitored by using the wavelength of maximum fluorescence emission (λ_{max}) of the tryptophan residues. Tryptophan in the aqueous environment has its maximum fluorescence emission around 350 nm, which is shifted to 320 nm when the aminoacid is placed in the hydrophobic core of proteins [*103*]. For Grh1 in solution, the λ_{max} is centered at 344 nm indicating the tryptophan residues are exposed to the solvent. The fluorescence signal shows a red shift, in a cooperative transition, from 344 to 352 nm upon increasing urea concentrations (Figure 10A), indicating further exposure of the tryptophan residues and complete loss of the protein structure. Furthermore, at low concentrations of urea, the fluorescence anisotropy values remain unchanged up to a concentration of 2.5 M, dropping then significantly from 0.14 to 0.05 when urea concentration increases to 7 M, thus suggesting a relevant decrease of the structural ordering around the tryptophan residues during urea denaturation (Figure 10B).

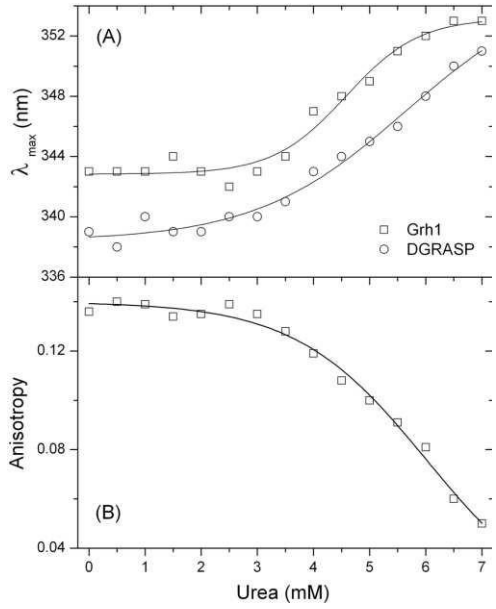

Figure 10: (A) Changes in the emission maximum (λmax) and **(B)** in the steady state anisotropy of Trp fluorescence as a function of the denaturant concentrations. The solid lines are fits using a sigmoidal Boltzmann function.

Since the three tryptophans present in Grh1 are found in the PDZ2, the same fluorescence experiments performed with DGRASP give similar results. However, in this case, the λ_{max} is at 339 nm, a slightly lower value than for Grh1, indicating that the tryptophan residues are less exposed to the solvent as compared to the whole protein. The presence of the SPR domain in the full-length protein seems to induce higher exposure of the inner regions of the PDZ2 domain, suggesting that they do not form two completely separated unities and they may, somehow, interact with each other.

Our observations of the urea-induced unfolding of Grh1 and DGRASP show weak cooperative transitions monitored by CD and somewhat more cooperative unfolding when looking at Trp fluorescence. This apparently disagreement can be explained by the origin of the chromophore under investigation in each method. Far-UV CD measures the optical activity originated from the peptide bonds, whereas fluorescence detects the emission of light generated by specific residues in the protein structure (in our case, Trp residues). We can thus see that CD is reporting unfolding of the overall protein structure, while Trp fluorescence is telling the same story from a more localized point of view. The differences in cooperativity seen from those methods indicate the coexistence of disordered and ordered regions both in Grh1 and in DGRASP, which is in agreement with our CD deconvolution and disorder prediction results (see above). The features observed so far, including low protein compaction but still significant amount of ordered secondary structure and low cooperativity during the unfolding transition, are characteristic of molten globule structures, a behavior already observed for a Grh1 homologue [*34*]. Interestingly, the SPR domain does not seem to be determinant for this, which is an issue still to be addressed in further details. Because the GRASP domain is the most conserved region within the GRASP family [*21*], we can strongly suggest that members of this family might all be molten globule-like proteins.

2.3.4 Effects of organic solvents

Based on the results shown in the previous sections, we conclude that Grh1 behaves as a molten globule like protein in solution and presents features attributable to proteins containing multiple intrinsically disordered regions. It has been shown that GRASP from *C. neoformans* (CnGRASP) experiences multiple disorder-to-order transitions upon changes in the dielectric constant of the medium or dehydration [*104*]. GRASPs are peripherally associated to membranes, so it is expected that disturbances in the physicochemical parameters induced by biological membranes may have some influence on their structure. A unique disturb induced by the biological membrane is the change in the dielectric constant (ε) nearby its surface [*105*,*106*]. Typically, a dielectric gradient is observed at the membrane/water interface, which can be modeled by an exponentially increasing function from ε= 2–4 at the first water layer up to 78 at approximately 5–6 nm from the interface [*106*]. In order to check whether Grh1 is also affected by those alterations in the medium, we performed CD experiments in the presence of organic solvents as mimetic models for the ε variation.

Figure 11 shows that the shape and intensity of the CD spectrum of Grh1 considerably

change in the presence of non-aqueous solvents manifested by the increase in the negative ellipticity around 222 nm. As observed in Table 1, the content of helical structure increases 43% and reaches a maximum in 35% methanol solution. Grh1 behaves similarly to CnGRASP up to this methanol concentration [*104*]. For further increase in methanol, a distinct pattern is observed: Grh1 gains β–sheet secondary structure and loses disordered regions as methanol increases (Figure 11A). The disordered regions decreased 41% in 45% methanol solution. A similar behavior is observed with high concentrations of ACN that induces β-sheet (23%) and helical (51%) conformations and reduces in 50% the disordered regions (Table 1 and Figure 11B). Hence, the decrease in ε induces the collapsed intrinsically disordered Grh1 to fold in a multiphasic manner, just as described by Uversky [*88*] for α-synuclein.

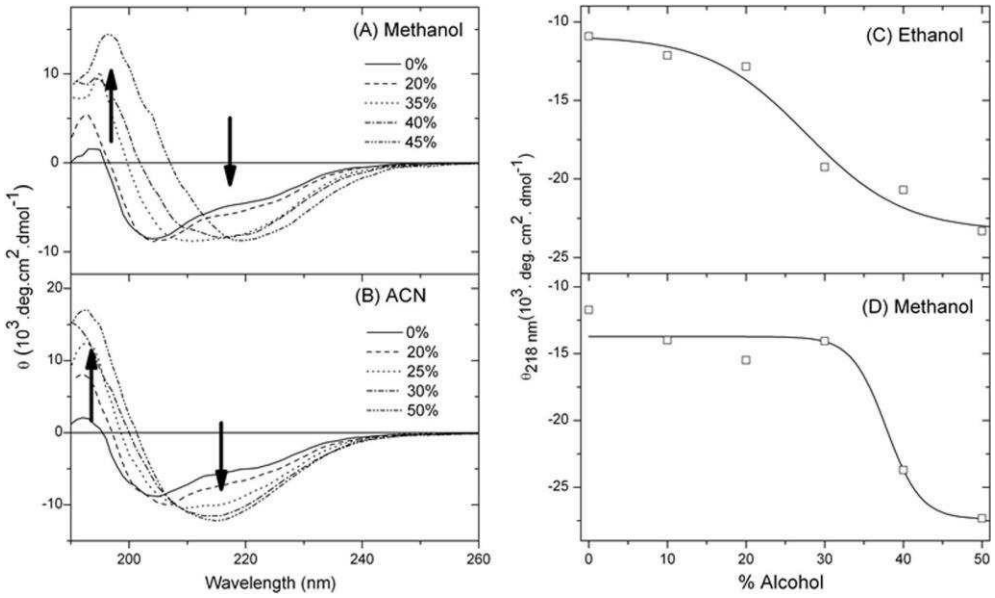

Figure 11: Far-UV CD spectra monitoring the effects of **(A)** methanol, and **(B)** ACN on Grh1 structure. Molar ellipticities at 218 nm upon increasing concentrations of **(C)** ethanol and **(D)** methanol.

Table 1: Secondary Structure Content of Grh1 as obtained from deconvolution of the respective CD spectra. The deconvolutions were performed using the Dichroweb software, with the k2d algorithm [*107*]. The data refer to CD spectra measured in increasing concentrations of (A) MeOH and (B) ACN.

(A) MeOH	α-helix	β-sheet	Turn	Disordered	NRMSD	(B) ACN	α-helix	β-sheet	Turn	Disordered	NRMSD
0%	0.12	0.22	0.17	0.49	0.067	0%	0.12	0.22	0.17	0.49	0.067
10%	0.14	0.22	0.16	0.47	0.099	10%	0.16	0.26	0.18	0.40	0.134
20%	0.17	0.25	0.18	0.41	0.134	20%	0.20	0.24	0.20	0.37	0.073
30%	0.17	0.25	0.19	0.39	0.100	25%	0.22	0.26	0.23	0.30	0.086
35%	0.20	0.26	0.21	0.33	0.093	30%	0.24	0.26	0.23	0.27	0.077
40%	0.17	0.32	0.21	0.30	0.072	40%	0.23	0.28	0.24	0.25	0.074
45%	0.15	0.33	0.23	0.29	0.093	50%	0.23	0.29	0.24	0.24	0.077

In all cases, the CD spectra at the end of the organic solvent variation show a pronounced minimum in the vicinity of 218 nm, typical of folded proteins with β-enriched structures. One can see the transition from α-helical (0% alcohol) to β-rich structures (50% alcohol) in ethanol and methanol (Figure 11C and D) as monitored by changes in the ellipticity at 218 nm. Uversky [*88*] described a similar observation when investigating the formation of oligomers of α-synuclein. Considering the fibrillar behavior of α-synuclein depending on the environment [*88*] and, being the formation of the β-rich Grh1 irreversible, we hypothesized that the gaining of β-sheet structure could, in fact, be also associated with the formation of fibrils.

2.3.5 Effects of Temperature

Far-UV CD was also used to analyze the thermally induced unfolding of Grh1. Figure 12 represents the far-UV CD spectra of Grh1 measured at different temperatures and shows that the Grh1 spectrum has its shape significantly changed as a function of the temperature. However, the spectra at higher temperatures are not typical of unfolded structures as observed in the thermal unfolding of globular proteins [*108*]. Instead of reaching a completely unfolded state, Grh1 irreversibly transitioned to a conformation still showing high contents of secondary structure. As the temperature is increased, the minima at 222 nm and at 205 nm become more and less intense, respectively, yielding a mid-point melting temperature (Tm) of 39.1°C (Figure 12B).

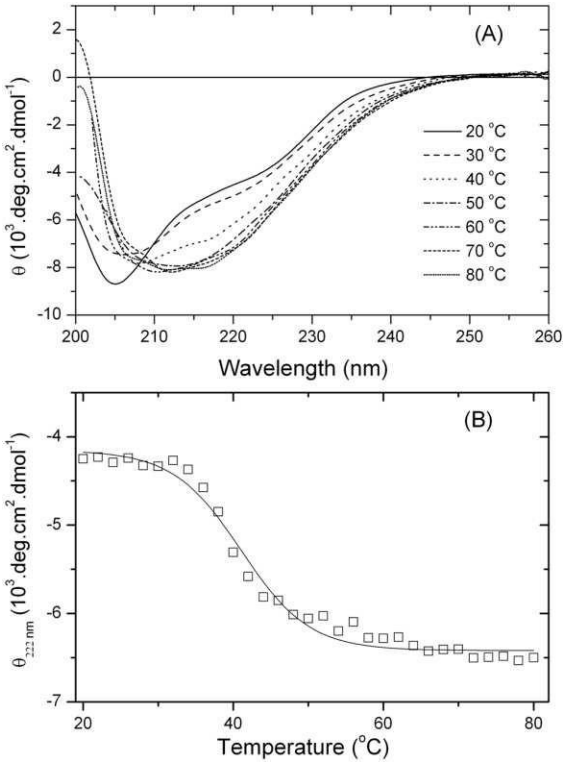

Figure 12: (A) Far-UV CD spectra of Grh1 upon heat-induced unfolding in aqueous solution from 20 to 80 °C. **(B)** Thermal unfolding monitored by the molar ellipticity values at 222 nm.

Interestingly, it has been previously observed a quite similar result for extended IDPs [*88*,*109*], where it has been proposed that the hydrophobic interactions at higher temperatures are the driving forces for the folding of the polypeptide chain. However, in the previous cases there is a transition from a fully unfolded state to a still unfolded one but with a small increase in helical content, whereas for Grh1 there is a "shape shift" from a folded conformation to a final unknown conformation, which is still rich in ordered secondary structure. Interestingly, the far-UV CD spectra progressively undergo a shift to spectra with a minimum at 218 nm, and whose shape and intensity measured at temperatures above 45 °C are close to those recorded in 40% methanol and 50% ACN solutions (Figure 11A and B), showing a β-sheet enriched conformation. Unlike other IDPs, in which temperature effects are reversible [*88*], once Grh1 reaches the β-sheet rich conformation, the structure is no longer changed upon cooling. The results in Figure 11 and Figure 12 suggest that the partial structure disturbances induced by either moderately higher temperature or decrease of ε are sufficient to trigger a transition to an ordered still unknown state of Grh1. Those observations upon changes in temperature and in the presence of organic solvents indicate that, depending on the environment, Grh1 assumes a transient conformation but above a determined threshold, a β-sheet rich conformation is adopted and changes are no longer

observed even at high temperatures (up to 80 °C).

2.3.6 Aggregation Prediction and Sequence Analysis

The appearance of considerable β-sheet contributions to the CD spectra of Grh1 either upon heating (Figure 11) or in the presence of organic solvents (Figure 12) prompted us to investigate whether those β-sheet conformations could be related to aggregation. Similar to the prediction of intrinsic disorder, there are now a number of algorithms to predict the protein regions prone to aggregation. One can have information on aggregation propensities by looking at specific residues that are known to be more common in, for example, amyloid fibrils, such as glutamine and asparagine. The server AGGRESCAN [*90*] evaluates the protein's primary sequence, classifying the residues in prone or not prone to aggregation. This classification is based not only on the nature of the residue itself, but also on its surroundings (in our case, we chose a five residue window, which means the residue will be evaluated together with the two previous and the two subsequent residues). With that classification, a Hot Spot (HS), the server creates a region where 5 or more residues are considered to be prone to aggregation. The longest the region and the aggregating nature of the residues, the higher the HS. The aggregation profile of Grh1 is shown in Figure 13, and we can see a number of short along with three long HS. While the predictor is not exclusive for fibril formation, since other aggregates can exist, it gives a good hint on whether or not a determined region is more likely to form fibrils.

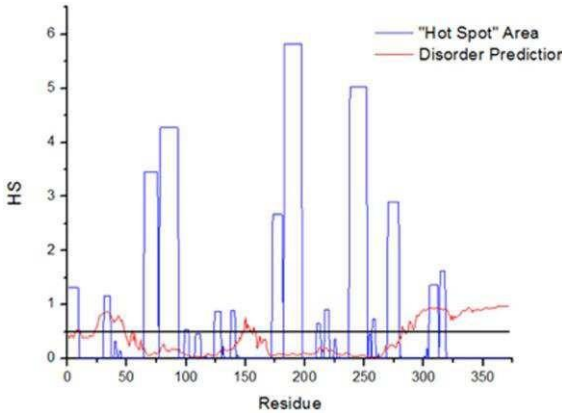

Figure 13: Aggregation prediction for Grh1, done in the AGGRESCAN server, represented by "Hot Spot" areas in blue. The red lines represent one of the disorder predictions shown in Figure 6.

The existence of potential aggregation spots brings the close link between aggregation and intrinsic disorder into play [*110*]. Hence, to check for correlations between

intrinsic disorder and aggregation in the case of Grh1 we also show in Figure 13 one of the disorder predictions presented in Figure 6. The black solid line represents the threshold for intrinsic disorder. The flexibility gained with a less compact structure can be used to help over- coming energy barriers needed for the formation of the aggregate. Several structural arrangements of disorder and aggregate-like regions in proteins have been proposed [*110*] and in one of them the amyloid core is flanked by intrinsically-disordered regions (IDRs), which could be the geometry adopted by Grh1 as suggested by the intrinsic disorder and aggregation propensities shown in Figure 13.

As for the final residues in the sequence, those in the SPR domain, it is reasonable not to observe aggregation since prolines are considered to be chain breakers, thus leading the score of a determined window in AGGRESCAN to 0. That means a domain such as the SPR would not aggregate. We can also think of that in terms of the structure of the fibril: to accommodate a proline into a β-sheet is very costly in terms of energy [*111*].

2.3.7 Ghr1 forms β-sheet rich amyloid fibers

2.3.7.1 8-anilino-1-naphthalenesulfonic acid (ANS) assay

Our bioinformatics analysis strongly suggested that Grh1 contains regions that are prone to aggregation, which, in conjunction with our results on the intrinsically disordered nature of part of Grh1 structure, indicate that Grh1 would be able to form β-sheet rich amyloid fibers. The formation of fibrils is a process that includes the formation of small oligomers that associate due to a destabilization of the native structure, leading to the formation of a number of partially folded intermediates, which possess increased aggregation propensity. This process is often called “monomer activation” [*112*]. In their review on the modeling of amyloid fibril formation, Gillam and MacPhee [*113*] cover the first moments of amyloid formation, called the lag phase, the mechanisms underlying the growth phase, where the formation of the proto-fibrils happens, until their assembly in amyloid fibrils, on the plateau phase. If we look at the whole process during time, we will have a sigmoid-like behavior much like the one we see in our CD experiments (Figure 11C and D).

To further investigate if Grh1 is really forming fibers depending on the environment conditions, we followed the well-established protocols based on the use of the fluorescence of extrinsic dyes [*111*]. ANS is a fluorescent dye commonly used in protein folding studies*114*. Although it is not specific for amyloid fibrils, the experiment we conducted followed previous studies related to fibril formation. Bolognesi *et al*. [*111*] were able to trace all the phases of fibril formation as a function of increasing concentrations of a fibril trigger. Even more

interesting in that report, the authors were able to establish a good relation between ANS fluorescence and the presence of proto-fibrils. Since ANS will bind to accessible hydrophobic cores in the protein, when the monomers assemble into proto-fibrils, there will be new hydrophobic sites created, thus increasing ANS fluorescence intensity. Keeping the stimulus by increasing the trigger concentration, the system is forced into the plateau phase, where the proto-fibrils assemble to form the proper amyloid fibrils. By doing so, the fibrils lose hydrophobic sites previously present, and then the ANS fluorescence decay [*111*].

Figure 14 shows how the ANS fluorescence will increase with increasing concentrations of ethanol (that we had seen on the CD experiments to lead to aggregation), until it reaches a maximum in 45% ethanol, and then decreases in 50% ethanol, which is in agreement with our CD data (Figure 11C). Although we cannot see the sigmoid-like time-course formation of the fibrils, we have data that is consistent with previous findings regarding ANS binding to proto-fibrils.

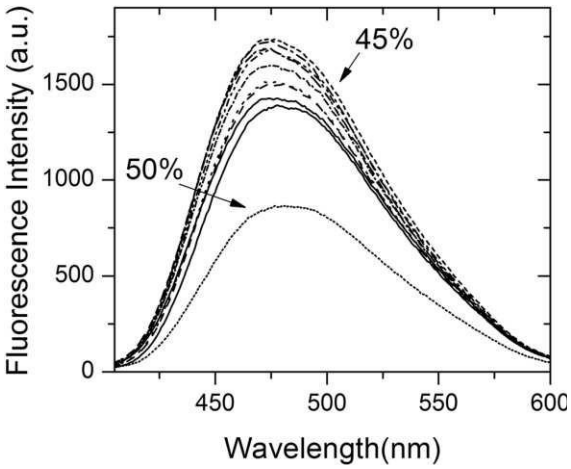

Figure 14: Fluorescence spectra of ANS bound to Grh1 with increasing concentrations of ethanol. The arrows point to the spectra in 45% and in 50% ethanol, emphasizing the reduction in intensity above 45% ethanol.

2.3.7.2 Thioflavine T (ThT) assay

The ANS assay described in the previous section indicates that Grh1 undergoes a structural transition from monomers to fibrils upon increasing ethanol concentration. To check whether those fibrils present amyloid features, we performed an assay based on the use of the fluorescence of Thioflavine T (ThT) in the presence of Grh1. ThT is a fluorescent dye used in the detection and characterization of amyloid fibrils *in situ* [*98*].

It works as a fluorescent rotor that binds into β-sheet cavities [*115*]. When in solution

the fluorescence is weak due to ThT freedom of rotation. When bound to fibrils, there is less torsional relaxation, leading to an expressive increase in fluorescence [*98*]. Although ThT can bind to amorphous aggregates and other structures with minor affinity, it is considered specific for amyloid fibrils [*98*]. In Figure 15A, we see weak fluorescence when ThT is in solution with Grh1 in its native form. However, when ThT is in solution with Grh1 previously submitted to the conditions we have seen to induce aggregation (we tested for temperature, methanol, ethanol and acetonitrile) there is at least a 10-fold increase in the fluorescence intensity. We tested our construction without the SPR domain (Figure 15B) in the same conditions and we observe the same increase in ThT fluorescence.

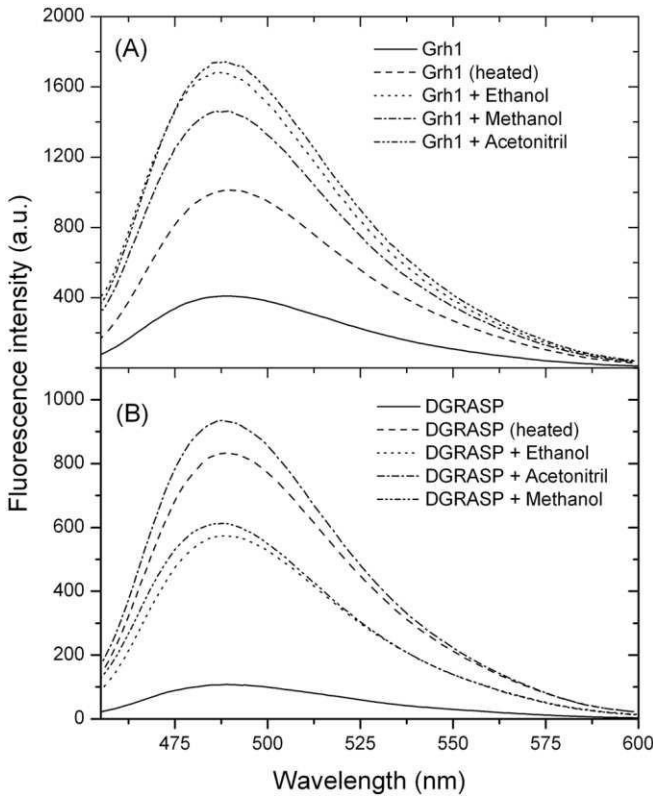

Figure 15: Fluorescence spectra for ThT bound to (A) Grh1 and (B) GRASP domain only, in different conditions.

Although the comparison between the ThT data for Grh1 and the GRASP domain cannot provide any insight into the route of fibril formation, it is nevertheless another proof that the SPR domain is not needed for the fibrillation to occur. Furthermore, we can see that different conditions led to different intensities in ThT fluorescence. For both Grh1 and DGRASP, ACN showed to induce the largest change, while heating led to a large change in DGRASP, but a not so pronounced one for Grh1, in which the effects of ethanol and methanol were markedly more pronounced. That could be the result of either the preparation of the

samples not being exactly equal, or it could be related to the pathways and the configuration that each condition induced.

2.3.7.3 Congo Red (CR) assay

CR is another widely used dye to probe amyloid structures [*98*]. The exact mechanism of binding is still unknown, but there are some models for it, such as ionic interactions between the sulfonate group of CR and basic residues in the aggregate [*116*]. It is possible to use the birefringence of the amyloid fibrils with CR to prove their existence but, since several participants are inherently birefringent (such as buffer salts), the technique is quite subjective and requires a known amyloid structure as control [*98*]. For that reason, we chose another approach based on a spectrophotometric assay. For this experiment we used pre-heated Grh1 to 50 °C to assure fibrillation. In Figure 16 we can see that the absorbance of CR between 400 and 700 nm increases linearly with the increase in pre-heated Grh1. We tested for the native form of Grh1, but there is no change in CR absorbance, showing that the binding only takes place with the protein in its fibrillar (pre-heated) form. Despite the fact that CR binding is one of the most accepted evidences of amyloid formation, it is now known that amyloid fibrils of different compositions may bind to CR through different mechanisms, which can change CR response [*98*]. The most pronounced change in absorbance intensity around 540 nm (in this experiment, the largest difference was in 533 nm) is believed to be characteristic of amyloid fibrils.

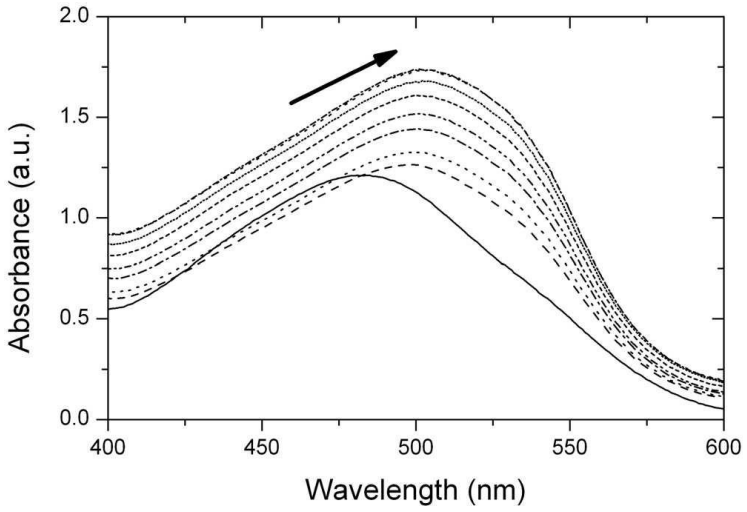

Figure 16: Absorbance spectrum for Congo Red free and bound to pre-heated Grh1.

2.3.7.4 Kinetics of fibril formation

To check fibril formation as a function of time, we used the strategy presented by Chan *et al*. [*117*], in which the authors use the so-called fibril intrinsic fluorescence in the visible range. Chan *et al*. [*117*] discuss the properties that allow a protein in its fibrillar state to fluoresce, while this is not seen with the protein in its native form. The authors suggest that it is the delocalization of electrons via multiple bond conjugation, present in β-sheet rich structures, that gives rise to the fluorescence emission in the visible range. This intrinsic fluorescence in the visible range has been used to give insights on fibrillation modes [*117, 118*].

We then followed that strategy by monitoring the fluorescence intensity of Grh1, when submitted to high temperature (50 °C), as a function of time and the result can be seen in Figure 17. Although a lag phase does exist, it is probably too fast to be detected in this manner. This suggests the most suitable fibrillation model in our case is the one described by Kumar *et al*. [*119*], with the best fitting mode being asymptotic, which accounts for a nucleation independent pathway, rather than sigmoidal. Based on the kinetics shown in Figure 17, we can see that the fibrillation process takes ca. 25 minutes to reach the plateau phase.

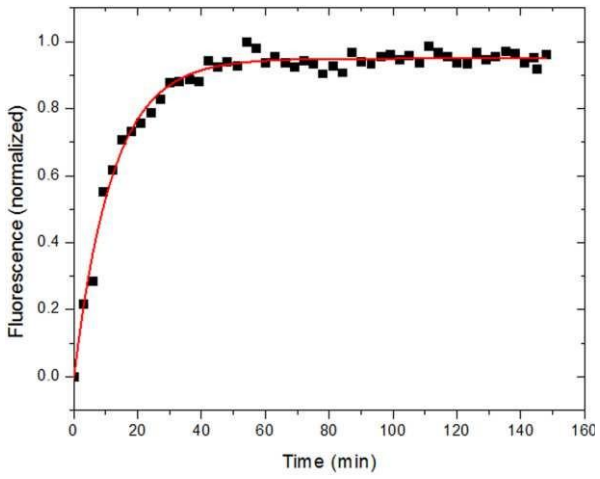

Figure 17: Normalized intrinsic fluorescence of Grh1 heated to 50 °C, as a function of time. Excitation wavelength: 357 nm Emission wavelength: 470 nm.

To actually see the fibril formation and respecting such constraint, we decided then to use the Fluorescence Lifetime Imaging Microscopy (FLIM), relying once more on the intrinsic fluorescent properties of the fibrils. While this technique does not tell us anything about the size of fibrils, the lifetime measurements can be of help in the matter of deciding whether we

have protofibrils or grown fibrils. We ran controls with Grh1 in its native state, and no fluorescence (as expected) was detected (data not shown). On the other hand, upon sample heating for 30 and 90 minutes, we could clearly detect the intrinsic fluorescence of Grh1 (Figure 18).

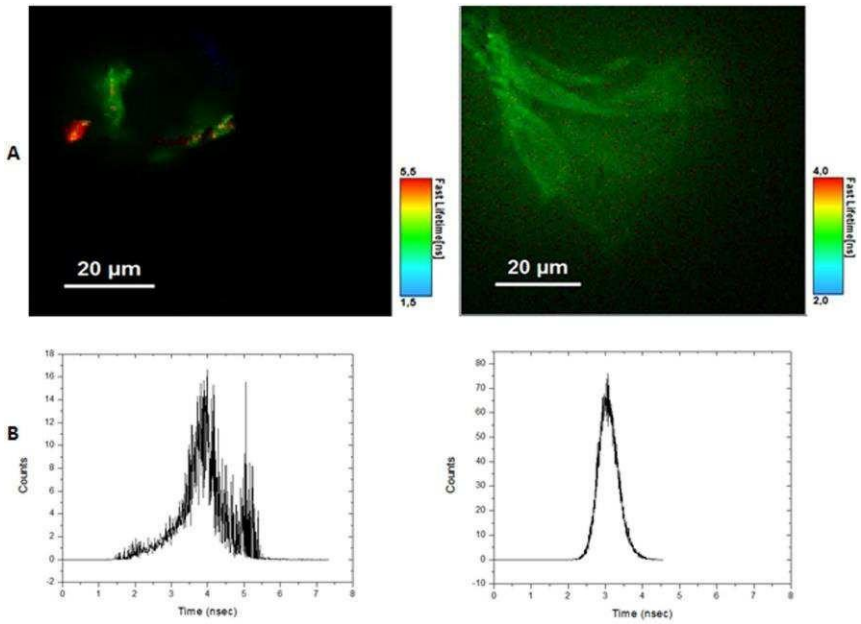

Figure 18: Results of the FLIM experiments. **(A)** Lifetime Microscopy Images of 15 µM samples and **(B)** Fluorescence Lifetime Histograms for samples heated for 30 minutes, on the left, and 90 minutes, on the right.

In Figure 18, we also present the histograms corresponding to the fluorescence lifetimes of the populations giving rise to the images in the upper panels of the figure. The images in Figure 18A as well as the respective histograms in Figure 18 show that the heating of the sample for 30 minutes produced a more heterogeneous distribution of fluorescence lifetimes than for the 90 minutes of heating. The presence of different colors in the left panel of Figure 18A clearly indicates the presence of a broader distribution of lifetimes, which is corroborated by the corresponding histogram. After 90 minutes, the particles gave rise only to green spots in the image. More quantitative information can be observed in Figure 18B: the lifetimes are longer and broader for samples heated up to 30 minutes, while within 90 minutes there is a more homogeneous distribution, and on average a shorter lifetime. These data are in agreement with what is described by Chan *et al*. [*117*], whose work showed a lifetime of fluorescence of 2 to 4 nanoseconds for amyloid fibrils, which is the value found in our experiments.

2.4 Conclusions

In this manuscript, we have described a biophysical characterization of Grh1 and its GRASP domain that revealed two significant aspects about Grh1, which are most likely linked: the presence of multiple intrinsically disordered regions that confer to Grh1 a molten globule-like feature and the capability of forming amyloid fibrils upon mild denaturing conditions, in an SPR-independent fashion. Grh1 structural dynamics in solution seems to be high but still showing a minimum stable tertiary structure. However, when a destabilizer condition, such as high temperature and/or the membrane surface, is introduced and the structure is slightly disturbed, an irreversible transition associated with amyloid fibril formation is induced. Interestingly, amyloid formation of b2m, a dialysis-related amyloidosis disease resulting from deposition of amyloid aggregates in skeletal tissue, is strongly enhanced in conditions that destabilize its globular structure [*120*]. Besides, the interaction between α-synuclein and lipids has been also shown to modulate amyloid fibril formation, depending on the relative proportion of the two species [*121*], suggesting that the membrane surface is capable of triggering fibrillation. It has been suggested that partially folded α-synuclein structures induced by increasing temperature is stabilized by self-assembly and that these oligomers may evolve into the fibril nucleus, besides having all the properties expected for a molten globules [*27*]. In general, misfolding intermediates play a key role in defining aberrant protein aggregation and amyloid formation in several different human diseases [*27*]. We observed that the GRASP domain is capable of forming fibbers in a SPR independent way, and since this is the most well conserved region along GRASP family, it is reasonable to expect the same amyloidogenic pattern for all members.

Amyloid fibrils are also found in a diversity of organisms, such as plants and bacteria [*110*], and *Saccharomyces cerevisiae* is not an exception. There are reports of amyloid proteins in yeast, such as the termination factor Nab3, that together with other two proteins forms a complex that is the major termination tool for short, non-coding RNAs [*122*].

Once thought to be disease-related only, today the idea of functional amyloids is widely accepted. Bacteria and even humans can use the properties of some fibrils to perform functions in the organism [*123*]. Such is the case of Sup35p: yeasts carrying the aggregated form of the protein have selective growth advantage [*124*]. In the case of Grh1, interestingly, only under growth it localizes to ER exit sites and early Golgi membranes, and the yeast stops growing above 37 °C [*124*], around the same temperature we determined that Grh1 forms fibrils. Upon stress conditions, like starvation and incubation at the non-permissive temperature of 37°C, Grh1 redistributes normally to a large compartment called compartment for unconventional protein secretion [*56*,*55*]. Thus, a hypothesis for further investigation is

whether the formation of fibrils by Grh1 takes part in membrane fusion events to help generating compartments involved in unconventional secretion [*56*]. Because we observed that both temperature and the membrane surface could affect the fibril formation, it is interesting to explore deeply the phenomenon when both perturbations are present together. Experiments to address this are currently being performed.

Understanding the relationship between protein structure and function is one of the fundamental questions in molecular biophysics. We proved that Grh1 is a marginally stable protein and undergoes folding reactions that involve different kinds of ordered forms depending on the environment. The functional diversity reported for Grh1 can then greatly benefit from the possibility of becoming more ordered or folded into stable secondary or tertiary structures and increase the specificity of binding. Furthermore, the irreversible quaternary structure it adopts (the amyloid fibrils) in some conditions might be a strategy of evolution to help survivability in undesired conditions.

3 In vivo amyloid-like fibrils produced under stress

Abstract

The participation of amyloids in neurodegenerative diseases and in functional processes has triggered the quest for methods allowing their direct detection in vivo. Despite the plethora of data, those methods are still lacking. We used the autofluorescence from the extended β-sheets of amyloids to follow fibrillation of *S. cerevisiae* Golgi Reassembly and Stacking Protein (Grh1). Grh1 has been implicated in starvation-triggered unconventional protein secretion (UPS) and here we suggest the idea of its participation also in heat shock response (HSR). Fluorescence Lifetime Imaging (FLIM) was used to detect fibril autofluorescence in cells (*E. coli* and yeast) under stress (starvation and higher temperature). The formation of Grh1 large complexes under stress was further supported by size exclusion chromatography and ultracentrifugation. Our data show the first-time *in vivo* detection of amyloids without the use of extrinsic probes as well as bring new perspectives on the participation of Grh1 in UPS and HSR.

Based on the manuscript available on BioRxiv, in 2021.

Fontana, NA, Rosse AD, Watts A, Coelho PSR, Costa-Filho AJ. *In vivo* amyloid-like fibrils produced under stress. 2021. BioRxiv

DOI: 10.1101/2021.02.02.429251

3.1 **Introduction**

Amyloid fibrils have been a subject of major interest over the years due to their pivotal participation in several neurodegenerative diseases [*125*] and, more recently, in functional processes [*126*]. Although the structural 3D arrangement of the fibrils and factors governing their formation have been thoroughly investigated [*127*,*128*], detecting amyloid-like fibrils *in vivo* is still not trivial. Aggregation has been monitored inside cells using GFP-labelled proteins combined with fluorescence methods [*129*]. The visualization of fibrils has been achieved using methods based on dyes that bind to amyloid plaques in excised brain tissue [*130*], and *in vivo* diagnostics of neurodegenerative diseases have been reported using Magnetic Resonance Imaging [*131*]. To directly observe fibrils inside cells, other biochemical and biophysical approaches are still necessary.

Recently, Pinotsi *et al* showed that the formation of amyloid fibrils by tau protein and lysozyme exhibited a characteristic fluorescence in the visible range[*118*]. The origin of such autofluorescence was attributed to the absorption/emission of electrons delocalized after the formation of hydrogen bonds in the typical β-sheet structure of amyloids, thus allowing low-energy electronic transitions to occur [*118*,*132*]. The specific molecular origin of the phenomenon is, however, still not completely understood [*132*]. Despite this uncertainty, the observed autofluorescence has been firmly correlated with amyloid formation in several cases, such as Amyloid-β [*133*] and α-synuclein [*134*]. Nonetheless, fibril formation monitoring was either restricted to the *in vitro* assembly [*133*] or *in vivo* detection using FRET between an extrinsic probe attached to the protein and the fibril [*134*].

The use of autofluorescence for direct detection of *in vivo* fibrillation without the use of an extrinsic probe has not been satisfactorily explored. One of the reasons could be the apparent lack of specificity in detecting the fibril signal due to the competing autofluorescence from the cells. Here, we report results on the *in vivo* formation of amyloid-like fibrils by one member of the Golgi Reassembly and Stacking Protein (GRASP) family without the use of an extrinsic dye for protein tagging.

GRASPs were initially implicated as participants in the structural organization of the Golgi apparatus[*17*], a central organelle in the conventional endoplasmic reticulum (ER)-to-Golgi pathway of protein secretion [*135*]. However, proteins can reach the plasma membrane and/or leave the cell via other mechanisms. Unconventional Protein Secretion (UPS) comprises alternatives through which (1) leaderless proteins (lacking the signal sequence for ER localization) are secreted and (2) proteins that use the conventional secretory pathway take a different route, traversing from the ER straight to the plasma membrane [*136*,*137*].

Different types of UPS routes have been reported, each dealing with different types of stress [*136*,*137*]. Among the four types of UPS reported thus far, Types III and IV share the common participation of GRASPs [*48*,*139*]. In particular, Type III UPS is characterized by the formation of a new GRASP-rich organelle, named Compartment for Unconventional Protein Secretion (CUPS) [*140*], which leads the secretory protein to the plasma membrane, where vesicle fuses, releasing its cargo.

Our group has been exploring the biophysics of GRASPs in the last few years [*14*, *34*,*141*,*142-145*]. In one of our last contributions [*141*], we described novel structural features of Grh1, the GRASP from *Saccharomyces cerevisiae*. We have demonstrated that Grh1 contains regions of intrinsic disorder, which seems to be a common feature among GRASPs. Furthermore, it was shown that Grh1 formed amyloid-like fibrils *in vitro*, and the fibrillation was independent of its C-terminal domain [*141*]. *In vitro* fibrillation has been also observed for both human GRASPs and seems to be another general feature within the GRASP family [*142, 146*]. A comprehensive review of the biophysics of GRASPs has been recently published [*14*].

The capacity of Grh1 to form amyloid fibrils is still of unclear biological significance. The presence of functional amyloid aggregates in yeast has been reported previously [*126*]. We hypothesized that the amyloid-like form of Grh1 also occurs *in vivo*, and the ensemble formed is closely related to the function of Grh1 in UPS, particularly in Type III during starvation [*147*], as well as upon increase in temperature (i.e., in Heat Shock Response - HSR) [*148*]. In the case of starvation, intracellular pH drops and becomes acidic [*53*], a condition that has been seen to trigger fibrillation *in vitro* [personal communication]. As for the temperature, we have recently reported fibrillation of Grh1 at temperatures greater than 37°C *in vitro* [*141*]. In the case of yeast, the optimal temperature for its growth is 30oC [*148*]. The cell can support mild temperature increases (for instance, from 37 to 41oC). HSR is a coordinated event that arrests cell growth through the aggregation of other proteins, thus impairing their function. This aggregation leads to the formation of Stress Granules (SG), which are disassembled by Hsps when thermal stress ceases, and the cell returns to normal growth [*148*].

Here, we address one issue, namely Grh1 fibrillation *in vivo*, whose contribution is two-fold: on the one hand, the direct detection of amyloid fibril formation *in vivo*, and, additionally, the demonstration of the formation of Grh1 fibrils inside the cell raises new insights towards better understanding basic aspects of UPS and HSR in yeast.

3.2 **Materials and Methods**

3.2.1 Protein Expression and Purification

The protocol for Grh1 expression in *E. coli* and purification is described elsewhere [*141*]. For the experiments with *E. coli* in acidic pH, cells were grown and expression was induced and carried out for 18 hours at 20 °C. Cells were pelleted by centrifugation at 8,000g for 10 minutes, and transferred for LB medium added of 50 mM MES and 20 mM sodium acetate, pH 4.6, and kept shaking at 20 °C for 1 hour.

3.2.2 Yeast Culture

The *Saccharomyces cerevisiae* strain Y470 was used in the FLIM experiments with excitation at 375 nm. All the other experiments without tagging or knockout were performed in the parental strain BY4741. The GFP-tagged and the knockout strains come from the commercial Yeast GFP clone collection (ThermoFisher Scientific). All cultures were grown in YPD medium (1% Yeast Extract, 2% Peptone, 2% Glucose).

For all experiments, a colony of the desired strain was placed in liquid YPD or SC-ura, and allowed to grow overnight at 30^{o} C. The following morning the colony was transferred to 200 ml of YPD, and allowed to grow again, this time under slow agitation until the culture reached an optical density at 600 nm of ca. 0.5.

For starvation, cultures were centrifuged and resuspended in 2% potassium acetate solution (as described by Cruz-Garcia *et al* [*147*]). For HSR, cultures were placed under agitation at 37 °C. Both experiments were run for 2 ½ hours, and the same time used for recovery, where the cultures were put back at optimal growth conditions.

3.2.3 Immunoprecipitation

Immunoprecipitation was carried out using the GFP-tagged strain, with the GFP-Trap Magnetic Agarose (Chromotek). Cells in the desired conditions were centrifuged at 12,000g for 10 minutes and the supernatant collected. The beads were previously equilibrated with dilution/washing buffer (10 mM Tris pH 7.5, 150 mM NaCl, 0.5 mM EDTA. pH adjusted to 8). Beads were added to the supernatant and the solution was left rotating end-to-end for 1 hour at 4 °C. Two washing steps were performed by separating the beads with a magnet until the supernatant was clear, discarding the supernatant and ressuspending beads with washing buffer.

For transmission electron microscopy experiments, the proteins were eluted by adding 50µL 0.2 M glycine pH 5.5. Although the protocol recommends pH 2.5, given the fact that Grh1 fibrillates in pH below 5.5, we decided to use this value (5.5) to avoid undesired fibrillation in the samples. The samples were incubated for 30 seconds under constant agitation, the supernatant was placed in another eppendorf tube, and the solution neutralized with 5 µL 1M Tris base, pH 10.4. For confocal and FLIM experiments, since the presence of the beads was not a problem, the elution step was not performed and the beads with trapped GFP taken to the microscope.

3.2.4 Lifetime Imaging Microscopy

FLIM experiments were performed in an IX71 Inverted Microscope (Olympus) equipped with a PicoQuant MT 200 confocal module. Excitation was set at 375 nm, and emission was detected from 405 nm. Data collection and analysis were performed with the SymPhoTime 64 software (PicoQuant). A Region of Interest (ROI) was delimited for analysis, and the nExponential Tailfit mode was selected. The number of exponential components was chosen based on the best distribution of the residuals and the best x^2 value found. To obtain the lifetime's histograms, the FLIM fit function was used based on the manual provided by PicoQuant (available at: https://www.picoquant.com/images/uploads/page/files/17319/4_td_flim.pdf). Decay curves presented are the best fits for each of the results.

3.2.5 Multiphoton Microscopy

Images were acquired using a LSM 780 Multiphoton AxioObserver (Zeiss), equipped with a titanium sapphire laser. Excitation was set at 880 nm, and emission recorded with a 515/30 nm filter. The microscope was available at the Laboratório Multiusuário de Microscopia Multifóton (Departamento de Biologia Celular e Molecular e Bioagentes Patogênicos, Faculdade de Medicina de Ribeirão Preto, Universidade de São Paulo).

3.2.6 Gel Filtration

Cultures in different conditions were centrifuged and pelleted in PBS, followed by sonication during 7 minutes, in cycles of 30 sec on and 30 sec off. To separate solid particulates, cultures were centrifuged at 20,000g for 20 minutes, and the collected supernatant was concentrated using a Vivaspin column (GE Healthcare, Buckinghamshire, United Kingdom). The concentrated supernatant was applied to a Superdex200 10/300 GL gel filtration column (GE Healthcare, Buckinghamshire, United Kingdom).

3.2.7 Ultracentrifugation

2 mL of cultured cells were harvested and resuspended in 300 uL lysis buffer (50 mM Tris, pH 7.5, 150 mM NaCl, 2 mM EDTA, 1 mM PMSF, 5% glycerol). Disruption was carried out by vortexing with acid-washed glass beads. 300 µL of RIPA buffer (50 mM Tris, pH 7.0, 150 mM NaCl, 1% Triton X-100, 0.1% SDS) were added to the solution, which was vortexed again for 10 sec. Centrifugation at 1,500g for 5 minutes was used to pellet cell debris. 200 µL of the soluble fraction was centrifuged in a TLA 100-2 rotor for 45 min at 100,000g and 4 ºC in an Optima TL Beckman ultracentrifuge.

3.2.8 Dot Blot

10 µL of resuspended precipitate (see Ultracentrifugation) was blotted in nitrocellulose membrane, which was then blocked with Blocking buffer (TBST - 10 mM Tris, 150 mM NaCl, 0.1% Tween 20- plus 1% w/v BSA) for 24 hours. Incubation with rabbit-polyclonal anti-GFP primary antibody in a 1:10,000 dilution (Invitrogen Cat. Number #A-11122) in Blocking Buffer was carried out for one hour, followed by three washes with TBST. Incubation with anti-Rabbit Secondary Antibody Solution Alk-Phos. Conjugated (Invitrogen™) followed and preceded for one hour. Washing and detection were performed as recommended for Novex® AP Chromogenic Substrate.

3.2.9 Transmission Electron Microscopy

The purified protein was analyzed at the Brazilian Nanotechnology National Laboratory, in a JEOL 3010. The ultracentrifuged and immunoprecipitated samples were analyzed in a FEI Tecnai 12 Transmission Electron Microscope, at the Sir William Dunn School of Pathology of University of Oxford (UK). A 120 kV of acceleration voltage was applied on the samples deposited in a 15 mA discharged copper grid and stained with 2% uranyl acetate. The images were analyzed with ImageJ [*149*].

3.3 Results

3.3.1 Grh1 forms *in vitro* amyloid fibrils under different conditions

One of the main challenges in monitoring the fibrillation of a specific protein inside the cell is to find a suitable experimental method to detect fibril formation under the conditions of interest. Fluorescence Lifetime Imaging (FLIM) is based on the measurement of the time

decay of the fluorescence signal after excitation at a determined wavelength and was the method of choice to first detect the autofluorescence of fibrils.

The formation of amyloid fibrils *in vitro* has been demonstrated for Grh1 [*141*]. In that study, it was shown that Grh1 fibrillates when submitted to either temperatures higher than 37 °C or to changes in the dielectric constant of the medium [*141*]. Those were two parameters intended to mimic Grh1 environment (or changes to it) in the cell, i.e., heat shock response and the presence of the membrane field, respectively. Here we complement that study by demonstrating that Grh1 also fibrillates when in acidic pH (≤ 5.5), a condition that has been shown to happen during starvation. We followed a similar protocol previously used [*150*] based on the autofluorescence of the fibrils detected using FLIM. The fluorescence decay times were also measured and used to distinguish changes in the fibril formation. The results are presented in Supplementary Figure 2 and it is clearly seen that Grh1 indeed form fibrils in all tested conditions. Moreover, the structures formed upon heating or in acidic pH have different fluorescence time decays (the decay is slower in acidic pH), thus suggesting differences in the structure formed and/or in the microenvironment where the fibrils are formed. Therefore, the pH-induced fibrillation *in vitro* reinforces our hypothesis of fibrillation in starvation conditions in yeast.

3.3.2 Grh1 is capable of fibrillating in a cellular environment

After showing that Grh1 can form amyloid fibrils *in vitro* under conditions that correspond to stress scenarios in the cell, the natural step after that was to ask whether Grh1 could also form fibrils within the cell. Hence, following the same expression protocol described elsewhere [*141*], we initially turned to heterologously expressed Grh1 in *E. coli* so as to place Grh1 in a cellular environment. Here, the idea was to perform experiments as if we had exchanged the *in vitro* buffer used before for the *E. coli* cytoplasm.

Figure 19 shows the FLIM results obtained from *E. coli* cells after excitation at 375 nm at room temperature (Figure 19A), at 37°C (Figure 19B-C) and at pH 4.6 (Figure 19D). By using 20 mM sodium acetate in de LB medium as described by Wilks and Slonczewski [*150*], we were able to prevent the bacteria to regulate its internal pH, thus a decrease in LB pH will be translated into a decrease in the pH of the cytoplasm.

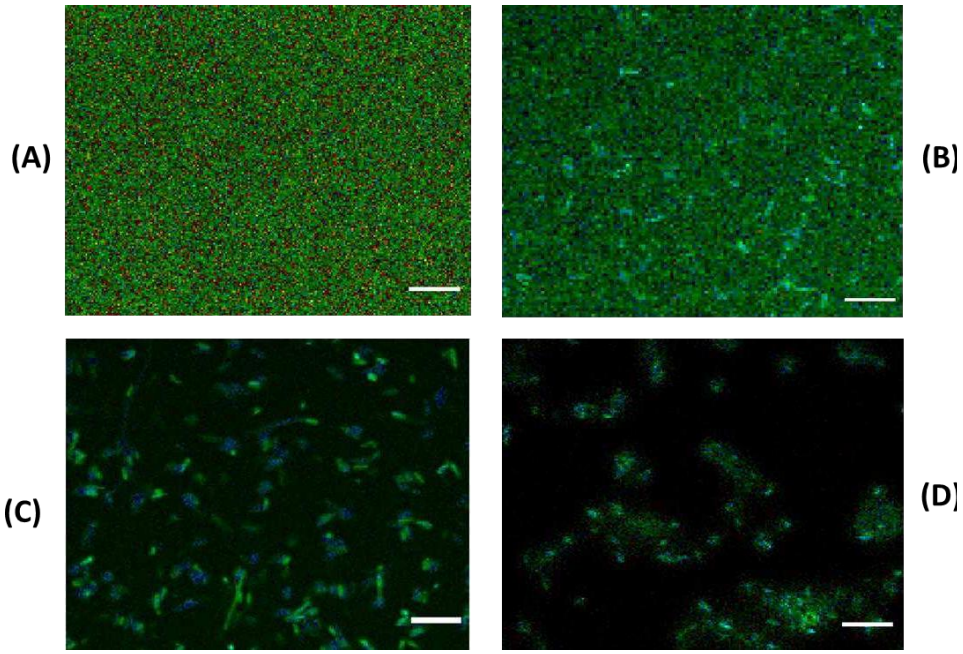

Figure 19: FLIM images of *E. coli* cells excited at 375 nm. The images show *E. coli* cells expressing: (A) Grh1 at room temperature. (B) ACBP in cells heated at 37°C after protein expression. (C) Grh1 in cells heated at 37°C after protein expression. (D) Grh1 in cells in an acidic medium (pH 4.6). Scale bar: 10 µm.

The green background in all images is due to the medium autofluorescence. Rod-like structures, resolved from the background autofluorescence and likely from Grh1, clearly appeared in the cell culture containing Grh1 heated at 37°C or in acidic pH (Figure 19C-D) (coloured in green and blue in Figure 1, where colours refer to lifetime values). We discarded random fibrillation due to protein overexpression by monitoring a negative control (Figure 19B), where the same *E. coli* strain overexpressing the non-amyloidogenic protein acyl-CoA binding protein (ACBP) did not show significant autofluorescence above the background signal. Controls in acidic pH did not show any signal either. Therefore, in the conditions that trigger *in vitro* fibrillation (increased temperature and acidic pH), Grh1 also fibrillates inside *E.coli*.

3.3.3 Fibrillation in yeast under stress

In cell Grh1 fibrillation was also investigated in its native environment in *S. cerevisiae* again via FLIM experiments. It is suggested that fibrillation of Grh1 is related to stress, and conditions previously described to trigger UPS Type III [*140*] and HSR in yeast cells [*148*] were used. Figure 20 shows FLIM images obtained from a yeast strain called Y270, which does not carry any mutations in *grh1* or related genes and is hereafter referred to as Wild-type (WT) yeast. As expected, there is no autofluorescence in the control cells (Figure 20C). Fluorescence is only observed when the cells are either heated at 37 ºC (Figure 2A) or submitted to starvation (Figure 20B), both being conditions known to trigger HSR and UPS Type III [*148*, *140*], respectively.

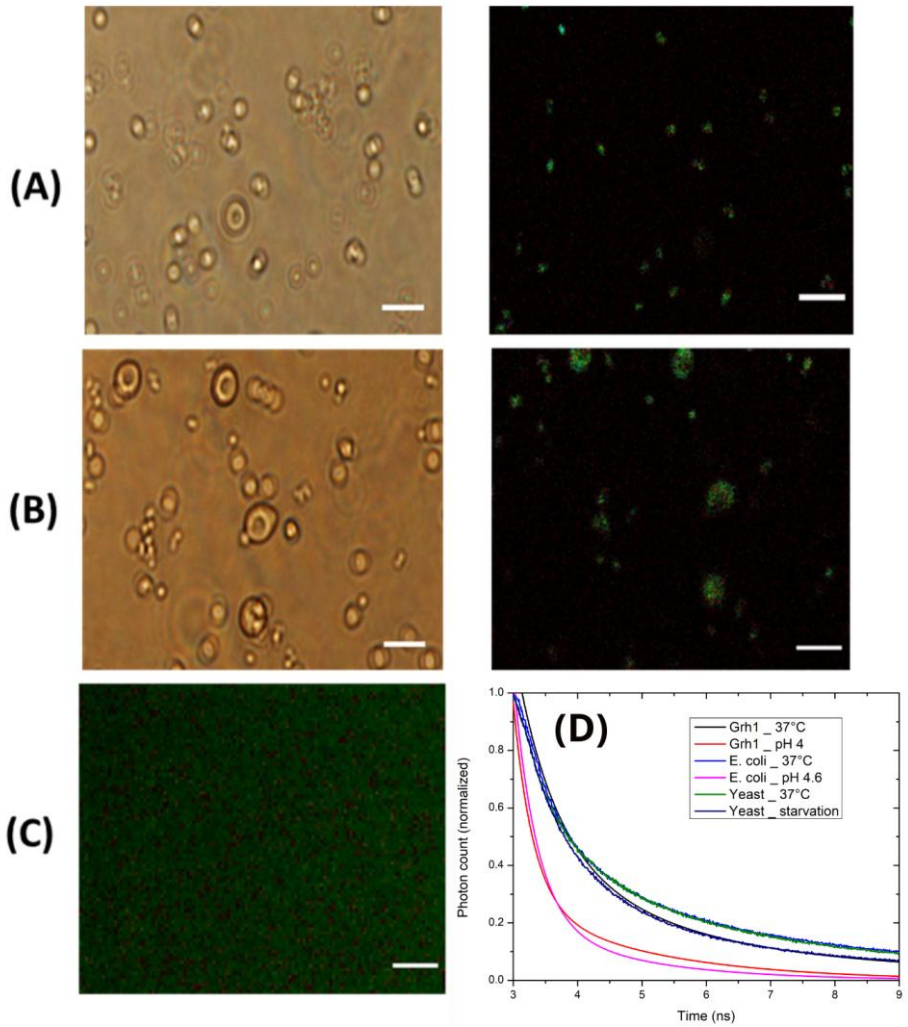

Figure 20: Yeast cell images in the following conditions: (A) heated to 37^{o}C, and (B) under starvation for at least 30 minutes (left: bright field image; right: FLIM image). (C) FLIM image of the control sample. (D) Time decays of fluorescence for purified Grh1 heated at 37°C (black), purified Grh1 in pH 4 (red), *E. coli* at 37°C (light blue), *E. coli* in pH 4.6 (pink), WT yeast at 37°C (green) and starved WT yeast (dark blue). Scale bar: 10 µm.

Time decays of the fluorescence in yeast under either starvation or heated at 37°C were measured, and compared with those from heated *E. coli* overexpressing Grh1 and from *in vitro* experiments. In Figure 20D, the differences between *in cell* time decays of fluorescence are expected, since lifetime depends on the fluorophore environment [*151*]. Comparing the fluorescence decays of the different samples, temperature stress in both cell types (*E. coli* and yeast) led to identical time decays (Figure 20D). This suggests differences in the environment of the fibrils upon temperature increase or during starvation, which is in agreement with the distinct responses of the cell to those stress conditions [*140, 148*].

3.3.4 The lack of Grh1 changes the autofluorescence signal

The results shown in Figure 19 and Figure 20 are indicative of *in cell* fibrillation of Grh1, but it could be argued that the fluorescence exhibited was due to other fibrillation processes taking place inside the cell. To better understand the origin of the observed fibrillation process, similar experiments were carried out, but this time with a Grh1 knockout yeast lineage.

As expected, under physiological conditions, no autofluorescence was observed. In the sample heated to 37°C (Figure 21A), however, there was a change in the pattern of fluorescence. Not only was the signal from Grh1 lost, but also some of the cells appeared as black dots (see red circles in Figure 21A right). Although it was not possible to determine the loss of signal quantitatively from this experiment only, the events occurring in the cell suggest considerable changes took place in HSR when Grh1 was not present.

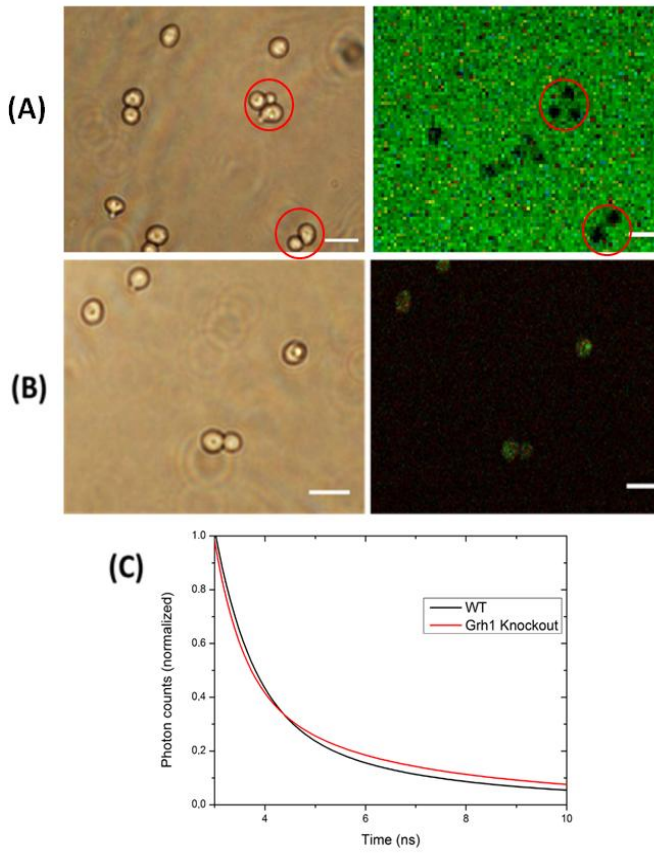

Figure 21: FLIM experiments with excitation at 375 nm of Grh1 knockout cells. (**A)** Heated to 37°C and **(B)** under starvation for at least 30 minutes. Left: bright field image. Right: FLIM image. **(C)** Time decays of fluorescence for WT (black) and Grh1 knockout (red). Scale bar: 10 µm.

In starvation, some autofluorescence in the Grh1-knockout cells (Figure 21B) was observed. To investigate this somewhat unexpected result, we further examined the pattern, in terms of lifetime values (colors in the right panels of Figure 20B and Figure 21B), of fibrillation in both Grh1-containing and knocked-out yeast. In Figure 20B, a heterogeneous signal, containing a broader range of lifetime values (color pattern in the figure) was observed. On the other hand, in Figure 21B, the lifetime is very similar for all events. An explanation for such difference would be that in Figure 20B, other entities, besides Grh1, are also fibrillating in response to starvation. As Grh1 was removed (knockout cells), the color pattern seen in Figure 21B became more uniform because the contributions to fluorescence arising from the fibrils of Grh1 were no longer present. The graph in Supplementary Figure 3 contains the distribution of events for both WT and knockout cells, and evidences the difference between the two groups. The decay of fluorescence in both samples (Figure 21C) was also different (4.8±0.1 and 0.78±0.027 for WT cells; 7.4±0.2 and 2± 0.12 ns for knockout), which confirms the contribution (or the absence of it) of Grh1 to the detected signal.

To further investigate fibrillation in starvation conditions we used a GFP-tagged strain and immunoprecipitated Grh1-GFP in cultures either grown in optimal conditions (control) or starved for 2 hours. The results for the control and test conditions can be seen in Supplementary Figure 4. While there is no signal coming from the control sample (Supplementary Figure 4A), in the immunoprecipitated sample from starved cells (Supplementary Figure 4B) the signal that arises presents a decay that is very similar to that seen from the whole cells in starved conditions (Supplementary Figure 4C). They both have the same slow lifetime (4.8±0.1 ns for the former and 5.0±0.4 ns for the latter). The slightly slower decay might be explained by the reorganization of the fibrils once released from the interior of the matured CUPS.

3.3.5 Grh1 forms higher-order complexes in certain conditions

A different strategy to test the formation of large complexes is size exclusion chromatography (SEC), in which large complexes (in our case, fibrils) are excluded from the separation column. To trace the Grh1 movement, we employed the GFP-tagged Grh1 yeast strain. Yeast cells were cultivated under the desired condition: control, under starvation, or submitted to temperature increase. The whole extract obtained from disrupted yeast cells in each condition was then applied in a SuperDex200 and the proteins tracked via their optical absorbance at 280 and 395 nm for proteins and GFP, respectively. Figure 22A shows the

results of SEC experiments using Grh1-GFP. For clarity, elution profiles were normalized and only the signal at 395 nm is shown. In the control experiment (black line), the signal from GFP appeared around 16 mL of elution. In starved cells (red line), the curve was shifted to the left, indicating that GFP (and consequently Grh1) was then too large to enter the column, being excluded at 9 mL. On the other hand, there were 2 populations in the non-permissive temperature condition (37 °C, blue line): one that was excluded from the column, and another that left the column at the same point as in the control condition. While SEC does not give information about the type of structure formed, it does indicate that, under stress conditions, Grh1 undergoes changes that significantly affect its size.

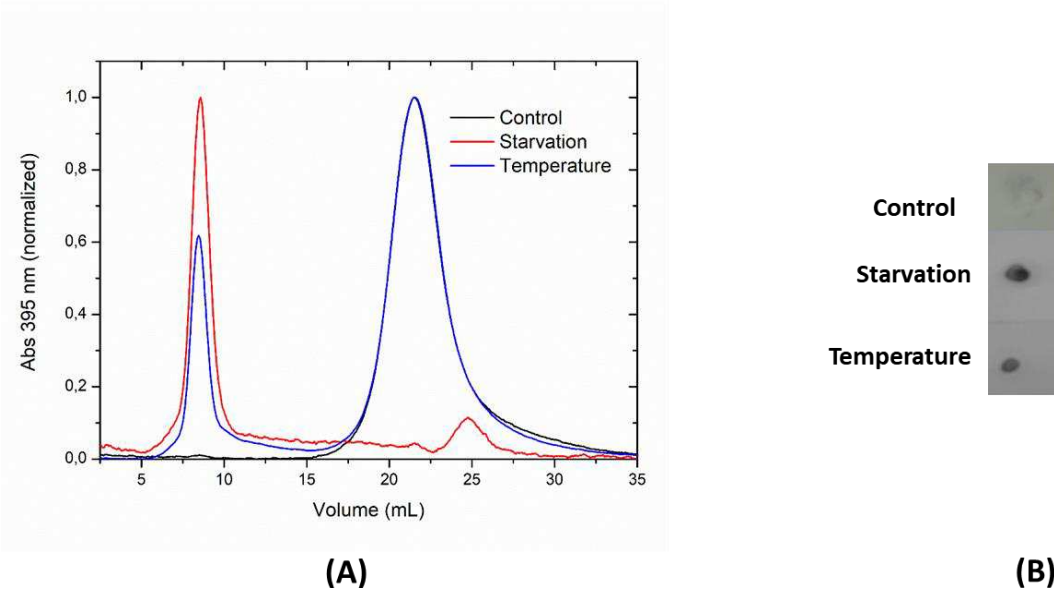

Figure 22: Results of the experiments monitoring the formation of higher-order complexes by using the yeast strain producing a GFP-tagged Grh1. (A) Elution profiles (normalized) of the size exclusion chromatography following the GFP signal (at 395 nm). (B) Dot blot of the pellet obtained from the ultracentrifuged samples. The detection was based on the use of an anti-GFP antibody.

To explore whether the observed size change in Grh1 is due to protein aggregation, ultracentrifugation in SDS was used to differentiate amyloid fibrils from other possible amorphous aggregates of Grh1 [*129*]. We also used the Grh1-GFP strain and performed a dot blot (Figure 22B) to detect the presence of Grh1 in the non-solubilized pellet. Confirming the SEC observations, Grh1-GFP fibrils were present under stress conditions, but not in the control, indicating that Grh1 formed SDS-insensitive large complexes when the yeast cells were submitted to starvation or non-permissive temperature. We can therefore infer that the size increase was not due to amorphous aggregation, but rather to amyloid formation.

3.3.6 Fibrillation reversibility

After incubation in starvation conditions, yeasts are capable of returning to their normal state when physiological conditions are restored [*147*]. In agreement with that, our data show that there was no autofluorescence from the sample that was subjected to starvation for 2 hours and then brought back to normal conditions (Supplementary Figure 5A), suggesting all the fibrillation events indicated by the autofluorescence in starvation conditions were reversible. Therefore, the fibrillation of Grh1 in this context seems to be reversible. Moreover, HSR is capable of sustaining the stress for 2 hours and the cells are able to go back to normal once optimal temperature is restored. Like starved cells, fluorescence from cells subjected to heating at 37°C for 2 hours (heat shock) was no longer seen when the cells were brought back to 30°C (Supplementary Figure 5B).

3.3.7 Visualizing Grh1 fibrils

To visualize the assemblies formed by Grh1 we used transmission electron microscopy and analyzed samples of purified Grh1 heated to 37°C for 30 minutes prior to preparation of the grids (Figure 23A), pellets of samples subjected to ultracentrifugation (Figure 23B) and Grh1-GFP precipitated using a GFP-Trap (Figures Figure **23**C and Figure **23**D). The results can be seen below.

The images of purified Grh1 show a pattern of oligomerization not usually seen for amyloid fibrils, with particles of size in between 15 and 20 nm that are 4 to 7.5 nm thick. Despite their unusual appearance, the amyloid signature has been previously confirmed [*141*]. There is a pattern of organization found on the grids (red circle of Figure 23A, zoomed in on the right), where 4 particles assemble in a rectangular-like shape that was seen in subsequent experiments.

In Figure 23B we have images from grids of pellets of ultracentrifuged content of yeast cells subjected to starvation. We know that in this condition Grh1 is found in the pellet (Figure 22B), and in the control (yeast cells grown in optimal conditions) the type of arrangement found in Figure 23 was not present. Figure 23B shows an arrangement of structures where one can see the resemblance with figure Figure 23A. The figure to the right on panel B represents the same condition but in a cleaner portion of a grid, where one can identify more clearly the arrangement (see red circle). More importantly, the size and thickness of each of the sides is compatible to what was found for purified Grh1 (16 to 21 nm for the former, and 4 to 7.5 nm for the latter).

On panel C, there are images of Grh1-GFP immunoprecipitated using a GFP-Trap, from cells in starvation condition. For this experiment we found more fibril-like assemblies, but it is still possible to distinguish small individual units that make up the whole structure. Two of them are evidenced by red arrows (see regular “breaks” in the fibrillar structure). On the bottom of the image there is another geometrical figure that resembles the previous ones. It can be seen in more detail on the right of panel C (zoomed in image). Each side of this rectangle, as well as the units identified in the figure on the left are 18-22 nm long.

The same can be observed on panel D, where we show an image of immunoprecipitated Grh1-GFP from cells subjected to heat shock. The small units identified on the previous image can be seen for this condition (see red arrows), and the organizational pattern is also found and one (inside the red circle) is highlighted on the right. Measuring the width and thickness of the particles, we have the same values found for the starvation condition.

Even though we cannot be sure that the structures observed in the grids of the ultracentrifugation experiments are Grh1, the sizes and pattern of organization strongly suggest so. These data corroborate the previous findings of the formation of higher order assemblies in stress conditions by Grh1, and might help explain its role in UPS and HSR.

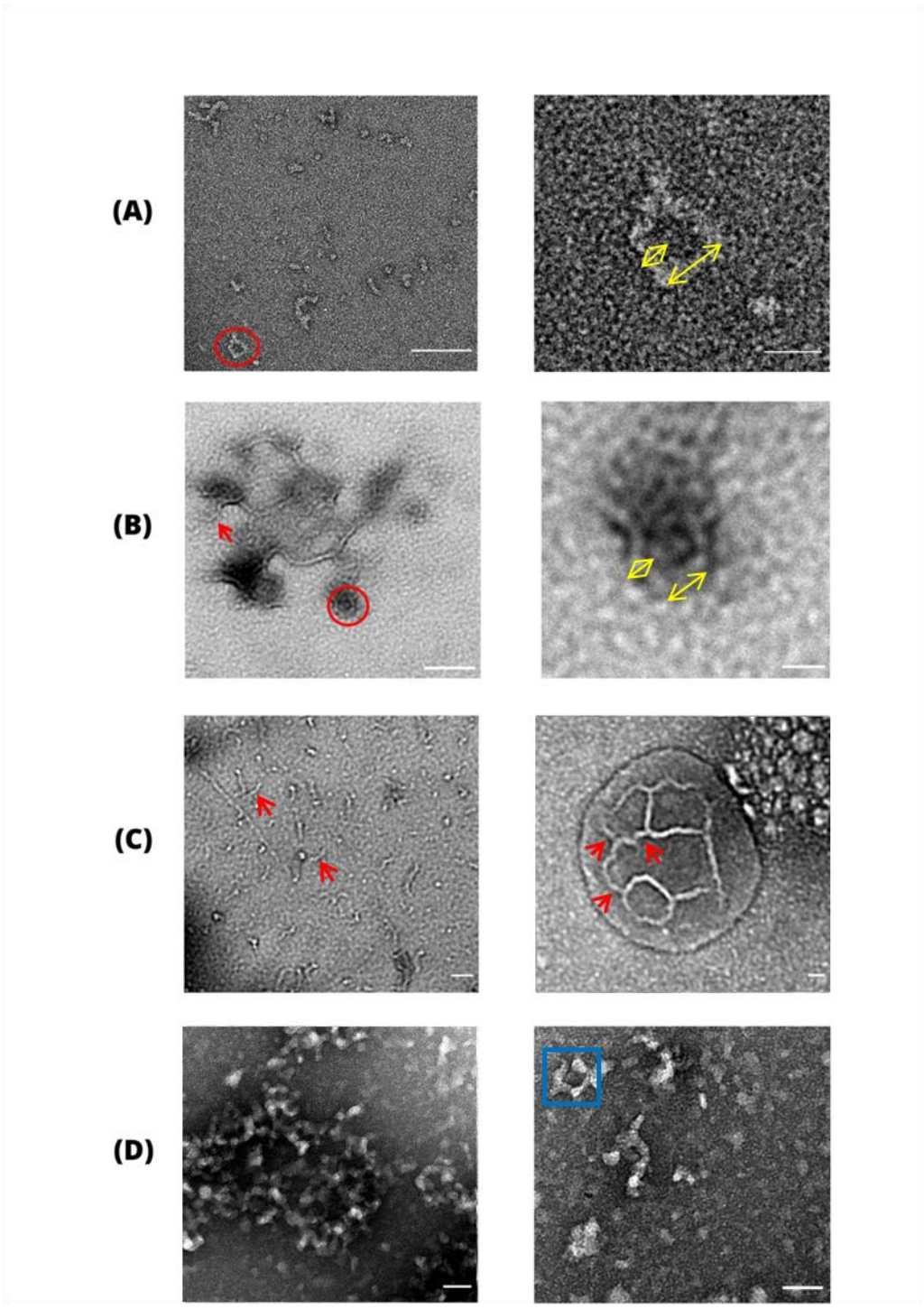

Figure 23: TEM images of: (A) purified Grh1 heated at 37^{o}C. (B) Grh1-GFP immunoprecipitated from yeast cells in heat shock. Right panels are zoomed-in images of the red circle seen on the left panels. Yellow double arrows indicate measured dimensions of particles. (C) Grh1-GFP immunoprecipitated from yeast cells in starvation. Red arrows indicate units of fibrils. (D) Pellets of ultracentrifuged yeast cells in starvation. Blue square highlights the structures found on the grids. Scale bar: (A), (B), (C) left panels:100 nm. (A), (B), (C) right panels, (D): 20 nm.

3.4 Discussions and Conclusions

Amyloid formation inside cells has been a subject of significant interest over the years. It has gained even more attention lately since various aggregation-prone proteins, whose potential formation of amyloid-like structures is not disease-related, have been described [[3]]. Nevertheless, detecting amyloid-like fibrils *in vivo* remains a challenge. Several reports have successfully probed aggregation within cells[4] by using chimeras of the target protein tagged with fluorescent reporters. In the case of aggregation-prone proteins, the foci formed inside the cells can, in principle, be visualized under the fluorescence microscope.[4] Despite the usefulness of this latter approach, in the specific case of Grh1, compartmentalization of the protein either in CUPS (in the case of starvation) or likely in stress granules during HSR can lead to the formation of 1 to 3 punctate structures, therefore hampering the direct identification of potential fibrils.

Grh1 fibrillation has been demonstrated *in vitro*[5] and we further expanded the list of triggering factors of that process to now include acidic environments (Figure S2). However, its occurrence within the cell and its potential implications were still unclear. Fibrils and changes in the cytoplasmic state are seemingly tools used by the cell to cope with different types of stress.[2, 6, 7] Our initial hypothesis was then that fibrils of Grh1 could form *in vivo* and would be necessary under specific conditions. The test of our idea was mainly based on the use of a label-free assay, firstly described by Pinotsi *et al.* in 2013.[8] Such a method for detecting amyloid fibrils relies on the intrinsic fluorescence in the UV-visible region that arises when the protein changes conformation and adopts the characteristic β-sheet rich structure of amyloids. Chan *et al.* [9] further described this fluorescence signature and how unlikely it would be for an experiment based solely on fibril autofluorescence to be used *in vivo* due to the competing autofluorescence from the cells. It was not a surprise, then, those publications using FLIM and intrinsic fluorescence that followed were based on either FRET experiments or changes in a reporter's physicochemical parameter when fibrillation happened.[10, 11]

Therefore, although *in vivo* FLIM of proteins without a reporter may not always be possible, we could show this can be a valuable approach for yeast cells. We specifically tested Grh1 *in vivo* fibrillation due to starvation (Type III trigger – Figures 2B and 3B) or to temperature increase (HSR trigger – Figure 2A), two stress scenarios where Grh1 seems to play a central role. During starvation, Grh1 leaves the Golgi membrane and relocalizes to be part of CUPS.[12] Upon heat shock, although there is hitherto no study describing the direct participation of Grh1, its increased expression when the yeast is subjected to thermal stress has been reported.[13] In control conditions, the autofluorescence signal arising from the cells was negligible when excited at 375 nm (Figure 2C).

Our data showed that the autofluorescence could be used to monitor the formation of the fibrils themselves (presence or absence – Figures 1, 2, and 3) and differences in the environment surrounding them induced by the distinct stress sources (Figure 2D). More specifically, the

alterations in pH, temperature, and starvation yielded distinguishable lifetime decays, therefore strongly suggesting that the fibrils are in different environments, which agrees with the idea of distinct cell responses and the corresponding Grh1 function in each case. It is interesting to note that the temperature stress in both cell types (*E. coli* and yeast) led to identical time decays, which indicates that the cell's HSR involves the formation of the fibrils in somewhat similar environments.

To further infer the participation of Grh1 fibrillation in each stress condition, we obtained FLIM and time decay data from a Grh1-knockout yeast strain under heat shock and starvation (Figure 3). The images from the heat-shocked knockout cells, unlike the images of the heat-shocked Grh1-containing cells (Figure 2C), surprisingly showed the cells as black dots, which indicates the lack of Grh1 led the cells to a different type of response to HS. As previously said, currently, no studies link Grh1 to the HSR. Still, some of the data available and our results reinforce the hypotheses of fibrillation of Grh1 in the context of HS. Gasch *et al.*[13], through microarray DNA experiments, measured the changes in transcript levels over time in response to several types of stress, including temperature. For Grh1, what they observed was an increase in transcription when the cell was subjected to heat shock (37°C).[13] Considering a stress situation where the cell stops its non-essential activities to save as much energy as possible, an increase in Grh1 transcription suggests a protein function in that scenario. Besides that, when the Grh1-GFP cell is subjected to a non-permissive temperature (37°C), the signal from GFP, which was initially more dispersed, coalesced into foci inside the cell, thus becoming brighter spots than before (Figure S6). As described by Alberti, Halfmann, and Lindquist,[4] proteins that fibrillate *in vivo* coalesce into microscopic assemblies, just like the ones we observed for Grh1.

On the other hand, the knockout cells showed a distinct response to starvation compared to HS. In this case, FLIM signals could be detected (Figure 3B), thus suggesting fibrillation of other proteins in the cell, described before for the protein Cdc19.[34] Despite the existence of this non-Grh1-related signal, we could find differences in the time decays (Figure 3C) and their distributions (Figure S2) measured from WT and knockout cells. Furthermore, sedimentation experiments and a modified version of the filter retardation assay (in the form of an SEC experiment)[4] were used to corroborate our FLIM data by showing that Grh1 was present in the fibrils formed within the yeast cells. To do so, we used a yeast strain expressing Grh1 tagged with GFP to allow for the immunoprecipitation of the Grh1-GFP chimera. The fibrils of Grh1-GFP were then detected using FLIM (Figure S3B) and compared with the data obtained for the whole yeast cell (Figure 2B). The pattern observed in those images and the similar lifetimes measured in both experiments (Figure S3C) allowed us to infer that the *in-cell* fibrillation was indeed due to Grh1.

To enhance our understanding of the fibril morphology, we used transmission electron microscopy to visualize the structures formed by Grh1. The TEM images from purified Grh1,

immunoprecipitated Grh1-GFP from cells in heat shock and starvation, and ultracentrifuged WT cells in starvation (Figure 5) all showed similar patterns where one can see the coexistence of fibril-like and square-like structures. The experiments here reported did not allow for atomic-resolution structural determination of Grh1-containing assemblies. Nevertheless, it was possible to distinguish short linear units in some images, whose dimensions are ca. 20 nm long and 6 nm thick. They are apparently linked to form the fibril itself and other more complex arrangements. Bruns *et al.* [14] showed that, upon starvation, Grh1 concentrates in large membraneous punctae in the cell to form the so-called compartment for unconventional protein secretion (CUPS). Despite the thorough description of the biogenesis of this new compartment, its detailed structure and composition were still not clear. Curwin *et al.* [15], in an elegant combination of correlative light and electron microscopy (CLEM) and fluorescence, advanced the knowledge on that issue by reporting CUPS were arranged in a somewhat spherical structure of convoluted tubules and vesicles, whose average diameter was ca. 200 nm. In the same paper, the authors proposed a pathway for CUPS formation that would consist of the segregation of Grh1 in tubular clusters, followed by the engulfment of this immature CUPS by a sheet-like structure called saccule. The exact origin of the saccule membrane was not determined, but Grh1-containing membranes were suggested as one possibility. Our TEM data (Figure 5) offer another possibility: the Grh1 higher-order structural arrangements. The GRASP's ability to form fibrillar structures, Grh1 among them, has been demonstrated.[5] In the Grh1 case, combining individual somewhat linear units seems to give rise to distinct 3D structures, such as the fibrils and the square-like seen in Figures 5B-C. Furthermore, in the right panel of Figure 5C, an even more complex arrangement involving an apparent network of tubules, whose rough average diameter was around 150 nm, can be seen. The dimensions of the chains formed by the units reported here are compatible with the images showing the different stages of CUPS maturation described by Curwin *et al.* [15] as the saccule. We could speculate that the 3D-sheet of unknown origin engulfing the immature CUPS and even the Grh1-containing vesicles described by Curwin *et al.* could be formed by Grh1 higher-order structures rather than their monomers. The reversibility of Grh1 fibril formation (Figure S4) is also compatible with a mechanism that needs to be turned on and off depending on the conditions triggering the cell stress.

Our data do not rule out the participation of secretory and endosomal membranes, but Grh1 structural plasticity and its ability to form complex arrangements seem to be a new piece of information that needs to be added as an alternative in the formation of compartments for UPS as well as for heat shock response. Furthermore, the capacity of Golgi-related proteins to undergo liquid-liquid phase separation (LLPS) has been recently demonstrated[16], which raises another exciting possibility regarding whether GRASP could also undergo such transition, a feature yet to be determined. LLPS as the source of membrane-less compartments has gained particular interest over the last few years[17,] and it might well be another aspect to consider when

tackling the problem of UPS and HSR.

In summary, here, we present solid evidence of *in vivo* formation of Grh1 fibrils under stress conditions. While the details on how exactly they function in both Type III UPS and HSR are yet to be fully revealed, our data reinforce the new concept of functional fibrils in yeasts as active factors in response to certain types of stress. As any first-time idea appearing in the literature, our findings seem to bring more questions than answers. Still, they undoubtedly offer new perspectives to better understand amyloids in vivo and Grh1 roles in UPS and HSR.

4 Liquid-liquid phase separation of Grh1

We showed in the previous chapters that Grh1 presents an IDP behavior and is also able to form amyloid-like fibrils both *in vitro* and *in vivo*. Based on the usual involvement of IDP and fibrils in liquid-liquid phase separation and also due to the observation that Golgins do indeed phase separate [*64*,*65*], we were rationally led to ask the question whether Grh1 could also undergo phase separation. Therefore, in this chapter, we present the initial results obtained when we tried to move one step forward in the issue regarding Grh1 supramolecular structures.

4.1 Materials and Methods

4.1.1 Turbidity measurements

For turbidity measurements, the absorbance at 600 nm of 30 µM of Grh1 in the appropriate buffer was measured in a Multiskan Go (Thermo Scientific) microplate reader.

4.1.2 Brightfield, fluorescence and DIC experiments

Microscopy experiments were performed in an IX71 inverted microscope (Olympus). The protein concentration was fixed at 30 µM. For fluorescence experiments the ThT concentration was 15 mM and a U-MWB2 mirror unit, with excitation BP460/490 used. 10µL of solution was placed onto a glass slide, covered with a coverslip and taken to the microscope. Images were analyzed using the software ImageJ [*149*].

4.2 Results

4.2.1 Bioinformatics

Before planning experiments in the laboratory regarding phase separation of Grh1, we decided to use bioinformatics tools to check whether or not our ideas were promising. There are some servers currently available that take into account, among others, information about intrinsic disorder propensity and the existence of low complexity domains within a protein sequence to predict that protein is capable of phase separating. The result for one of such predictors, PScore [*153*] (available at

http://abragam.med.utoronto.ca/~JFKlab/Software/psp.htm), is represented in Figure 24. PScore is based on the expected number of long-range, planar sp2 pi-pi contacts [*153*]. Planar pi-pi interactions are more prevalent in protein regions that lack secondary structure and are more accessible to the solvent [*153*], being relevant for intrinsic disorder and, therefore, another way to look for regions more prone to phase separation.

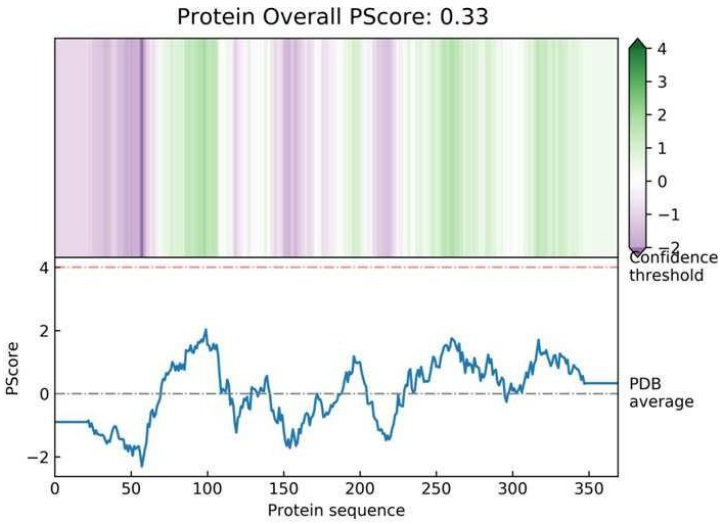

Figure 24: Results of the predictor PScore using the Grh1 sequence. The upper panel shows the colored regions in which the score is higher than the PDB average in green, and the ones with a lower score are colored in purple. The lower panel sows the actual scores represented in the upper panel. Figure prepared by the author.

The protein overall PScore is 0.33, which puts it as a protein predicted to be able to phase separate. As expected, the SPR domain that we know to be highly disordered is predicted to phase separate in its entirety. But there are two other regions, one in PDZ1 (around residues 70-100) and one in PDZ2 (a smaller region comprising residues 185-200), that could be involved in LLPS as well. Given our observations of disorder within the GRASP domain [*141*] that is not a surprising finding.

Predictors such as PScore are considered first-generation prediction tools [*154*]. They are based on specific protein features assumed as the driving force for LLPS. Recently, another predictor became available for the community, called PSPredictor [*155*] (available at http://bio-comp.ucas.ac.cn/llpsdb). This is considered a second-generation predictor, given the fact that it uses machine learning to improve its results. In the PSPredictor scale, Grh1 has a score of 0.8511, therefore being predicted to phase separate.

4.2.2 Turbidity Assays

One of the standard methods for detecting phase separation, although not being very specific, is the assessment of the medium turbidity [*156*]. When a protein undergoes phase separation and assembles into droplets, it increases the turbidity of the solution. The tests can be performed by eye just checking if, visually, the solution becomes turbid or by measuring the absorbance of the solution at 600 nm.

LLPS is mediated by factors that affect multivalent interactions, such as pH, temperature, protein and salt concentration [*72*]. As a first and explorative step, we sought to examine the effect some of these factors would have on the turbidity of the solution in the presence of Grh1. A graph with these results can be seen in Figure 25.

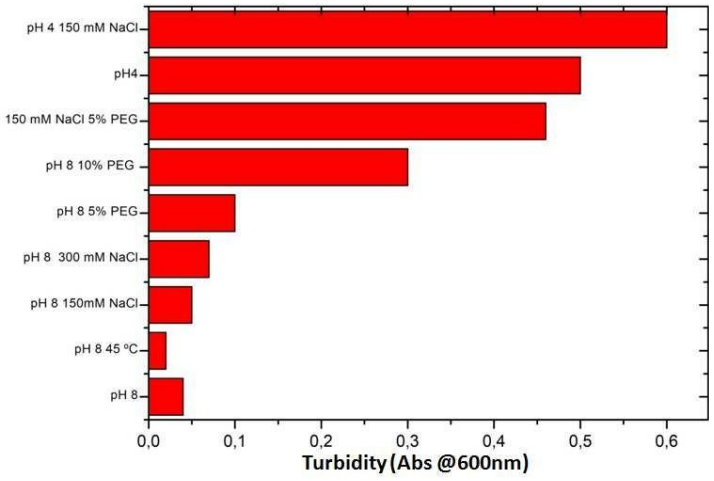

Figure 25: Results of turbidity measurements of Grh1 in different solutions. Turbidity was measured as the optical absorption at 600 nm. Figure prepared by the author.

As one can see in Figure 25, it seems that a low pH and concentrations of polyethylene glycol (PEG) above 5% would be good candidates for conditions triggering LLPS of Grh1. Solutions containing 5% of PEG and high concentrations of salt (150 and 300 mM NaCl) had little effect separately, but were effective in boosting each other effects (see 150 mM NaCl, 5% PEG condition). PEG is used as a macromolecular crowding agent with the aim to approximate the protein in solution to concentrations experienced in the native environment. The phenomenon of molecular crowding affects the properties of molecules because it reduces the volume of solvent available, thus making the effective concentration of molecules higher in the solution [*157*].

Since different concentrations of PEG had such different effects, we performed a series of measurements with different concentrations of this molecular crowding agent. The results can be seen below in Figure 26, which shows that PEG only begins to affect turbidity of the solution at a concentration of 4%, and even so the change is very subtle. Larger changes occur only with a concentration of 6% or higher.

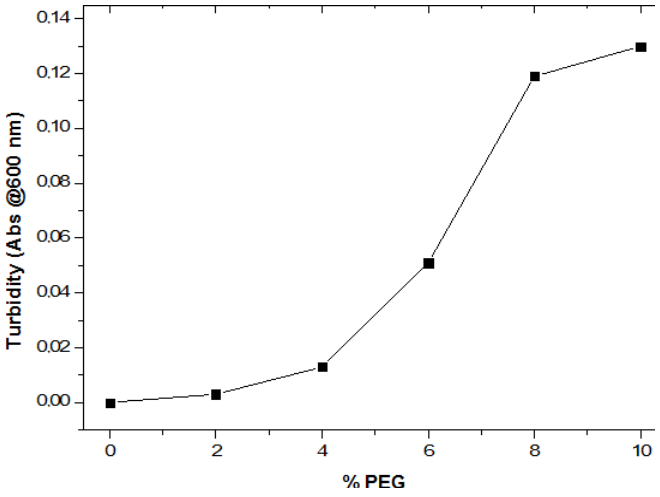

Figure 26: Results of turbidity measurements for Grh1 in solution with various PEG concentrations. Figure prepared by the author.

4.2.3 Microscopy studies

Based on the turbidity results, we decided to take some of the samples in conditions seen to augment turbidity to the microscope and check whether we could detect the characteristic droplet formation of LLPS. The results are represented in the images of Figure 27.

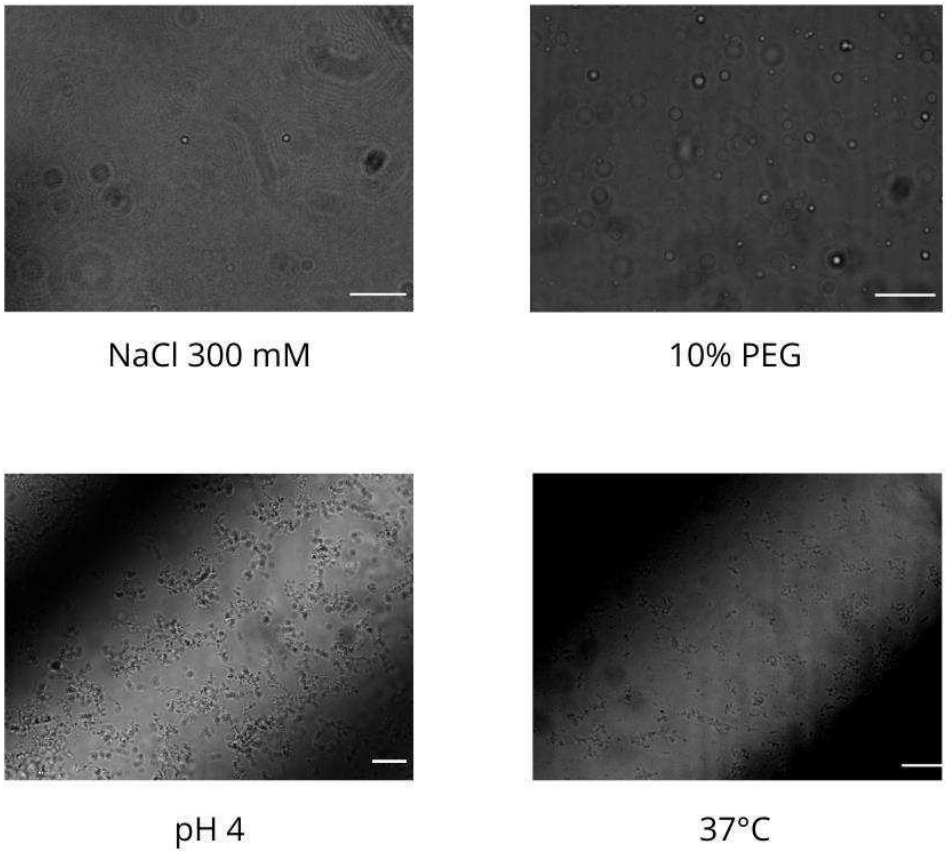

Figure 27: Micrographs of solutions of Grh1 at 30 µM in different conditions. Images of conditions NaCl 300 mM and 10% PEG were acquired in 100x magnification, brightfield. Images of conditions pH4 and 37°C were acquired in 60x magnification, DIC. Scale bar: 20 µm. Figure prepared by the author.

As suggested by the turbidity measurements (Figure 25), the presence of a high concentration of salt (300 mM NaCl) led to the formation of only a few droplets in the solution. The presence of 10% PEG, however, triggered the formation of many of them. Interestingly, low pH (pH 4) and high temperature (37°C) led to the formation of different structures that we hypothesized to be the result of a liquid-to-solid transition. It is necessary to study further these conditions to be able to say what is really happening in the process, but one explanation could be that the amyloid formation triggered by the LLPS (both temperature and low pH are conditions for Grh1 fibrillation; see Chapter 2) can be driving the transition further into another phase. This type of liquid phase separation followed by a liquid-solid transition has been reported before for the FUS protein, for which the liquid droplets convert with time into an aggregated aberrant state, in a liquid-to-solid phase transition [*158*].

We also performed initial experiments mixing the different conditions, and obtained intriguing results. As one can see in Figure 26, 2% PEG had no effect on the solution turbidity. In fact, when this condition was investigated on the microscope, there were no droplets formed at all. However, 2% PEG in the solution at pH 4 prevented the formation of

the gel/solid-like structures shown in Figure 27. Instead, the field was filled with droplets, suggesting the formation of a separated liquid phase (Figure 28).

One of the criteria, besides the spherical shape, normally used to confirm that LLPS actually occurred is the observation that these droplets are permeable. Being a liquid assembly, proteins and other molecules must be able to come in and out of the droplet in a dynamic manner. We used this condition (pH 4, 2% PEG) that we found to trigger the formation of such droplets to evaluate if a dye (ThT) was able to diffuse to the interior of them. The results are presented in Figure 28.

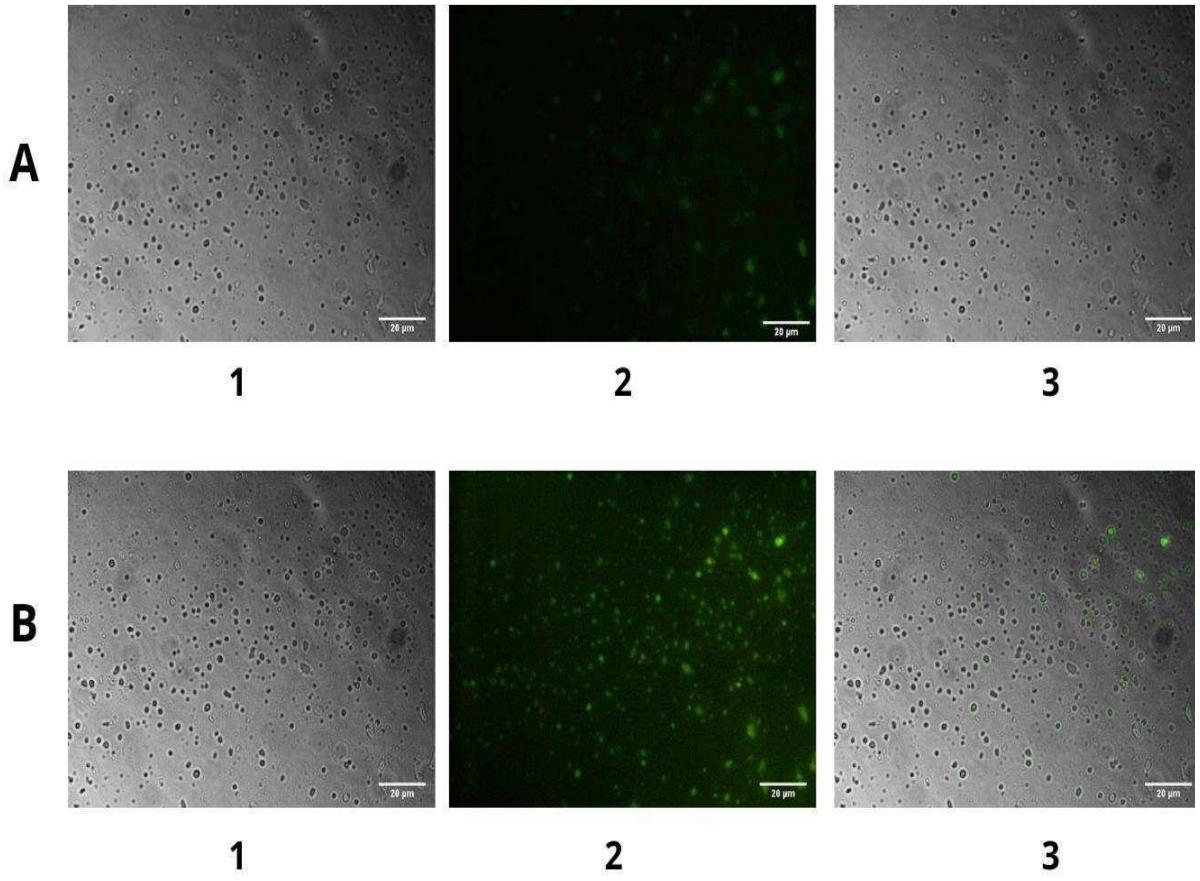

Figure 28: LLPS studies of Grh1 in pH 4 and 2% PEG. A and B represent the same sample at time 0 **(A)** and after 20 min **(B)** 1: Brightfield images. 2: ThT fluorescence images. 3: Merge. Scale bar: 20 µm. Figure prepared by the author.

In Figure 28, we show the data on monitoring the formation of droplets as function of time by measuring two different moments (0 and 20 min) of the same field of view with the same exposure. It is clear the increase in the fluorescence of ThT from the beginning of the

experiment (Figure 28A-2) to 20 minutes later (Figure 28B-2). The positions of the fluorescent spots coincide with the positions of the droplets visualized in panels 1 of Figure 28 (merged in panels 3), thus showing that ThT localizes within the droplets. At first the signal from ThT is very weak, therefore the merged image (panel 3 on Figure 28A), has a fainted green colour.

Another characteristic of liquid droplets is their ability to undergo fusion (coalescence). We followed several droplets for many minutes and were able to capture in good detail only one coalescence event. Figure 29 shows a series of frames when a small droplet fuses with another. More attempts will be necessary in order to make any statistical assumptions regarding fusion events. But these initial results along with what was shown in the previous figures are very encouraging.

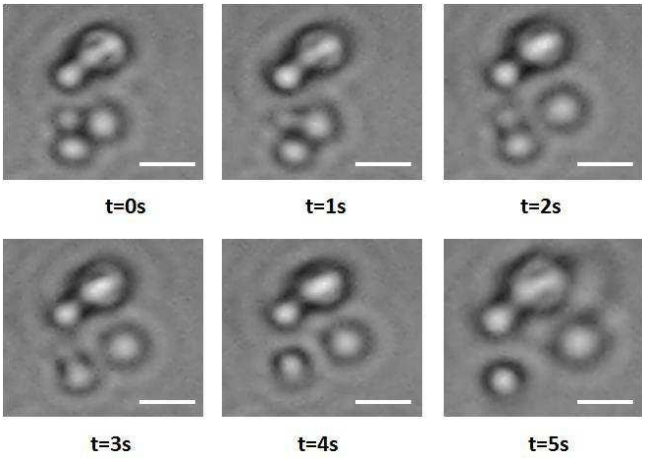

Figure 29: Time series showing the fusion event of Grh1 droplets in pH 4 and 2% PEG. The top droplet in each panel was used as a reference. Scale bar: 5 µm. Figure prepared by the author.

4.2.4 Conclusion

Phase separation became a popular theme in Biology very recently, and the discovery of LLPS by Golgins [*41*,*65*] led to the hypothesis of the Golgi being a phase separated organelle [*66*]. Given the close relationship between intrinsic disorder and phase separation it was natural to associate GRASPs with this idea.

We were able to show here the characteristic formation of droplets in conditions that were described before for proteins that undergo LLPS [*78*,*159*] (Figure 27). They have around 3 µm in diameter, although more experiments are necessary to do actual statistical measurements. They are permissive to the surrounding medium (Figure 28), and capable of fusion (Figure 29), other criteria that must be met for LLPS [*156*].

It is interesting to note that the low pH seen to induce LLPS also triggers Grh1 fibrillation (see Chapter 2). There are reports of phase separation inducing and/or accelerating fibrillation of proteins, such as TDP-43 [*160*]. The increase in fluorescence inside the droplets within time, seen in Figure 28, could be an indication of Grh1 fibrillating and then accumulating ThT (ThT is considered a marker for fibrillation, since it binds somewhat specifically to the cavities of fibrils [*115*]). Although we cannot make assumptions at this point, this result is another indication that we have a promising case of study in our hands. Furthermore, when the yeast cell faces starvation there is a drop in pH [*161*], which highlights the relevance of evaluating such condition.

It will be interesting, also, to see how other conditions are affected by the presence of PEG and other components such as salt. The idea is to gradually increase the level of complexity of the medium as we understand the factors separately. Due to time constraints, the experiments discussed here are rather simple and exploratory. They are, nevertheless, very promising.

5 Grh1 Golgin partner: Bug1

This chapter is dedicated to describe the initial experiments with Grh1 Golgin partner, Bug1, performed in collaboration with the undergraduate student Ariane Duarte Rosse, and therefore it presents a somewhat less traditional organization. We tried to describe all the attempts made so as to have a logbook of them that will be of further use for those who come afterward.

5.1 Materials and Methods

5.1.1 Bioinformatics Tools

5.1.1.1 Disorder prediction

Prediction of disordered regions was performed using the Database of Disordered Protein Predictions (D2P2, http://d2p2.pro/) [162]. The predictors used were: Espritz-D [163], Espritz-X [163], Espritz-N [163], IUPred-L [164], IUPred-S [164], PV2 [165], PrDOS [166], VSL2b [167], VLXT [168].

5.1.1.2 Coiled-coil prediction

For the prediction of coiled-coil regions in Bug1 sequence we used the Waggawagga server (https://waggawagga.motorprotein.de/) [*169*]. The coiled-coil tools applied were Marcoil, Multicoil, Multicoil2, Ncoils, Paircoil and Paircoil2. Window size was set at 21.

5.1.2 Protein expression and purification

The pet28 plasmid containing the gene encoding Bug1 (~150 ng) was transformed into 25 uL of BL21[DE3] Rosetta thermo-competent cells. The transformation process consisted of 20 minutes of incubation of the cells with DNA on ice, followed by heat shock (42 ºC for 45 seconds) and other 2 minutes on ice. The cells were then incubated with 900 µL of LB medium for 50 minutes at 37 °C under agitation at 200 rpm. Incubation was followed by centrifugation at 14 krpm for 30 seconds. The supernatant was removed and the cells

were resuspended in the remaining liquid, that was spread on plates containing LB medium with 1.5% w/v agar, and 40 µg/mL of Kanamycin for selection of the plasmid, and 34 µg/mL of Chloramphenicol for selection of the bacterial strain (these concentrations will also be used for expression of the protein). The cells were left growing in the plates for 16 hours at 37 ºC.

For expression, one colony of Rosetta containing the plasmid was incubated in 10 mL of LB with added Kanamycin and Chloramphenicol at 37 °C and 200 rpm for 16 hours. After this time, this pre-culture was added to 1 L of LB medium with antibiotics, and left for growing for about 3 hours, until the optical density (O.D., absorbance at 600 nm) was 0.8 – 1. When the O.D. was achieved, 0.5 mM of IPTG was added and the temperature in the shaker lowered to 20 °C. Expression was carried out for 18 hours.

After expression the cells were collected by centrifugation at 8,000 g for 5 minutes. The pellet was resuspended in working buffer (300mM NaCl. 40 mM HEPES, 10% Glycerol and 0.5 mM β-mercaptoethanol) and the cells were lysed by sonication. The insoluble material was resuspended in working buffer plus 2 M of urea and left in the freezer at -80 °C for 30 minutes. It was then thawed and subjected to sonication and centrifugation again. This time the soluble fraction was collected and loaded in 2 mL of equilibrated Ni-NTA superflow column (QIAGEN). The loaded column was submitted to gentle agitation at 4° C for 20 minutes, eluted, washed 2 times with working buffer and once with working buffer plus 20 mM imidazole. The protein was eluted in working buffer plus 300 mM imidazole. To cleave the His-Tag, purified Tev protease was added to the solution and the reaction occured for at least 3 hours. The buffer was washed off imidazole by dialysis against working buffer, and the solution was again loaded in nickel column, the protein being collected this time in the flow through. This fraction was concentrated and the remaining contaminants were removed by size exclusion chromatography on a Superdex 200 10/300 GL gel filtration column (GE Healthcare Life Sciences). The protein was concentrated by centrifugation in a Sorvall RC 6 plus centrifuge (Thermo Scientific), using an Amicon Ultra Centrifugal Filter with a NMWL of 30 kDa (Merk Millipore).

5.1.3 Circular Dichroism

Far-UV (190–260 nm) CD experiments were carried out in a Jasco J-815 CD Spectrometer (JASCO Corporation, Japan), using a quartz cell with a path length of 1 mm. Bug1 was in 10 mM sodium phosphate buffer, pH 8.0 and at final concentration of 5 µM. All far-UV CD spectra were recorded with a scan speed of 50 nm/min and at time response of 1

s. Chemical stability experiments were performed in the same buffer and increasing urea concentration (0–8.0 M). The spectra were averaged, baseline-corrected and smoothed with a Savitsky-Golay filter using CDTools software [*93*].

5.1.4 Steady-State Fluorescence

Intrinsic and extrinsic fluorescence were monitored using a Hitachi F-7000 fluorimeter equipped with a 150 W xenon arc lamp. The excitation and emission monochromators were set at 2.5 nm slit width in all experiments. The protein concentration was 5 µM for Bug1 in 40 mM Hepes, 300 mM NaCl, 10% glycerol. For tryptophan fluorescence experiments, the selective tryptophan excitation wavelength was set at 295 nm and the emission spectrum was monitored from 300 to 400 nm. The fluorescence of tryptophan across chemical denaturation was measured in increasing concentrations of urea (0–8 M).

5.1.5 Differential Scanning Calorimetry

DSC experiments were done in a Nano-DSC II from Calorimetry Sciences Corporation, CSC (Lindon, Utah, USA). Protein solutions at concentrations of 100 µM were kept under vacuum for 10 min before usage and scans were recorded from 15-95°C at an average heating rate of 0.25 °C/minute and 3 atm pressure.

5.2 Results

5.2.1 Bioinformatics

Golgins are known for having regions of intrinsic disorder [*170*], so we decided to first use online servers that evaluate protein primary sequences to generate predictions of disorder for Bug1. The results can be seen Figure 30. The N-terminal of Bug1 is predicted to be entirely disordered (Figure 30A) by all servers, while the C-terminal bears some scarcely distributed disordered regions. Taking together the data from those predictors and considering disordered the regions for which at least 75% of them agree, we obtain the result in Figure 30B. Only three small regions in the C-terminal are predicted to be disordered. That agrees with what has been described for other proteins in the family: Golgins take advantage

of rigid (i.e. fully structured) membrane-bound regions (the C-terminal) and also of flexible segments (the coiled-coil N-terminal) to perform their tethering functions [*170*].

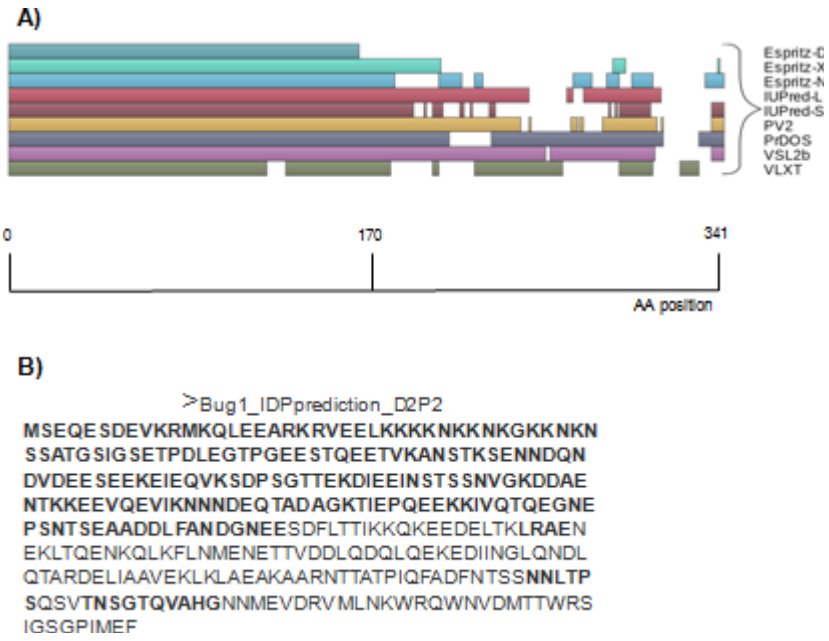

Figure 30: (A) Prediction of intrinsic disorder for Bug1. The nine colored bars represent the location of intrinsically disordered regions (IDPs) as predicted by the different servers. **(B)** The highlighted portions of Bug1 sequence represent regions where there is 75% agreement between all predictors. All data is available at: http://d2p2.pro/. Figure prepared by the author.

Like disorder predictors, there are servers available online that predict the organization of proteins into coiled-coil structures. Coiled-coils are defined as segments of α-helices with many topologies that result from an arrangement of “knobs-into-holes” packing, with seven amino acids forming the basis, where the first and fourth ones are hydrophobic residues [*171*]. These motifs direct the folding of the helices that will generally be buried in the structure to hide their hydrophobic side from the solvent [*172*]. Waggawagga is a comparative tool available online that allows for the visualization of prediction of coiled-coil regions by different servers [*169*]. We ran Bug1 sequence through the website and obtained similar results with all predictors. One of them is depicted in Figure 31 below. All servers agree with a region of coiled-coil structure comprising residues 190-280. The coiled-coil segment, then, would be neither in the region predicted to be highly disordered nor in the rigid membrane-bound C-terminal either.

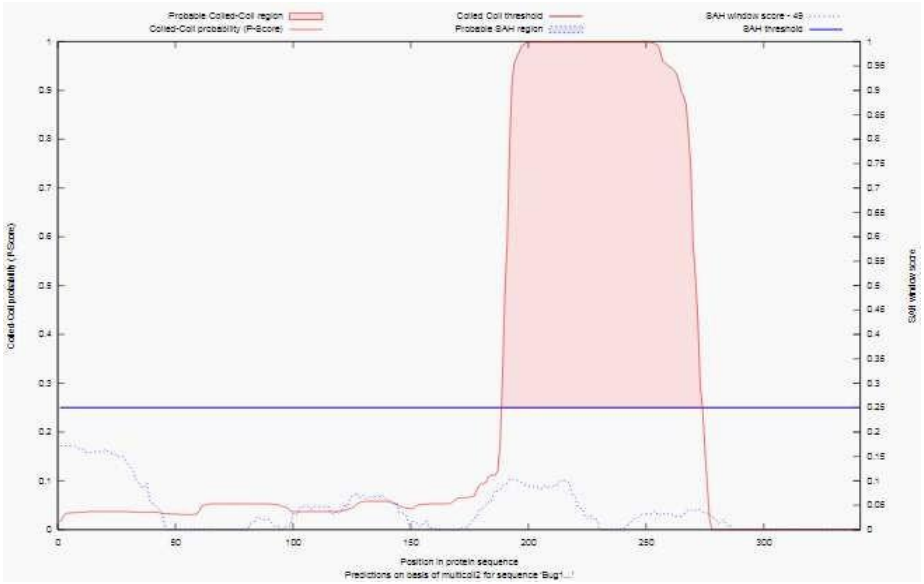

Figure 31: Prediction of coiled-coil formation by Bug1 sequence. On the right there is the score for single α-helice domains (SAH), represented in the graph by the dotted blue line. Figure prepared by the author.

5.2.2 Expression and purification

5.2.2.1 An unconventional protocol is able to purify Bug1

Our group has made several attempts to obtain purified Bug1. The presence of the SUMO tag in the C-terminus of the protein proved to be inefficient, leading to a high degree of proteolysis. We then decided to try working with the protein in pet28 with a TEV protease cleavage site in its N-terminus. That led to another problem, commonly faced by people trying to purify proteins and that often makes it impossible to obtain the target: the expression of the protein in the insoluble fraction of inclusion bodies. The most common strategy adopted in this situation consists in solubilising of such bodies, followed by refolding of the solubilized protein [*173*]. The solubilisation is often done by chaotropic agents, such as urea, in very high concentrations (>8 M) or using detergents such as sarkosyl. Although good in getting the job done, these approaches often lead to aggregation of the protein during the refolding step. Furthermore, they require extensive steps of purification and sometimes result in a low yield of the recombinant protein [*173*].

By using a mild-denaturation protocol, a version of the one described by Singh et al [*173*] with changes in incubation time (see Methods), we were able to obtain Bug1 pure and in high quantities (Figure 32).

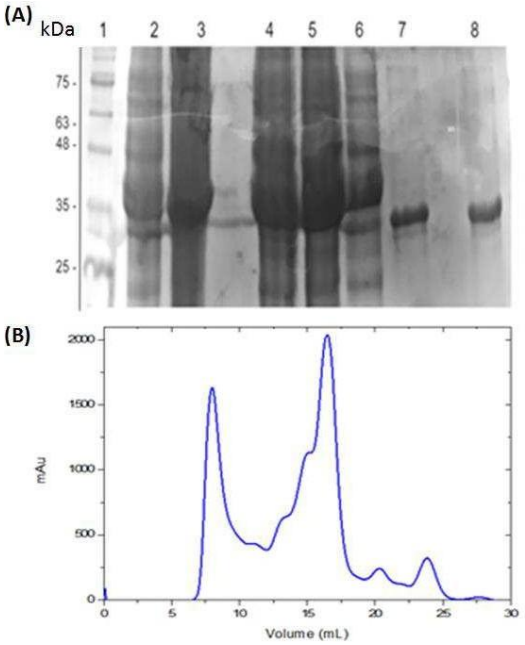

Figure 32: Results of: **(A)** Bug1 purification seen in an SDS-PAGE: (1) Ladder, (2) Soluble fraction, (3) Insoluble fraction, (4) Soluble fraction post-freezing, (5) Eluate, (6) Washing, (7) Fraction of 300 mM Imidazole and post-cleavage, (8) Size exclusion chromatography (fraction of 16 mL). **(B)** Size exclusion chromatography of Bug1. The first peak represents the void of the column. Figure prepared by the author.

5.2.3 Structural Behaviour in solution

The protocol described in the previous section allowed the production of Bug1 protein in adequate quantity and purity for the biophysical studies. We then used Circular Dichroism (CD) to verify the integrity of the Bug1 protein produced according to the protocol described above and, consequently, the success of the refolding. The CD spectrum of Bug1 in aqueous solution has negative bands around 208 nm and 222 nm and a positive band near 196 nm (Figure 33), which are typically seen in the CD spectrum of proteins with an α-helical structure [*174*]. Furthermore, the ratio of molar ellipticity $[\Theta]_{222}/[\Theta]_{208} = 1.18$, suggests the presence of a coiled-coil structure [*174*]. This is another confirmation of Bug1 as a member of the family of Golgins.

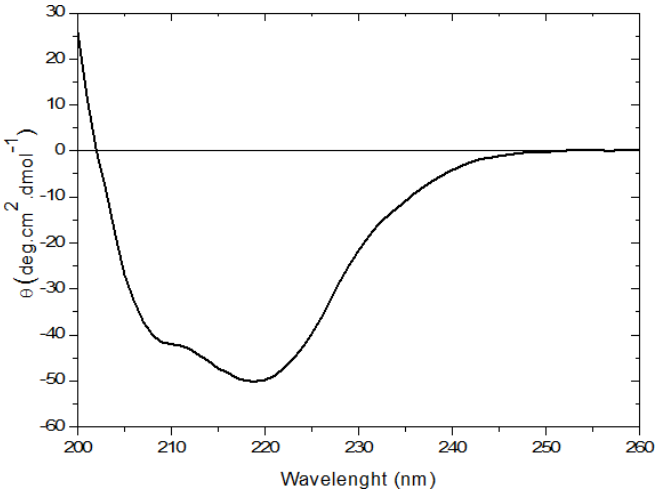

Figure 33: Far-UV CD spectrum of Bug1. The $[\Theta]_{222}/[\Theta]_{208}$ ratio of 1.18 confirms the coiled-coil nature of the structure. Figure prepared by the author.

To further explore the biophysical characteristics of Bug1, we evaluated how the secondary structure changes in denaturing conditions. To do that, we used increasing concentrations of urea in the circular dichroism experiments. The changes in ellipticity at 222 nm were used to monitor the degree of denaturation of Bug1, as the denatured fraction (F_d, calculated as $(\theta - \theta_{0M}) / (\theta_{8M} - \theta_{0M})$). The results are presented in Figure 34. The results show that Bug1 follows a very cooperative transition between folded and unfolded states, with a mid-point at around 2 M of urea. This cooperative behavior is indicative of a well-structured protein, opposite to what we thought initially based on the disorder prediction (Figure 30).

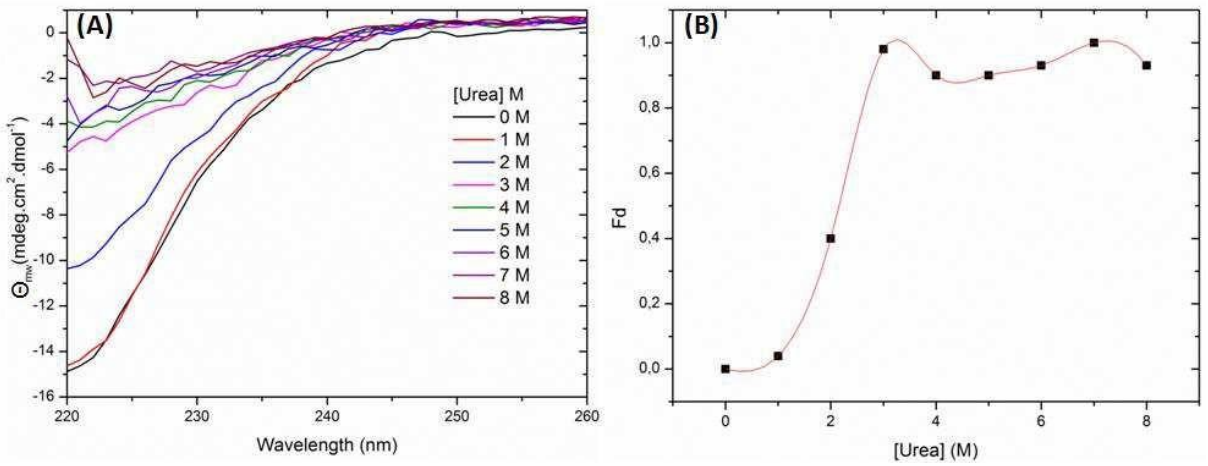

Figure 34: (A) Bug1 far-UV CD spectra in different urea concentrations. **(B)** Denatured fraction (F_d) of Bug1 upon increasing urea concentrations. The ellipticity at 222 nm was used to estimate F_d. In B, the line is a guide for the eyes only. Figure prepared by the author.

We also used the intrinsic fluorescence of tryptophan present in Bug1 to monitor its chemical stability. When free in solution tryptophan fluorescence has a maximum around 350 nm. The residues buried in a hydrophobic core have a shift to a maximum wavelength of emission around 320 nm. This blue-shift is due to the change in polarity of the medium [*175*]. It is noteworthy that while in the CD we were looking at the whole protein, in the intrinsic fluorescence experiments we are looking at the areas close to the tryptophan residues. The tryptophan is a local-probe, so it will give information about its vicinity.

Bug1 has 3 tryptophan residues, which are located in the C-terminus of the protein. Figure 35 shows that when Bug1 is in its native state the tryptophans have an emission maximum at 345 nm, suggesting that they are more exposed to the solvent. Following the fluorescence during chemical denaturation showed that upon increasing urea concentration the maximum was shifted to 356 nm and that the urea concentration of mid-transition in this case was 3 M (Figure 35B).

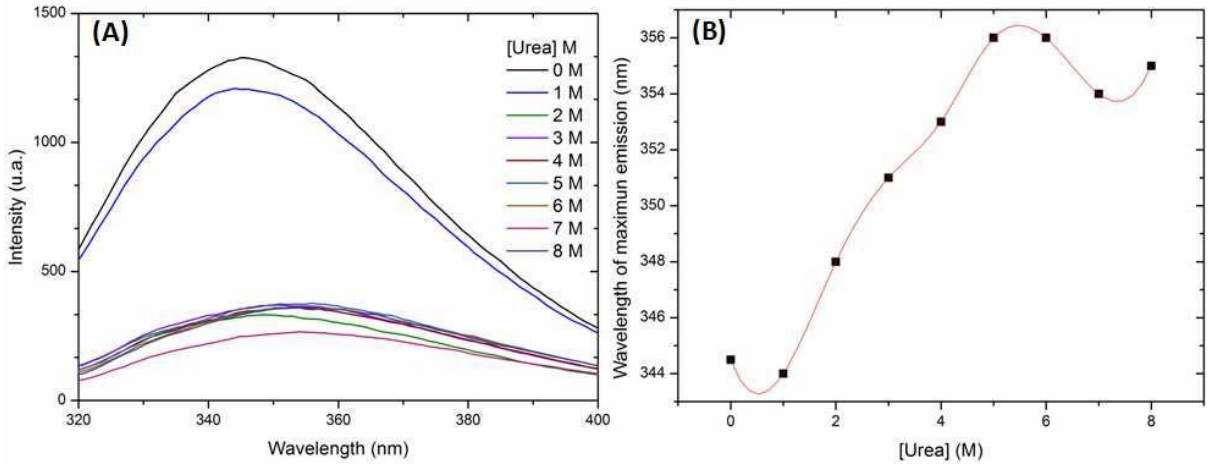

Figure 35: Chemical denaturation of Bug1 monitored via steady-state fluorescence. **(A)** Tryptophan fluorescence profile in different urea concentrations. **(B)** Wavelength of maximum emission of the tryptophan versus urea concentration (M). In B, the line is a guide for the eyes only. Figure prepared by the author.

If we compare the denaturation curves in Figure 34B and Figure 35B we can see that the transition monitored by the local probes (tryptophans) presents a lower cooperativity when compared with the one that represents the global denaturation of the protein (Figure 34B). However, the concentration needed to reach the mid-point of transition is higher when we are looking only to the tryptophans (Figure 35B): 2 M for the former and 3 M for the latter. That suggests the region where the tryptophans have higher stability (being necessary more urea to perturb it), yet maintaining accessibility to the solvent (wavelength of maximum emission without urea = 345 nm). Besides, the lower cooperativity indicates that this region

loses structure when unfolding in a less orchestrated manner when in comparison with the whole protein, suggesting more flexibility.

To further characterize the product of our expression/purification protocols, we then moved to study the thermal stability of Bug1. In this case, we made use of Differential Scanning Calorimetry (DSC) and the respective thermogram is shown in Figure 36. One can readily see that the unfolding peak indicates a transition without any intermediate states occurring around 55ºC.

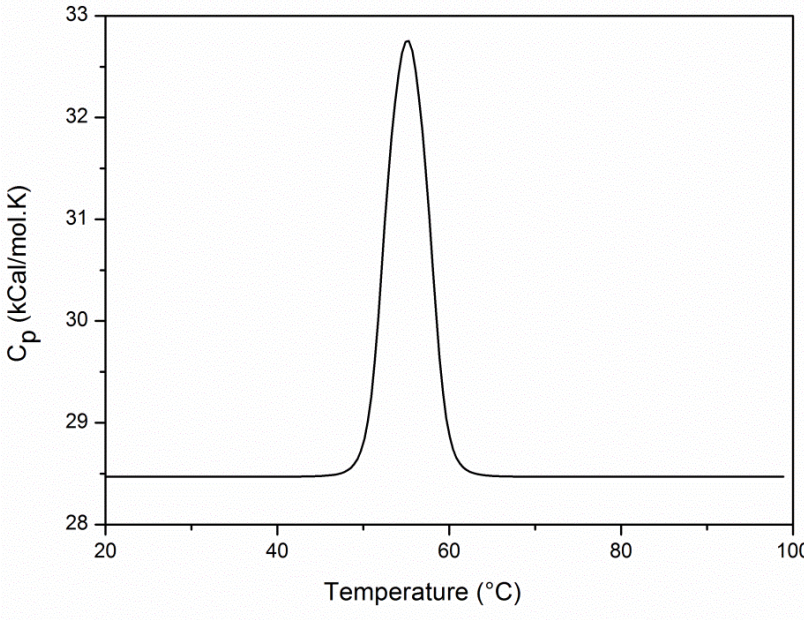

Figure 36: Thermal unfolding of Bug1 monitored by DSC and showing a T_m of 55 °C. Figure prepared by the author.

5.3 Conclusion

The purification of Bug1 was successful when using a mild denaturation protocol. Several attempts had been made before using traditional refolding methods, but they were ineffective in removing Bug1 from inclusion bodies (experiments not shown in this thesis because they were not performed by nor with the aid of the author).

The experiments shown here are only a small part of a biophysical characterization, and much more is necessary to paint a more complete picture of the structure of Bug1. What they can tell us is that Bug1 follows the basic organization of Golgins, having part of its structure folded as a coiled-coil (predicted by different servers and presented in Figure 31 and evidenced by the CD spectrum shown in Figure 33).

Even though the protein is predicted to be highly disordered (see Figure 30), the transition from folded to unfolded state is very cooperative (Figure 34), what suggests a high degree of order in the structure. We will need more data to explain the apparent contradiction of the C-terminal being more flexible and having a less cooperative transition in the unfolding experiments than the protein as a whole (see Figure 34 and Figure 35). It is also important to note that we plan to carry out experiments using more points in between concentrations from 0 to 4M of urea to be able to trace the transitions in more detail.

Having Bug1 in our group opens new possibilities to study protein-protein and protein-membrane interactions and can help broaden our knowledge on protein secretion. Furthermore, in the light of the recent reports regarding Golgins and LLPS [*64*], the biophysical characterization of Bug1 is the first step for other exciting discoveries.

6 The exquisite structural biophysics of the Golgi Reassembly and Stacking Proteins

Abstract

Golgi Reassembly and Stacking Proteins (GRASPs) were firstly described as crucial elements in determining the structure of the Golgi complex. However, data have been accumulating over the years showing GRASPs can participate in various cell processes beyond the Golgi maintenance, including cell adhesion and migration, autophagy and unconventional secretion of proteins. A comprehensive understanding of the GRASP functions requires deep mechanistic knowledge of its structure and dynamics, especially because of the unique structural plasticity observed for many members of this family coupled with their high promiscuity in mediating protein-protein interactions. Here, we critically review data regarding the structural biophysics of GRASPs in the quest for understanding the structural determinants of different functionalities. We dissect GRASP structure starting with the full-length protein down to its separate domains (PDZ1, PDZ2 and SPR) and outline some structural features common to all members of the GRASP family (such as the presence of many intrinsically disordered regions). Although the impact of those exquisite properties *in vivo* will still require further studies, it is possible, from our review, to pinpoint factors that must be considered in future interpretation of data regarding GRASP functions, thus bringing somewhat new perspectives to the field.

Based on the manuscript published in the International Journal of Biological Macromolecules, in 2020.

Mendes LFS*, Fontana NA*, Reddy ST*, Uversky VN, Costa-Filho AJ. The exquisite structural biophysics of the Golgi Reassembly and Stacking Proteins. Int J Biol Macromol. 2020 Dec 1;164:3632-3644

* These authors contributed equally to this work.

DOI: 10.1016/j.ijbiomac.2020.08.203

6.1 Introduction

6.1.1 The Golgi apparatus

The Golgi apparatus is a complex organelle with a “manufacturing” functionality (i.e., a center for modifying, sorting, and packing of proteins and lipids for secretion), besides acting as the major delivery system in all eukaryotic cells. Especially because of its relatively large size in Plantae and Metazoa, the Golgi apparatus was one of the first organelles to be discovered, awork of Camillo Golgi. In the late 1960s, the pivotal role of the Golgi apparatus in secretion was thoroughly established by George Palade and co-workers, who tracked secretory proteins as they proceeded from the endoplasmic reticulum (ER) to the Golgi [*176*]. After that, with the development of GFP-tagging technology in the early 1990s [*177*], it became evident that the Golgi apparatus is a highly dynamic organelle [*178*]. Furthermore, in a recent commentary note, Nobel laureate James E. Rothman suggested the possibility that the Golgins (large rod-like Golgi proteins that form a coiled-coil over most of its length), although still functioning in a limiting way as tethers to capture cognate vesicles, would have a far more fundamental role in the Golgi apparatus organization [*66*]. In his view, the Golgi could exist not as a flattened membrane sandwich but as a liquid-crystal formed by the phase separation of cytosol-derived proteins with Golgi membranes [*66*]. Recent data showing that several Golgins undergo liquid-liquid phase separation [*64*,*65*] are a step forward in understanding the role of phase separation in Golgi structure and also bring attention to the exquisite properties of Golgi-related proteins.

Apart from newly suggested aspects, it has been established that the Golgi apparatus is a central membrane-bound organelle located in the perinuclear region of the cell, where it plays a crucial role in intracellular trafficking, sorting, and modification of proteins and lipids. To properly execute their function, the flattened cisternae need to be correctly packed into individual stacks, which are then laterally connected to form a compact ribbon structure in Metazoans [*179*]. Recent efforts to unravel the mechanisms of Golgi structure formation have targeted the Golgimatrix proteins, including the Golgi Reassembly and Stacking Proteins, Golgins, Rabs, and other GTPases, as well as actin and microtubule cytoskeletons. Despite having their individual specific functions, the Golgi structural proteins act together to hold the proper structure of the organelle [*180*].

6.1.2 Structure and function of the Golgi Reassembly and Stacking Proteins

Golgi Reassembly and Stacking Proteins (GRASPs) constitute a family of peripheral membrane-associated proteins first identified as an essential factor in Golgi cisternae reassembly after mitotic times [reviewed in references [*181*,*182*]. The genome of the Metazoans encodes two GRASP proteins, called GRASP55 and GRASP65 [reviewed in reference [*27*]. The discovery of GRASP65 came after the observation that the sulphydryl modifying reagent N-ethylmaleimide (NEM) affected the rebuilding of stacked cisternae in a cell-free system [*17*]. GRASP65 is one of the main targets of NEM and, together with its Golgin partner GM130, was one of the first structural factors observed in Golgi reassembly and stacking [*17*]. In the seminal work of Barr et al., it was shown that GRASP65was doubly anchored to the cell membrane: first through a myristoylation of its glycine-2 and second via the direct interaction with GM130 [*17*]. Later, again using a cell-free-based system, it was shown that GRASP55 is also a component of the Golgi stackin gmachinery [[*18*], reviewed in [*183*]]. Using biochemical assays, Short et al. found that GRASP55 had a specific Golgin partner, called Golgin45 [*184*], and could be both myristoylated and palmitoylated in vivo [*185*]. GRASP55 is preferentially located in the medial/trans-Golgi through the binding with Golgin45 [*184*], even though its interaction with GM130 was also observed using a yeast two-hybrid system [*18*].

Although GRASP55 and GRASP65 were originally assigned as main components of the Golgi reassembly machinery, subsequent single and double knockout models of these members of GRASP family led to controversial conclusions. Mammalian cell models silenced for the genes coding the pair GRASP55/GRASP65 or GRASP55 and GRASP65 separately, either by siRNA depletion [*186*], microinjection of antibodies against GRASP55/65 [*18*,*15*], inactivation by Killer-red [*187*] or through CRISPR-Cas9 [*188*], showed Golgi ribbon unlinking and/or Golgi stacking failure phenotypes. However, GRASP65 [LacZ] knocked-in mouse by homologous recombination [*189*] and mouse knocked-out of GRASP55 [*58*] showed no obvious developmental or growth defects, along with an insignificant Golgi disturbance. Furthermore, Golgi organization was not affected in cells with double gorasp1/gorasp2 gene depletion when both Golgin45 and GM130 were overexpressed [*180*]. Therefore, mammalian GRASPs did not seem to be essential for cell viability, and the loss of the individual GRASPs did not show significant effects on the stacking of Golgi cisternae. Up to that point, the role of GRASPs in cisternal stacking was still not clear. To finally rest the case on the participation of GRASP in the Golgi structure, Grond et al., in a very recent publication, generated a mouse in which both GRASPs were knocked out [*19*]. It is clear from the electron micrograph images that the Golgi cisternae remained stacked, but were laterally disconnected from each

other and showed a significant decrease in the cross-sectional diameters [*19*]. These data finally lead to the conclusion that the “Golgi Reassembly and Stacking Proteins”, although members of the Golgi matrix and with a role in its organization, are not involved in the stacking of the Golgi cisternae.

Mammalian GRASPs do not show direct involvement in the classical secretory pathway, even though they could act as chaperonins [*190*] and also play an indirect role in the correct protein glycosylation within the Golgi [*191*]. On the other hand, an increasing number of reports has implicated GRASPs as pivotal participants in unconventional protein secretion (UPS) [reviewed in great detail in reference [*44*]].More specifically, GRASPs were shown to be involved in UPS of type III (for soluble proteins through autophagosome-like vesicles) and type IV (membrane proteins bypassing the Golgi but still addressed to the early steps of the conventional secretory pathway) [*44*]. The involvement of GRASP in type III UPS was firstly observed by Kinseth et al. [*21*]. In this seminal work, it was shown that, upon silencing of the GRASP gene in D. discoideum, a deficiency in the secretion of acyl-CoA binding protein (ACBP) was perceived under cellular stress, which resulted in sporulation defects and ACBP accumulation inside the cell [*21*]. GRASP participation in type III UPS was later observed also in Cryptococcus neoformans [*51*] and in S. cerevisiae. Cabral et al. described the presence of a vesicular intermediate important for ACBP secretion [*192*] and Bruns et al. showed that type III UPS in yeast uses a new cellular compartment, which was called CUPS (Compartment for Unconventional Protein Secretion) [*54*]. Recently, new discoveries have been made on the components of CUPS [*57*], and, although much remains unknown, it is now established that CUPS somehow contains GRASP, which leaves the Golgi and relocates to the cytoplasm, when cells are subjected to starvation [*21*]. However, even within the type III UPS, GRASP was shown to play somewhat “different” roles depending on the molecule to be secreted. For example, unlike the ACBP case, recent studies revealed that GRASP55 and the “unfolded protein response” control Interleukin-1β aggregation and its unconventional secretion [*58*].

The involvement of GRASPs in type IV UPS has been shown in two illustrative cases: secretion of the Cystic fibrosis transmembrane conductance regulator (CFTR) and α-integrins. The CFTR is a transmembrane protein belonging to the ‘C’ branch of the ABC transporter superfamily, but unlike other members of this family, it works as an anion channel that permits the diffusion of anions such as Cl− and HCO3 − [reviewed in reference [*193*]]. A common deletion of the phenylalanine 508 (ΔF508 CFTR) leads to defects in both its ER exit and its cell surface expression, promoting the so-called cystic fibrosis [*194*]. Gee et al. showed that, upon ER stress, the ΔF508 CFTR can exit the ER in a GRASP55-dependent

type IV UPS pathway, rescuing the healthy phenotype [*195*]. Another example is the secretion of α-integrins (αPS1 and αPS2) in Drosophila. αPS1 is normally addressed to the plasma membrane via classical secretion. However, during some stages of Drosophila development, αPS1 can bypass the Golgi and be secreted via the GRASP-dependent type IV UPS pathway [*196*]. A similar situation was also observed for αPS2 [*30*]. Interestingly, in all those cases, the activation of the GRASP-dependent type IV UPS passed through the reallocation of GRASP to the ER exit-sites [reviewed in references [*44*,*197*]].

How exactly GRASPs act in UPS is still unclear. Although in some cases there is a direct interaction with the cargo protein, in others, no evidence of such interactions was observed [*197*,*44*]. UPS pathways are triggered by various cellular stresses, with nutrient starvation being one of the most common [*44*]. GRASP55 was discovered to be de-OGlcNAcylated upon energy deprivation and to regulate autophagosome maturation [*198*]. GRASP55 can also be phosphorylated by PKCα in response to an increase in the intracellular Ca+2 concentration, modulating Golgi structure and function [*199*]. These observations suggest that GRASPs could act as a nutrient sensor for stress detection, but this is something that needs to be demonstrated.

In the context of their involvement in many different cell functionalities, GRASPs were shown to be very promiscuous in mediating protein-protein interactions, a property that will be discussed in more detail below. Figure 37 illustrates the remarkable binding promiscuity of human GRASPs by presenting their corresponding protein-protein interaction (PPI) networks generated by Search Tool for the Retrieval of Interacting Genes (STRING, http://string-db.org/, accessed in 2020) [*200*] using the medium confidence level of 0.4. In the GRASP65-centered network (Figure 37A), there are 200 nodes (proteins) involved in 5636 interactions. Since the expected number of interactions among proteins in a similarly sized set of proteins randomly selected from human proteome is equal to 581, this PPI network has significantly more interactions than expected. Results of the analogous analysis of the GRASP55 interactivity are shown in Figure 37B. This network includes 96 proteins linked by 807 edges. Therefore, both human GRASPs can be considered as important hub proteins involved in numerous interactions. The vast number of functionalities associated with GRASPs and also their role as hubs in the cell interactome lead to a common and reasonable question: how can apparently “not-so-complex” proteins be so promiscuous when it comes to the number of interactions and cell functionalities? In this review, the exquisite molecular biophysics of GRASPs is discussed, in particular, how the promiscuity in cell functionalities correlates with their structural plasticity.

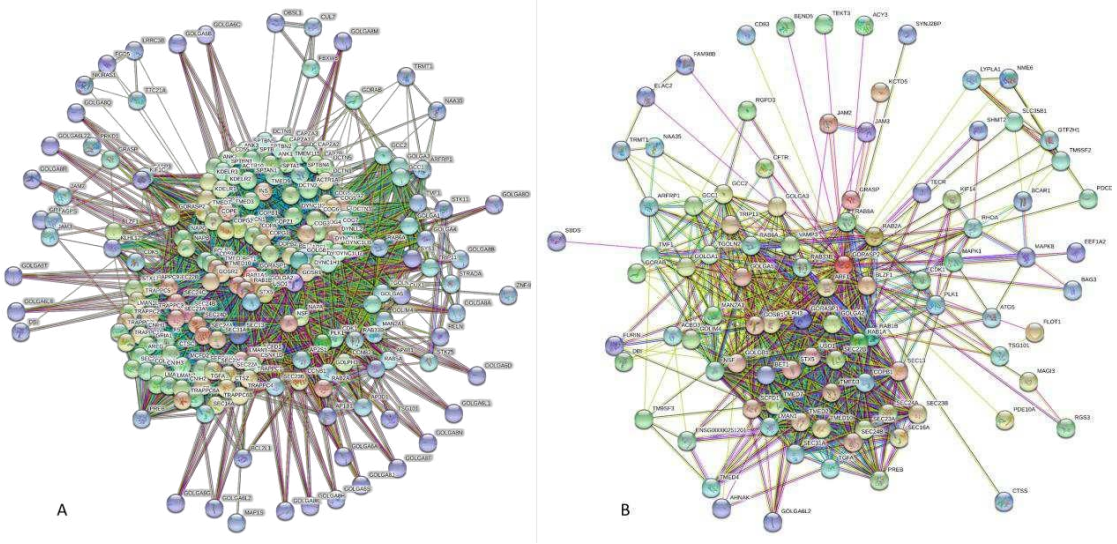

Figure 37: Analysis of the interactome of human GRASP65 (**A**) and GRASP55 (**B**) conducted by Search Tool for the Retrieval of Interacting Genes (STRING, http://string-db.org/, accessed in 2020) that generates a network of predicted associations based on predicted and experimentally-validated information on the interaction partners of a protein of interest [*200*]. In the corresponding network, the nodes correspond to proteins, whereas the edges show predicted or known functional associations. Seven types of evidence are used to build the corresponding network, where they are indicated by the differently coloured lines: a green line represents neighbourhood evidence; a red line - the presence of fusion evidence; a purple line - experimental evidence; a blue line – co-occurrence evidence; a light blue line - database evidence; a yellow line – text mining evidence; and a black line – co-expression evidence [*193*].

6.2 Full-length GRASPs

GRASP65 was the first GRASP to be identified through unstacking processes using mitotic cytosol that generated short cisternae and vesicles. It was then isolated in SDS-PAGE and subjected to microsequence analysis [*17*]. Comparing the sequence of that newly identified protein using BLAST analysis, two positive matches were found: 30% identity with a S. cerevisiae sequence and 40% with a S. pombe one. Human and rat partial matches were also found. Even though none of those sequences had any function assigned to them, this was the first hint that GRASPs were conserved proteins.

GRASPs are cytosol-oriented proteins and, having no transmembrane domain, are targeted to the Golgi via N-myristoylation of its glycine at position 2 [*17*,*201*] in most cases. GRASP structure is constituted by two domains: a well-conserved one, termed GRASP domain, and a non-conserved less-studied domain called SPR (i.e. Serine and Proline Rich). The GRASP domain is the N-terminal part of the protein, comprising residues 1–201 in GRASP65, being necessary and sufficient for dimerization [*24*]. Wang et al. were able to show that they are arranged as a trans-oligomer [*60*]. Although most of the data reported thus far has been related to the GRASP domain, it has been shown that phosphorylation

sites, probably important for trans-oligomerization, are contained in the C-terminal SPR domain [reviewed in reference [*5*]]. Since GRASP domains alone form more stable dimers than the full-length proteins, phosphorylation of the SPR was suggested as a means of enabling unstacking during mitosis [*30*]. Upon phosphorylation, oligomers breakdown at the onset of mitosis, and the Golgi cisternae can disassemble and be distributed to the daughter cells,where they will form a new Golgi apparatus upon dephosphorylation of GRASPs [*202*]. This effect of GRASP phosphorylation in unstacking during mitosis needs to be reconciled with the new findings from reference [*19*].

In recent years, an increased amount of structural information about GRASPs has emerged, thus complementing the cell-based assays that led to their discovery and first characterization. To date there is no full-length GRASP with known 3D structure, but there are crystallographic structures for GRASP domains of some organisms, which will be discussed in the following session. The inability to crystalize a full-length GRASP is likely due to the disorder and flexibility of its SPR domain[*34*]. A scheme with the main characteristics of GRASPs and their suggested positioning in the Golgi is presented in Figure 38.

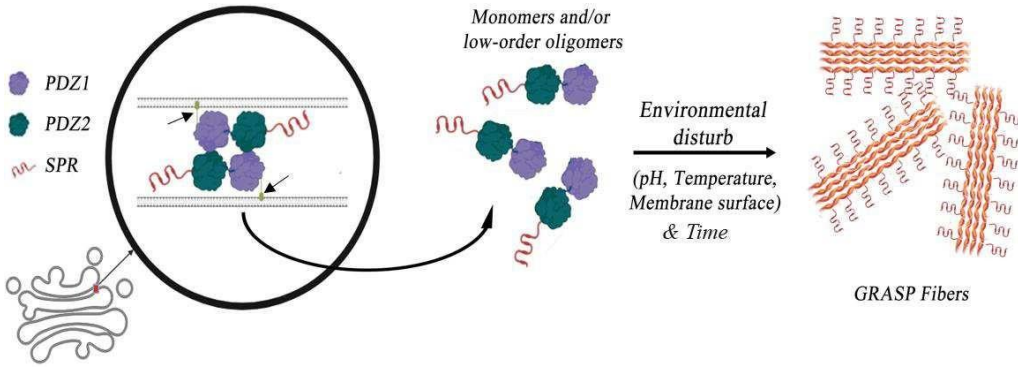

Figure 38: A schematic representation of GRASP location between the Golgi cisternae and their structural transition into amyloid structures. Left side of the figure represents the Golgi apparatus and a portion of the stacked system zoomed in. The PDZ subdomains are represented as globular structures coloured in different pattern to emphasize the *trans* character of the dimer. The disordered SPR domain is shown in red. The arrows indicate a didactic representation of the post-translational modification at residue 2 that allows GRASPs to interact with the membrane. After been released from the Golgi and dispersed in solution, GRASPs tend to fibrillate under perturbations in pH, temperature and dielectric constant. Even in a very diluted situation *in vitro*, it was shown that after some days there is also a tendency for fibrillation in human GRASP55. Possibly structural changes occurring over time tend to decrease the energy barrier necessary for initial nucleation. In our model, the SPR domain is flanking the fibrils since fibrillation was shown to be SPR-independent. The figure was built using BioRender and Adobe Fireworks CS6.

The first structural characterization of a full-length GRASP orthologue in solution, GRASP from *Cryptococcus neoformans* (CnGRASP), was published in 2016 [*34*]. Data from a combination of several biophysical tools indicated that CnGRASP is less compact than a

regular globular protein and due to high structural flexibility shows increased solvent accessibility of its hydrophobic core. These findings placed CnGRASP within a novel category of functional proteins[*85*] uncovered by a recent revolution in structural biology based on the discovery of what was named intrinsically disordered proteins (IDP) [reviewed in references*203*,*204*]. IDPs have been reported in all proteomes [reviewed in references*85*,*205*] and their impacts on many cellular processes are well-documented [reviewed in references*91*,*206 208*,*209*]. It was clear that CnGRASP structural properties closely resembled those of a class of collapsed IDPs, called molten globule-like proteins [*34*]. These are not extended-disordered structures, like those observed for α-synuclein, casein, and many others [*210*,*211*], but rather a compact protein structure with high levels of secondary structure elements and low number of tertiary contacts, which defines the overall structural flexibility in a particular timescale of μs-ms (which is why they are called “molten” [*210*]). The presence of intrinsically disordered regions in GRASPs have been later observed for other GRASP orthologues, thereby suggesting it as a general feature of the family [*141*,*145*]. GRASP65, as an example, was named for its apparent molecular mass on an SDS-PAGE but, in fact, its theoretical mass is only 46.5 kDa. This anomalous SDS mobility comes mainly from the fact that the SPR domain is predicted as fully disordered (a theme that will be discussed latter in the text) and IDPs are formed by a significant lower content of hydrophobic amino acids, which perturbs SDS binding, leading to a “gel shift” towards an apparent larger molecular mass [*212*,*213*]. This aberrant gel mobility is not observed for the isolated GRASP domain [*143*].

If GRASPs have this unusual structural plasticity, a natural issue that arises is: how could the cellular environment affect GRASP behaviour? GRASPs are membrane anchored proteins, mainly located in the Golgi, and that eventually relocate to participate in other processes, especially in UPS [*21*]. It was observed that GRASPs were particularly sensitive to changes in the dielectric constant of their microenvironment, especially for values going from 20 up to 55, close to those observed at the membrane surface [*104*]. The membrane environment induced multiple disorder-to-order transitions in GRASP, which showed very distinct behaviour under the conditions that mimic the vicinity of the membrane surface compared to those found in bulk solution [*104*]. The balance between being more-ordered or more-disordered might have a great impact on GRASP functionalities. For example, GRASP great sensitivity to protease activity, which has been shown to occur *in vitro* as well as *in vivo*, is likely due to the abundant presence of intrinsically disordered regions throughout GRASP structure [*143*].

The intrinsically disordered nature of GRASPs might help explaining how they are able to interact with so many different partners and to be part of different processes inside the cell. GRASP55 has been seen to interact with multiple partners of the PtdIns3K UVRAG complex, component of autophagosomes generated upon amino acid starvation [*214*]. Upon glucose deprivation, GRASP in *S. cerevisiae* relocates to form a new organelle responsible for type III unconventional protein secretion [*54*]. This organelle, called CUPS, is enriched with GRASP, and a plethora of new proteins seem to assemble around it [*56*]. Furthermore, the high flexibility of GRASPs confers the ability to undergo extensive structural changes in different scenarios. Recently, the *in vitro* formation of amyloid-like fibrils has been reported for GRASP in *S. cerevisiae* [*141*] and both human GRASPs [*145*,*142*]. Many "higher ordered" assemblies, such as amyloid fibrils, use the high flexibility of the native structure as an advantage to overcome energy barriers that would otherwise be too difficult to transpose [*110*]. It is common to have regions of intrinsic disorder flanking regions that undergo fibrillation, and that seems to be the case of GRASP in *S. cerevisiae*. The SPR domain is not necessary for fibrillation (what is expected given its proline-rich nature), but even within the GRASP domain, the "hot spots" for aggregation [*90*] are surrounded by regions predicted to be intrinsically disordered [*141*]. At first, amyloid formation was thought to be a "special" ability of some proteins, derived from mutations that would destabilize the structure and lead to diseases such as Alzheimer [reviewed in reference [*215*]]. Today, fibrillation is seen more like a structural change achieved by virtually all proteins when they are under proper conditions. Furthermore, cases of functional amyloids have been reported, which led to a revision of the idea of amyloids being solely linked to diseases [reviewed in reference [*216*]]. It is thus plausible to consider the fibrillation of GRASPs as the formation of a functional structure within the cell.

Recently, GRASP55/GRASP65 were reported to fibrillate *in vitro* in a nucleation-dependent manner *via* a sequence of events that seemingly comprises a lag-phase (aggregation of misfolded monomers into oligomers), growth phase (reorganization of the intermediate oligomers into organized protofibrils), and plateau phase (association of proto-fibrils into amyloid-like fibrils) with increasing incubation time at physiological conditions (such as 37℃ and pH 7.4) [*145*,*142*]. On the other hand, GRASP in *S. cerevisiae* was shown to undergo a nucleation-independent aggregation, forming fibrils within minutes at temperatures from 37℃ and above, upon changes in the dielectric constant or low pH [*141*] (Figure 38). Given the strong connection of GRASPs and stress, the assessment of these exquisite features is important and might help in understanding how GRASPs can use them to perform many different functions.

The conditions shown to trigger GRASP fibrillation in *S. cerevisiae* can be easily translated to an *in vivo* context, such as the change in pH in the cytoplasm of stressed cells [*217*]. Also, the change in the dielectric constant might mimic the changes experienced by GRASP when leaving the membrane (making it less affected by the “membrane field”). *In vivo* data on GRASP fibrillation and their impact on UPS will expand our view over these supramolecular assemblies of GRASP.

6.3 The GRASP domain

6.3.1 Structure and oligomerization

The conserved N-terminal half of GRASPs is conveniently called GRASP domain (DGRASP). DGRASPs are conserved across the eukaryotes and structurally formed by two-PDZ sub-domains connected in tandem [*27*,*143*]. PDZs are widespread protein–protein interaction modules involved in the dynamic regulation of signaling pathways and scaffolding, and usually exist as parts of multimodule proteins [*218*]. There are several excellent reviews dealing with PDZ structure and function already available in the literature [*218*].

DGRASP is the best studied portion of GRASPs with several crystallographic models already available (Figure 39A). The first structure was determined by Truschel *et al.* of the human GRASP55 GRASP domain (DGRASP55) using protein crystallography and showed an unusual PDZ fold adopted by this domain [*28*]. Eukaryotic PDZs are structurally formed by a $^{+}NH_3-\beta_1\beta_2\beta_3\alpha_1\beta_4\beta_5\alpha_2\beta_6-COO^{-}$ secondary structure arrangement, with the binding groove formed by both β_2 and α_2 [*28*], besides a conserved GLGF region located in the loop connecting *β*1 and *β*2 [*218*]. DGRASP55 is an exception to this rule and shows a circular permutation of the first two β-strands, which are located at the end of the secondary arrangement in a $^{+}NH_3-\beta_3\alpha_1\beta_4\beta_5\alpha_2\beta_6\beta_1\beta_2-COO^{-}$ organization [*28*]. This unusual PDZ organization for eukaryotes is not so uncommon in prokaryotes [*28*]. The structure of the mammalian GRASP65 GRASP domain (DGRASP65) was later determined and showed an apparently similar fold to DGRASP55 [*29*]. A second conclusion derived from the crystallographic structures is that DGRASPs are formed by structurally similar PDZ domains albeit their low sequence identity (Figure 39B) [*28*,*29*].

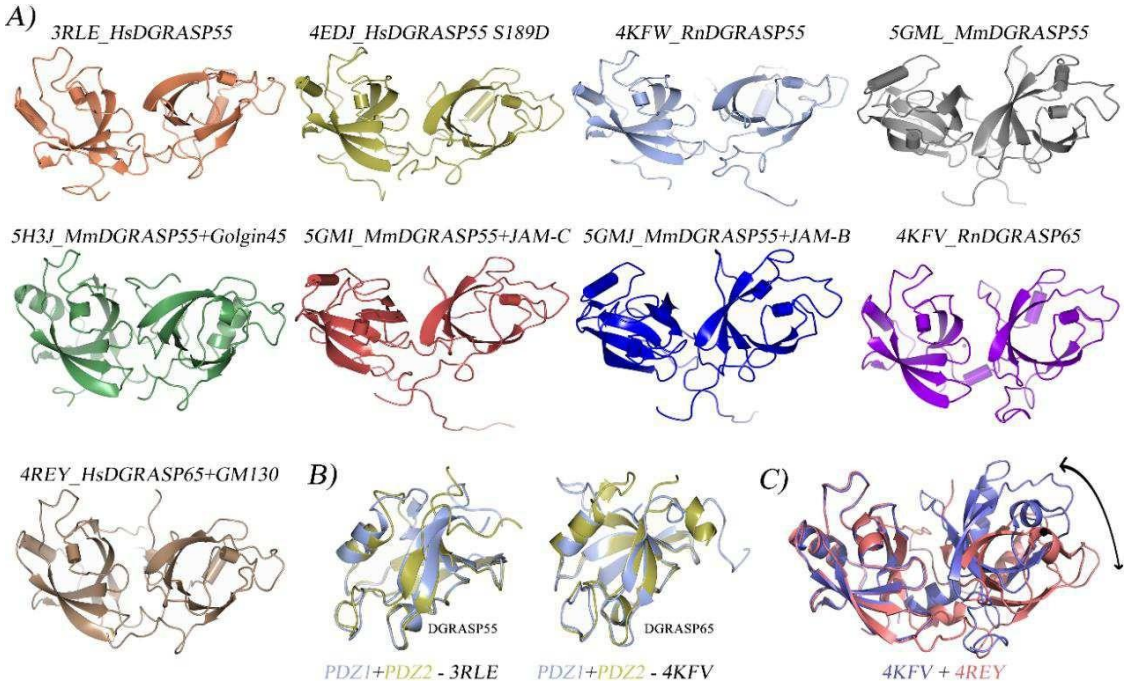

Figure 39: A) DGRASP structures solved by high resolution protein crystallography are illustrated. The overall structural pattern is conserved between the models. Only mammalian DGRASP structures have been reported thus far. **B)** Structural superposition of PDZ1 and PDZ2 of both DGRASP55 and GRASP65 showing the structural conservation between both subdomain inside the DGRASP structure. **C)** Structural superposition of apo DGRASP65 (4KFV) and DGRASP65 with bound GM130 peptide (4REY). The superposition was made by keeping the PDZ1 fixed. The black arrow illustrates the degree of reorientation between both PDZs after binding. The figures were built using Pymol and Adobe Fireworks CS6.

The GRASP oligomerization has been a subject of debate in the literature, and the most accepted model suggests that mammalian GRASPs form dimers *in vivo*, and the inter GRASP interaction is driven by a conserved internal peptide in PDZ2 (IGYGYL) inserting into a binding pocket in PDZ1 [*24*,*28*]. Interestingly, the internal peptide region mapped in the DGRASP55 structure matches in size the binding groove of PDZ1 [*28*]. However, the heterologous purifications of either DGRASP55 or DGRASP65 resulted in mostly monomeric forms of those proteins [*29*,*221*]. Furthermore, GRASP55 is not capable of interacting with GRASP65, although they have conserved PDZ1 domains and internal peptide sequence in PDZ2. A report focusing on GRASP intermolecular interaction was published and conclusions were taken from crystallographic packing contacts and symmetry expansion [*29*]. The molecular system in the asymmetric unit was monomeric, but the authors claimed that a feasible dimer of both DGRASP55/65 could be formed using a 2-fold axis symmetry expansion [*29*]. Using this procedure, a low interaction surface formed by the contact of two laterally positioned PDZ2 contributed in synergy with a possible C-terminal insertion inside the PDZ1 of another pair of dimers to create the high-order oligomeric species [*29*].

However, this C-terminal region was artificially engineered when isolating the DGRASP from the SPR, so the possible contribution of the SPR to GRASP dimerization is still open for debate. Therefore, isolated DGRASP does not seem to spontaneously form oligomers *in vitro.* Since it was previously observed that DGRASP forms oligomers *in vivo*, some specific environmental factors or conditions present *in vivo* might be key to dimerization.

The interaction between DGRASP65 and its Golgin partner, GM130, was addressed using a peptide mimicking the GM130 C-terminus [*222*]. There was a previous assumption, based on biochemical data, that the binding site for GM130 on GRASP65 involved residues 189–201, the region where the internal peptide responsible for dimerization is located [*223*]. The crystal structure of the DGRASP65/GM130 peptide complex showed that PDZ1 instead is responsible for the canonical PDZ-GM130 peptide binding, and a conserved hydrophobic cleft between PDZ1-PDZ2 also participates in an array of secondary interactions, both being essential for the complex formation [*222*]. The secondary array of interactions involves the ^{973}IPFFY^{977} region of GM130 interacting with Y36 and C103 from PDZ1, and residues Q111, W113, D140, V136, G138, L143, L152, and M164 from PDZ2, besides A108 from the linker connecting the two PDZ domains [*222*]. The secondary participation of several residues in PDZ2 might be the cause for the erroneous biochemical conclusion regarding the involvement of this subdomain in the binding of GM130. However, there are still conflicting biochemical data showing that a ΔPDZ1-GRASP65 is sufficient for the complex formation with GM130 [*223*]. It could be that the SPR domain also contributes for the interaction and the binding mechanism changes, when the isolated DGRASP65 is used, although this explanation looks less likely because DGRASP65 and the GM130 peptide have a high binding affinity with a K_D of (108$\pm$28) nM [*222*]. Besides, there is a rigid body reorientation of the two PDZs to accommodate the GM130 peptide (Figure 39C). The authors also speculated about a GRASP oligomerization based on crystal packing, claiming that GM130 is responsible for a DGRASP65-hexamer formation [*222*]. Although they showed that the coiled-coil region of GM130 can form a hexamer-like structure in solution, no conclusive data indicating the existence of a hexameric GRASP have been reported so far in the literature. Future biochemical and structural studies are needed to enlighten those points.

As for DGRASP55, its 3D structure in the presence of a peptide mimicking the Golgin45 C-terminal region has been recently reported [*224*]. The data showed a binding mode similar to the one observed in DGRASP65/GM130 complex, although the secondary array of interactions involved different sites at the PDZ1/PDZ2 interface. Therefore, the canonical PDZ-peptide interaction is mediated by PDZ1 in both cases involving DGRASPs and the Golgins [*224*]. A special feature of DGRASP55 and Golgin45 interaction was the

formation of a zinc finger-like structure that stabilizes the complex. This zinc finger-like structure is formed between C393 and C396 of Golgin-45 and H18 (β_1) and C103 (β_2) of DGRASP55. The authors also suggested that DGRASP55 oligomerization was mediated by Golgin45. In the crystal packing, it was observed that each C-terminal Golgin45 mimicking-peptide was capable of interacting with three different DGRASP55 molecules, suggesting a new possible way to form GRASP55 oligomers in the *medial*/*trans* Golgi interfaces [*224*]. Whether this arrest of GRASP55 by the Golgin45 truly happens *in vivo*, or even in solution with the full-length proteins or the isolated domains, remains to be demonstrated.

Although GRASP oligomerization could be mediated/controlled by the Golgins, it has been observed that GRASPs act as tethering factors *in vivo* without Golgin interference [*28*]. In an artificial cell model using the native proteins tagged with a mitochondrial targeting sequence derived from the bacterial actin nucleator protein ActA of *Listeria monocytogenes*, both GRASP55 and GRASP65 were capable of inducing mitochondria clustering [*28*,*225*]. Moreover, when mutated versions of both proteins known to block PDZ1 binding properties were tested, the degree of mitochondria clustering was strongly diminished [*28*,*225*]. The overall data showed that, although the Golgins could play a role in GRASP55/65 oligomerization, we cannot rule out that GRASPs might form oligomers *in vivo* by themselves when the full-length proteins are introduced in the native conditions.

GRASPs are anchored to the membrane surface of the Golgi cisternae by a dual mechanism involving the aforementioned interactions with the Golgins and, secondly, protein lipidation, mainly myristoylation of the conserved glycine-2 [*27*]. Heinrich *et al* explored the double anchoring of DGRASP55 using the G2 myristoylation and a C-terminal His-tagged bound to a Ni-NTA-DGS (a synthetic diacyl lipid with a His-tag binding head group) to mimic the GRASP55/Golgin45 interaction. With that mimetic system, they observed, on one hand, that myristoylation was not essential for DGRASP55 binding to the membrane, and, on the other hand, when myristoylated, DGRASP55 had a fixed upright orientation on the membrane incompatible with *cis* interactions, thus concluding that myristoylation was required only for an efficient tethering [*83*]. However, the mimetic of GRASP55/Golgin45 used in that study was not ideal, because Zhao *et al.* showed later that the interaction involved mainly GRASP55 PDZ1 and not PDZ2 [*224*]. Nevertheless, it is interesting to observe that the orientation of GRASP on the membrane might be restricted due to myristoylation and the potential important role played by the membrane surface especially on PDZ1. A previous report showed that the binding energy provided by the myristate is weak with a K_D of $10^{-4}\,M$, which is insufficient to fully anchor a protein to a cellular membrane [reviewed in reference [*226*]]. To date there are no experimental data for a possible direct

interaction between GRASP and the membrane surface. Therefore, the membrane surface might also participate in GRASP anchoring and, consequently, in inducing changes in DGRASP structure and/or oligomerization tendency. GRASP monomerization and Golgi membrane release were previously observed to be necessary in the Δ508-CFTR unconventional secretion [*227*]. An interplay between GRASP oligomers in the membrane field and GRASP monomers in solution could be the missing link and should be explored in the future.

A well-known mechanism controlling GRASP oligomerization is protein phosphorylation [*27*,*15*,*228*,*199*]. Phosphorylation of DGRASP65 S189 residue by PLK1 was shown to break GRASP65 oligomers, leading to Golgi ribbon impairment [*229*]. Since residue S189 is conserved, Truschel *et al.*, using DGRASP55 and the phosphomimetic mutation (S189D) as a model, observed that there was an allosteric effect, caused by the S189D region, that propagated all the way through to the predicted internal peptide responsible for GRASP dimerization [*221*]. More specifically, Y198 was one of the main residues involved in DGRASP dimerization and it shifted 6.9° in the S189D DGRASP55 structure compared to the native one [*221*]. The shift was caused by a loss of a native polar S189-E157 contact in the S189D mutant. E157 is located at the beginning of helix α_2, and the loss of this polar contact induces a disturbance propagating through α_2 and, consequently, inducing shifts in the β-strand where the internal peptide is located. The authors also showed that this DGRASP55 phosphomimetic had decreased tethering capacity *in vivo* using the artificial model of anchoring GRASP55 into the mitochondria membrane [*221*]. However, in order to observe a significant number of DGRASP55 dimers in solution, the authors had to increase the DGRASP55 concentration to 10 mg/ml and still the amount of dimers was significantly lower than the monomer population [*221*]. Although we now know how DGRASP oligomerization is blocked, it is still not clear how it really occurs.

6.3.2 The unusual structural biophysics of DGRASPs

Since the appearance of the GRASP55/GRASP65 paralogy is a recent trend in evolution, the structural similarity of these two proteins is not a surprise [*29*]. However, GRASP55 and GRASP65 play very different roles when it comes to cell functionalities. GRASP55 seems to be more involved in UPS [*44*,*197*], energy sensing in the Golgi [*198*], and membrane tethering during autophagy [*230*], whereas GRASP65 participates in the dynamics of the Golgi, especially during Golgi ribbon formation [*231*], Golgi fragmentation in apoptosis [*232*], and modulation of the Golgi structure and microtubule organization during cell division [*228*,*233*]. A phylogenetic analysis of eukaryotic DGRASPs indicated that the duplication of GRASP55 and GRASP65 is Metazoa-specific [*234*]. An extensive study of

GRASPs outside Metazoa might enlighten the original GRASP function spanning all the way back to the last eukaryote common ancestor. But what do we know about DGRASP structure outside Metazoa? The answer so far is “not much”. There are no crystallographic structures available for non-metazoan DGRASPs besides a communication of a short *Saccharomyces cerevisiae* GRASP PDZ1 domain construction [*235*]. Although it suggests that this Fungi PDZ1 adopts the same circular permutation as the mammalian DGRASP PDZs, the absence of β_2 in this construction compromises more detailed analyses.

A recent report has expanded the knowledge on DGRASP outside Metazoa, but still within the Opisthokonta clade [*143*]. Holomycota are a basal Opisthokonta clade, sister of the Holozoa and mainly formed by the kingdom of Fungi (Figure 40A). Fungi are single-GRASP organisms without any obvious GM130 and Golgin45 homologues [*23*]. Therefore, they precede GRASP55/GRASP65 duplication and might be an interesting model to unravel the GRASP55/GRASP65 original function. A fact observed in the Fungi DGRASPs studied up to date is their molten globule-like structural behavior in solution, similar to the observed in the full-length structures [*34*,*141*,*143*]. The chemical unfolding of fungi DGRASPs is characterized by very low cooperativity, as evidenced by the shallow sigmoidal curves (Figure 40B) [*143*]. This is an indicative that the tertiary contacts inside Fungi DGRASPs are not well formed, leading different parts of the protein structure to unfold in different ways [*88*]. The same behavior is observed for other collapsed IDPs that, similarly to fungi DGRASPs, are highly dynamic and characterized by low conformational stability, which is reflected in the low steepness of the transition curves induced by strong denaturants [*88*]. This is the opposite of what is observed for well-structured proteins, where unfolding usually takes place in a highly cooperative way, closer to an “all or none” transition (Figure 40B) [*143*]. Furthermore, limited proteolysis and solution NMR analyses showed significant amounts of disordered structures in the Fungi DGRASPs (Figure 40C) [*143*]. This large number of disordered regions present in the Fungi DGRASPs leads to some unusual features, such as high sensitivity to proteolysis [*143*], disorder-to-order transitions according to some changes in the physicochemical properties of the solution [*141*], and fibrillation tendency [*141*,*145*].

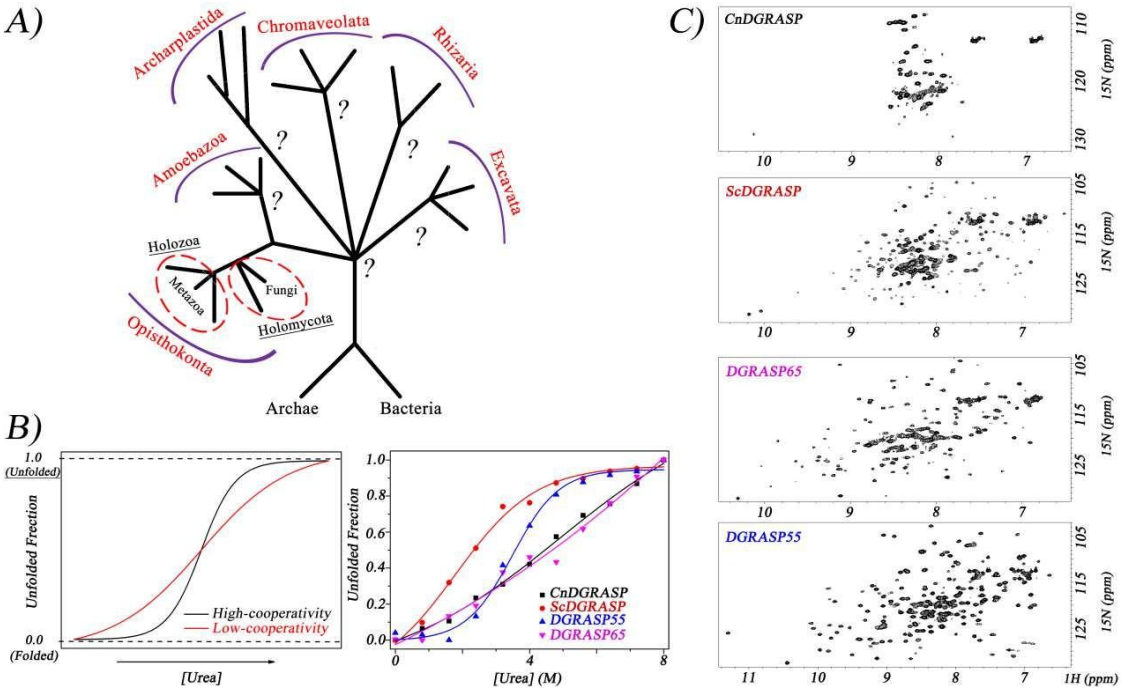

Figure 40: A) Schematic tree of life with the eukaryote branches highlighted. Our current "high-resolution" knowledge about DGRASP structure remains limited to the Metazoa extremity, with some low-resolution data for a couple of Fungi examples. The figure illustrates the great number of unknown pieces in our GRASP jigsaw puzzle. **B)** DGRASP structure unfolding using the chaotropic agent urea and monitored as a function of the unfolded fraction, measured by steady-state fluorescence. The data was adapted from [*143*]. The left panel shows representative curve models for a "well-behaved" structure following a protein unfold pattern considered of high-cooperativity and a "not-so-well-behaved" one with a low-cooperativity transition. The latter is typical of proteins enriched with intrinsically disordered regions and/or with lower tertiary contacts. **C)** 1H-15N HSQC spectra of fungi and human DGRASP showing the great number of disordered regions inside the fungi DGRASPs. The data was adapted from [*143*]. The figures were built using Adobe Fireworks CS6.

How could the intrinsic disordered nature of the Fungi DGRASPs be transferred to the correspondent mammalian paralogues? In a molecular biophysics study using Fungi and human DGRASPs as models, it was observed that, from a structural biophysics point of view, DGRASP65 behaves more similar to fungi than to DGRASP55 [*143*]. Such similarity includes the amount of disorder and the lower-tertiary contacts responsible for the high cooperativity of the unfolding transition, typically observed in well-behaved proteins. Besides, in the phylogenetic analyses, the cluster of mammalian DGRASPs and fungi suggest that the last common ancestor of these systems is rather similar to the subgroup of DGRASP65/fungi DGRASPs than to DGRASP55 [*143*]. This indicates that DGRASP65 might have kept most of the functions seen in more ancient DGRASP. Even for the fungus, which has a single GRASP gene but with a fragmented (or partially fragmented) Golgi complex, the *cis*-Golgi is the more obvious conserved part of this organelle [*143*]. This is the case of *S. cerevisiae* GRASP, which was observed to be associated with the *cis*-Golgi via its acetylated N-terminal

region [*23*]. This does not exclude the possibility for DGRASP55 to perform this “ancienter” GRASP function but suggests that this protein might have evolved under different evolutionary pressure. However, it is not clear at the moment whether such unusual DGRASP65/Fungi phenotype is an ancient feature or has evolved in parallel later in evolution. In this evolutionary context, based on phylogenetic analyses, it is concluded that the appearance of Golgin45 and GM130 represents a Holozoan feature, which therefore precedes the GRASP55/GRASP65 duplication [*234*]. Unraveling whether the common ancestor of GRASP55/GRASP65 could interact with both Golgins and if this feature appeared later in evolution might give some clues on the evolution of GRASP functionalities.

6.3.3 DGRASP PDZs – how similar are they?

PDZ1 and PDZ2 on GRASP share a sequence identity in the order of 30-40% [*27*,*28*]. However, as previously discussed, the crystal structures of mammalian DGRASPs suggested that, albeit their relative low sequence identity, they share a high degree of structure conservation (Figure 39B). In the previous section we discussed the role of PDZ1 as a mediator of the canonical interaction of DGRASPs with the Golgins, while PDZ2 assists such interaction with secondary contacts. But how common is this for other protein partners? One fact is that mammalian GRASPs are very promiscuous in mediating protein/protein interaction (see Figure 37). They were observed to be part of a complex with RAB2 [*184*], and to interact with: cargo receptors from the conventional secretory pathway [*190*], TGF-α [*185*], the potassium channel tetramerization domain-containing protein 5 [*236*], SEC16A and ΔF508 CFTR [*237*,*63*], JAM-B and JAM-C during spermatogenesis [*238*], LC3-II and LAMP2 [*230*], CD83 [*239*], membrane-type 1 matrix metalloproteinase and furin [*240*], with itself during dimerization [*24*] and with an artificial SPR construction [*28*]. In such large array of protein partners, most of the interactions involved mainly PDZ1 [*28*,*144*,*222*,*223*]. A recent study, where a Fungi DGRASP was used as a model, reported that the binding pocket of PDZ1 is more promiscuous than that of PDZ2 [*144*]. In this case, a more malleable binding groove could account for this higher promiscuity in protein/protein interaction. Concomitantly, PDZ2 would participate in other types of interactions that would stabilize the complex and previous crystallographic studies were conclusive in this aspect [*222*,*224*].

An interesting observation was made when the structure of DGRASP65 with GM130 was determined: the superposition of the structures of DGRASP65 apo- and holo-forms using PDZ1 as a template showed a 32.6° rotation of the PDZ2 domain upon binding of the GM130 peptide (Figure 39C) [*222*]. The same phenomenon was not detected for DGRASP55 and Golgin45 [*224*], but a somewhat similar tendency for rigid body reorientation was observed in the structure of DGRASP55 with the JAM-B/JAM-C C-terminal peptide,

which was also characterized by a 33° rotation of PDZ2 towards PDZ1 [*238*]. Therefore, this reorientation is not an exclusive property of DGRASP65 and seems to be a more general phenomenon. Using Adapted Biasing Force molecular dynamic simulations, it was shown that DGRASP55 samples a large free energy conformational space in the apo-form at physiological temperature [*144*]. However, this free energy space is severely reduced when the protein goes to the bound state, suggesting that the complex is stable and the relative movement of the PDZs is more restricted [*144*]. One unexpected observation was that all the holo-structures of DGRASP55, including those with the different rigid-body reorientation, were sampled in the free-energy conformational space of the apo-form [*144*]. Kinetic experiments might unravel whether the complex formation is through a conformational selection or induced fit process, but the large degree of accessible free-energy regions between both PDZs explain how this protein can be so promiscuous when it comes to protein-protein interactions.

6.4 SPR domain

GRASPs have variable extensions of their primary sequence depending on the organism. The GRASP domain contains around 200-220 amino acids, therefore the large variations in GRASPs extension are due to the changes in the SPR size (Figure 41A). The SPR domain is neither conserved in size nor in sequence in closely related species [*27*]. There are differences even inside the same organism, for instance GRASP55 and GRASP65 SPR sequences are quite different. However, this non-conserved domain with still obscure structure and function occupies nearly half of the sequence of most GRASPs. The SPR domain was already shown to have multiple phosphorylation sites, and this post translational modification can have great impact on GRASP oligomerization and membrane anchoring [*186*]. Hence, the best established SPR functionality is the regulation of DGRASP activity through phosphorylation, although the molecular details remain elusive.

One intriguing issue is why would nature evolve to give GRASPs a domain, usually larger than the GRASP domain, just to control oligomerization? The SPR was also shown to contain caspase cleavage sites important for Golgi fragmentation in apoptosis [*31*] and phosphorylation sites necessary for spindle pore formation and Golgi reorientation to the leading edge in migratory cells [*32*], which are all related to SPR function as regulator of the DGRASP activity. The SPR of GRASP55 was observed to interact with Beclin-1, regulating autophagy [*214*]. The SPR of GRASP65 can interact with Mena and Dja1, playing a role in Golgi structure formation [*231*,*241*]. Therefore, the SPR might still have several unknown roles in GRASP function.

It is still unclear how the SPR domain is folded in solution. However, some patterns are reproduced throughout several GRASP orthologues. For instance, Mendes *et al* showed that the fully disordered pattern of the SPR domain is a high conserved feature of the GRASP family, despite their variation in size and amino acid sequence [*34*]. Disorder is predicted based on the low complexity of the amino acid sequence, especially due to the lower content of hydrophobic amino acids and high content of charged/polar residues [*33*]. A disorder prediction using PONDR® VSL2 [*167*] and the same protein sequences used by Mendes *et al* [*34*] clearly shows that the SPR domains of GRASPs are characterized by high intrinsic disorder propensity (Figure 41B). A low resolution structural analysis based on the reconstruction of the CD spectrum of the SPR domain from the circular dichroism spectra of the full-length CnGRASP and the isolated GRASP domain indicates the SPR domain has the same CD profile observed for fully disordered structures [*34*]. Another interesting statistic is that, on average, 33% of the amino acids that form the SPR domain are serine (10%), proline (16%) and threonine (7%), explaining how this domain can be the target of so many protein kinases (Figure 41C).

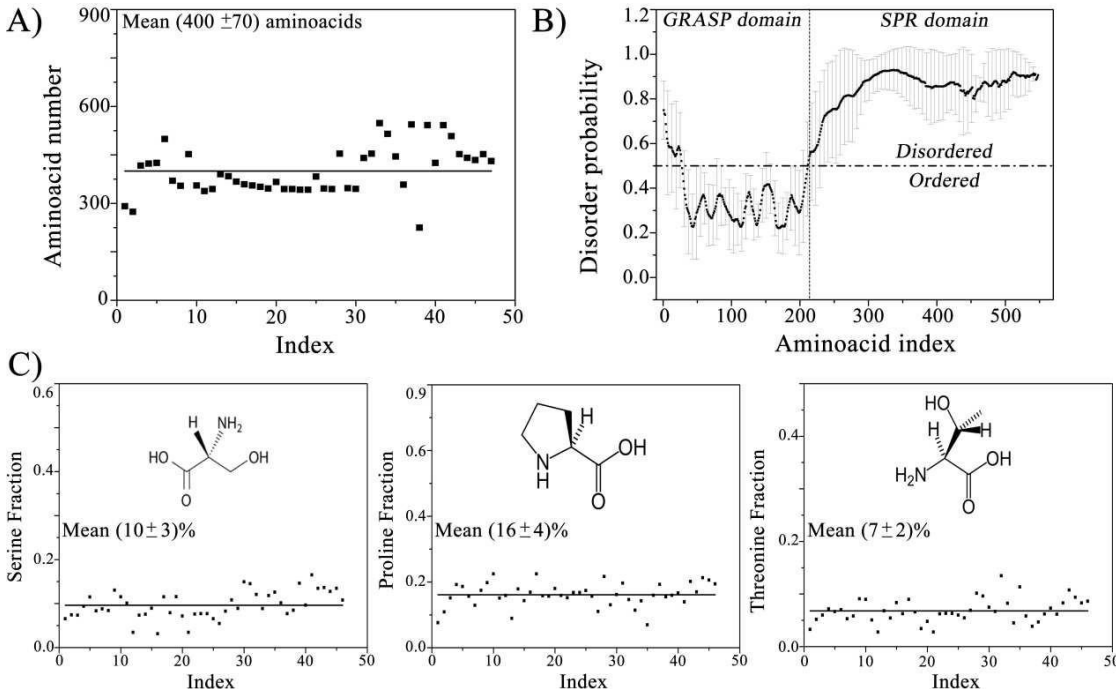

Figure 41: A) The amino acid content of different GRASP orthologues is plotted as a function of an index number given to each sequence. The line represents the simple average number of amino acids that comprise the GRASP sequences used. This representation was chosen to clearly illustrate the degree of variability. Note that there are GRASP sequences with less than 300 amino acids and some of nearly 600**. B)** The sequences used in (A) were evaluated for their disorder probability using VSL2. The curve shown is an average curve over the whole sequence database and error bars represent the standard deviation. A region with probability higher than 0.5 is considered to be disordered. **C)** The serine, proline and threonine content of the GRASP sequences used in (A) are shown. The representation is the same used in (A). The GRASP orthologue database was collected from [*34*]. The figure was built using Origin 8.0 and Adobe Fireworks CS6.

Although it is already known that the SPR domain is rich in serine and proline, it is important to note that their total amount is somehow conserved for different orthologues. Also, one should keep in mind that according to the accepted classification of residues as order- and disorder-promoting, serine, threonine, and proline are grouped into the category of disorder-promoting residues [*242*], with proline being the most disorder-promoting of the 20 common amino acid residues [*100*]. To give a better perspective of the peculiarities of intrinsic disorder distribution within the sequences of GRASPs and to show the rich disorder-based functionality of these proteins, Figure 42 represents the results of the analysis of the sequences of human GRASP65 and GRASP55 by DiSpi (Figures Figure **42**A and Figure **42**C) and D2P2 computational platforms (Figures Figure **42**B and Figure **42**D). It is clearly seen that the C-terminal halves of both human proteins are predicted to be highly disordered. Furthermore, GRASP65 and GRASP55 are highly decorated with various posttranslational modifications and include multiple predicted disorder-based protein binding sites, known as molecular recognition features, MoRFs, with very significant parts of these proteins representing such disorder-based binding regions (see Figures Figure **42**B and Figure **42**D).

Therefore, it can be seen that the SPR domain plays a significant role in GRASP function, likely as a controlling hub of structural changes. The analyses discussed above, most of them based on computational methods, undoubtedly show that experimental studies with the full-length GRASP are still needed to completely unravel the biophysics of the SPR domain.

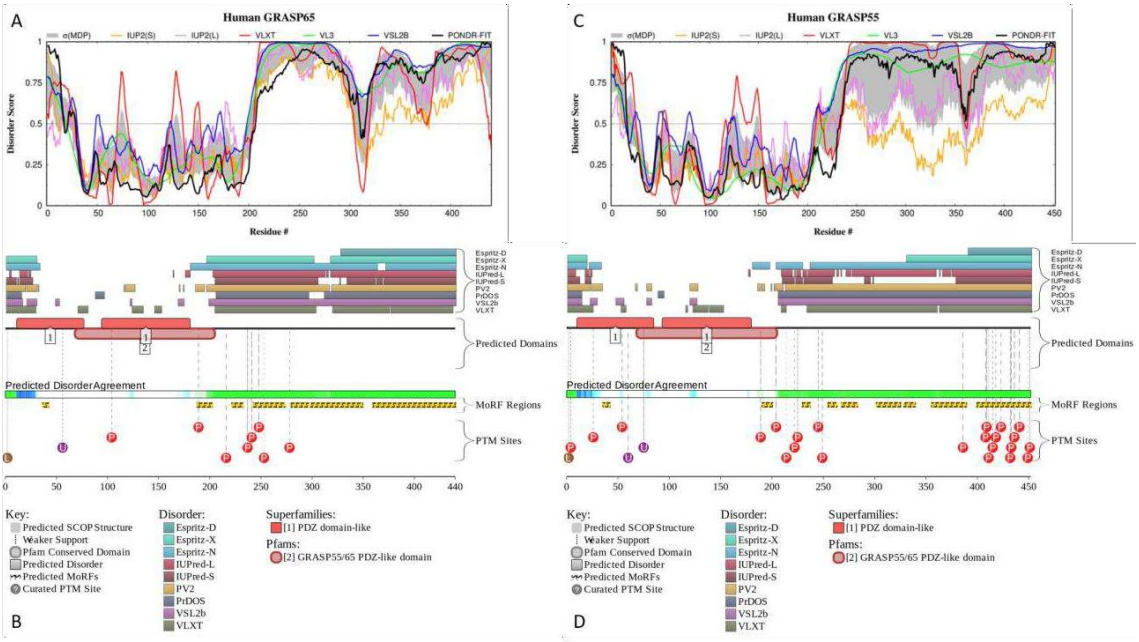

Figure 42: Evaluation of the intrinsic disorder predisposition and disorder-based functionality of human GRASP65 (plots A and B, UniProt ID: Q9BQQ3) and GRASP55 (plots C and D, UniProt ID: Q9H8Y8) by DiSpi (plots A and C) and D2P2 computational platform (plots B and D). DiSpi is a web-crawler that aggregate the results from a set of commonly used predictors of intrinsic disorder, such as PONDR® VLXT [*168*], PONDR® VL3 [*167*], PONDR® VLS2B [*245*], PONDR® FIT [*92*], IUPred2 (Short) and IUPred2 (Long) [*164*,*246*, *247*], and enables the rapid generation of disorder profile plots for individual polypeptides as well as arrays of polypeptides. On the other hand, D2P2 (http://d2p2.pro/, accessed in 2020) is a database of predicted disorder for a large library of proteins from completely sequenced genomes [*162*] that in addition to using the outputs of IUPred [*164*,*246*], PONDR® VLXT [*168*], PrDOS [*166*], PONDR® VSL2B [*167*,*245*], PV2 [*162*], and ESpritz [*163*] represents several disorder-based functional annotations, such as location of various posttranslational modifications and predicted disorder-based protein binding sites, known as molecular recognition features, MoRFs. It is known that many disorder-based binding regions are characterized by the presence of less disordered sub-regions, which are not capable of folding on their own, but can undergo binding-induced folding at interaction with its binding protein partner. In disorder profiles, such regions are typically manifested as local “dips” within the regions with high disorder score [*248*,*249*]. In D2P2, the presence of MoRFs is evaluated by ANCHOR algorithm [*250*,*251*].

6.5 Future perspectives

GRASPs have been discovered more than two decades ago, and while the function first assigned to them (and from which they received their name) has been a matter of extensive debate among the scientific community, the number of processes that involve GRASPs has dramatically increased in the last decade. Cell-based assays discovered a wide range of interactions and roles for GRASPs, but structural data have been falling behind, impairing the understanding of the molecular basis for such promiscuous behavior. DGRASP structures were determined and more data regarding secondary and tertiary structures, proteolysis sensitivity, stability, and so on for the full-length GRASPs have been recently reported. This is making possible to establish a link between cell and molecular

biology, and there is a good prospect that we will be able to shed more light on GRASPs capabilities.

The structural plasticity can be at least partially explained by the intrinsic disordered nature of regions not only in the SPR but also within the GRASP domain. This plasticity also allows for structural changes that can confer different functionalities, such as the case of GRASP fibrillation, a change that happens *in vivo* in very specific conditions and seems to be involved in the yeast response to stress. Furthermore, there are several recent reports in the literature demonstrating the propensity of the Golgins to undergo liquid-liquid phase separation [*64*,*66*]. It is thus stimulating to suggest that the macromolecular organizations of Golgins and Golgi matrix proteins could be an important building block of the Golgi structure as well as a modulator of its dynamics. This hypothesis will certainly benefit from future studies aiming at understanding the liquid-liquid phase separation and fibril formation propensities of Golgi-related proteins. Of course, those supramolecular arrangements can also be important in UPS specially by the necessity of a physical and/or chemical stress to trigger its activation and this should also be a theme to explore in the near future. Since most of these studies using Golgins and GRASPs were performed using non-native situations (like overexpression and/or artificial diluted conditions), future kinetic and thermodynamic studies of those supramolecular complexes, both in vivo and in mimetic conditions, might give valuable information on the specific cellular triggers that could be used to control their formation.

Moreover, several quests on GRASP structure/function relationship remain largely unknown. Regarding the structure of full-length GRASPs, it is intriguing how little is known about the SPR organization in solution and conformational responses to the several different post-translational modifications that have been already observed *in vivo*. Why would nature evolve to give GRASPs a domain, usually larger than the two PDZs, with the sole functionality of being a controller of GRASP oligomerization? In that context, the conflict of data from *in vivo* and *in vitro* studies regarding GRASP association still remains. A hypothesis that could account for such differences is the absence of the GRASP myristoylation and, therefore, the consequent absence of the membrane-field perturbations in the *in vitro* analyses available in the literature. Further studies on membrane-associated GRASPs will contribute to seek for conformational changes induced by the lipid membrane, and their potential role in GRASP oligomerization.

Finally, another intriguing open question is related to the presence of two GRASPs in Metazoan organisms. Although some data are now available in the literature, it is not clear why, despite their structural similarities, there is a seemingly more frequent involvement of

GRASP55 in UPS, while GRASP65 appears to be more Golgi-related. Besides, why is there a special association of GRASP65 with GM130 and GRASP55 with Golgin45 showing up in evolution if both Golgins are Holozoa-specific proteins? It is clear that these associations give the Metazoans unique functionalities, but an extensive study of GRASP outside this branch of the eukaryotic tree might give some information on the specific points of divergence and on the initial GRASP function coming all the way from LECA.

7 General conclusions and future perspectives

Grh1 belongs to a family of proteins that possesses many different functions inside the cells as it was discussed throughout this thesis. Our group previously showed that the GRASP from *Cryptococcus neoformans* (CnGRASP) had regions of intrinsic disorder in its GRASP domain as well as in its SPR. This had never been reported before (in fact, GRASPs in general lacked biophysical characterization by then) and could help explain the promiscuity of these proteins and the astonishing number of processes they are involved in.

The yeast *Saccharomyces cereviseae* has a disperse Golgi complex rather than a stacked one, and for this reason the "classical" GRASP function, that is, to keep the Golgi membranes stacked together, has no place for Grh1. Even so, Grh1 shares the structural organization of other GRASPs, being a homolog of the human GRASP65. Grh1 was chosen as a model for the GRASP family, and the initial goal of this project was to generalize the findings of intrinsic disorder. In a broader sense, we wanted to understand GRASPs to pave the way for a better understanding of the Golgi complex and the secretion pathways.

We used a plethora of biochemical and biophysical methods to characterize Grh1, and our initial results confirmed that it has regions of intrinsic disorder in the SPR, as well as in the GRASP domain. However, the protein is not of the extended-IDP type, being classified as a molten globule. It neither has a fully folded, compact and globular structure, nor a totally flexible and lacking secondary structure.

Trying to understand the behavior of Grh1 in different environments and carrying on with the idea of comparing our results with previous findings for CnGRASP, we tested the protein in different conditions such as higher temperature and the presence of ethanol. To our surprise, the CD results showed a steep transition to a β-sheet rich structure that led us to hypothesize it was forming amyloid fibrils. At that moment, the project gained new objectives (more were to come) and new methods were used to test for Grh1 fibrillation. We used the classical experiments to prove that Grh1 is capable of forming fibrils *in vitro* and also added the FLIM technique that only recently had been applied to this end. This was the first observation of fibril formation by GRASPs, and later our group would show that it was the case for the two human GRASPs as well.

Our next step was decided taking into consideration that: some of the conditions we saw to trigger fibrillation of Grh1 were very mild, like 37°C. Interestingly, 37ºC is considered to be a stress condition for the yeast. When in starvation the yeast faces a drop in cytosolic pH, and low pH is another condition that triggers Grh1 fibrillation. GRASPs have increasingly

been reported to be involved in UPS (that mostly deals with stress situations), and Grh1 is the marker for the formation of CUPS. So it seemed reasonable to ask ourselves if Grh1 could fibrillate inside the yeast as well.

We employed different techniques and were able to show that, when the yeast faces starvation, Grh1 forms amyloid-like fibrils like the ones we observed *in vitro*. The fibrillation of Grh1 in this context has profound implications for Type III unconventional protein secretion and CUPS formation, and can change the way we understand these processes. We also proved fibril formation by Grh1 in heat-shock condition. While there are no reports of GRASPs being involved in the HSR, Grh1 is upregulated when the cell is in HS, and it shares protein regulators with some Hsps, the main proteins involved in the HSR. This finding might be the first in the assignment of GRASPs to yet another process in the cell. Another important contribution was the use of FLIM to detect fibril formation *in cell*. We acknowledge that the use of the technique without external probes attached to the target protein makes it less specific, but we were able to show that it is possible to obtain relevant data in some cases, especially when combining different cell lines, like we did with the wild type and Grh1-knockout yeast strains.

Recently, liquid-liquid phase separation became a hot topic in cell biology. The discovery of liquid phase separation involving the Golgins led to the hypothesis of a phase-separated Golgi, that in turn led us to the hypothesis of phase-separated GRASPs. Our initial findings with Grh1 made us confident that these proteins do phase-separate. Although more experiments are necessary for statistical purposes and to assess more conditions, we were able to show the characteristic droplet formation, fusion and diffusion.

As for Grh1 interacting partners, we were able to purify Bug1, the Golgin partner of Grh1, and begin a biophysical characterization that confirmed its coiled-coil organization. It is worth emphasizing that to date, there is no data available on Golgins in solution. Therefore, we hope the data reported in this thesis on Bug1 production and initial characterization will help to fill that gap by being the starting point of future studies on Bug1.

There is still much to be done, and every one of our findings opened a new set of questions to be answered. It would be interesting to have a purified construct of Grh1 tagged with a fluorescent probe such as GFP to perform more elaborated experiments concerning LLPS, such as fluorescence recovery after photobleaching (FRAP). Considering Grh1 fibrillation in stress conditions, and the possibility of GRASPs being phase-separated in the Golgi, it is important to understand how these two phenomena are linked. FLIM experiments

in the conditions seen to trigger LLPS concomitant with droplet formation tracking could be a good starting point.

In conclusion, this thesis gave important contributions to the field of GRASP biophysics. The findings here discussed can greatly impact our understanding of the Golgi and Unconventional Protein Secretion.

References

[1] Harter, C., and Reinhard, C. (2000) The secretory pathway from history to the state of the art, *Subcell Biochem 34*, 1-38.

[2] Kalies, K. U., and Hartmann, E. (1998) Protein translocation into the endoplasmic reticulum (ER)--two similar routes with different modes, *Eur J Biochem 254*, 1-5.

[3] Golgi, C. (1898) Intorno alla struttura delle cellule nervoses. XXV. Sulla struttura delle cellule

nervose dei ganglin spinali.

[4] Wei, J. H., and Seemann, J. (2010) Unraveling the Golgi ribbon, *Traffic 11*, 1391-1400.

[5] Ramirez, I. B., and Lowe, M. (2009) Golgins and GRASPs: holding the Golgi together, *Semin Cell Dev Biol 20*, 770-779.

[6] Kreis, T. E., Lowe, M., and Pepperkok, R. (1995) COPs regulating membrane traffic, *Annu Rev Cell Dev Biol 11*, 677-706.

[7] Duden, R., and Schekman, R. (1997) Insights into Golgi function through mutants in yeast and animal cells, In *The Golgi Apparatus* (Berger, E. G., and Roth, J., Eds.), pp 219-246, Birkhäuser Basel, Basel.

[8] Schweizer, A., Clausen, H., van Meer, G., and Hauri, H. P. (1994) Localization of O-glycan initiation, sphingomyelin synthesis, and glucosylceramide synthesis in Vero cells with respect to the endoplasmic reticulum-Golgi intermediate compartment, *J Biol Chem 269*, 4035-4041.

[9] Dunphy, W. G., Brands, R., and Rothman, J. E. (1985) Attachment of terminal N-acetylglucosamine to asparagine-linked oligosaccharides occurs in central cisternae of the Golgi stack, *Cell 40*, 463-472.

[10] Roth, J., Taatjes, D. J., Lucocq, J. M., Weinstein, J., and Paulson, J. C. (1985) Demonstration of an extensive trans-tubular network continuous with the Golgi apparatus stack that may function in glycosylation, *Cell 43*, 287-295.

[11] Schekman, R. (1992) Genetic and biochemical analysis of vesicular traffic in yeast, *Curr Opin Cell Biol 4*, 587-592.

[12] Szul, T., and Sztul, E. (2011) COPII and COPI traffic at the ER-Golgi interface, *Physiology (Bethesda) 26*, 348-364.

[13] Glick, B. S., and Nakano, A. (2009) Membrane traffic within the Golgi apparatus, *Annu Rev Cell Dev Biol 25*, 113-132.

[14] Mendes, L. F. S., Fontana, N. A., Reddy, S. T., Uversky, V. N., and Costa-Filho, A. J. (2020) The exquisite structural biophysics of the Golgi reassembly and stacking proteins, *Int J Biol Macromol*.

[15] Wang, Y., Seemann, J., Pypaert, M., Shorter, J., and Warren, G. (2003) A direct role for GRASP65 as a mitotically regulated Golgi stacking factor, *EMBO J 22*, 3279-3290.

[16] Feinstein, T. N., and Linstedt, A. D. (2008) GRASP55 regulates Golgi ribbon formation, *Mol Biol Cell 19*, 2696-2707.

[17] Barr, F. A., Puype, M., Vandekerckhove, J., and Warren, G. (1997) GRASP65, a protein involved in the stacking of Golgi cisternae, *Cell 91*, 253-262.

[18] Shorter, J., Watson, R., Giannakou, M. E., Clarke, M., Warren, G., and Barr, F. A. (1999) GRASP55, a second mammalian GRASP protein involved in the stacking of Golgi cisternae in a cell-free system, *EMBO J 18*, 4949-4960.

[19] Grond, R., Veenendaal, T., Duran, J. M., Raote, I., van Es, J. H., Corstjens, S., Delfgou, L., El Haddouti, B., Malhotra, V., and Rabouille, C. (2020) The function of GORASPs in Golgi apparatus organization in vivo, *J Cell Biol 219*.

[20] Tie, H. C., Ludwig, A., Sandin, S., and Lu, L. (2018) The spatial separation of processing and transport functions to the interior and periphery of the Golgi stack, *Elife 7*.

[21] Kinseth, M. A., Anjard, C., Fuller, D., Guizzunti, G., Loomis, W. F., and Malhotra, V. (2007) The Golgi-associated protein GRASP is required for unconventional protein secretion during development, *Cell 130*, 524-534.

[22] Kondylis, V., Spoorendonk, K. M., and Rabouille, C. (2005) dGRASP localization and function in the early exocytic pathway in Drosophila S2 cells, *Mol Biol Cell 16*, 4061-4072.

[23] Behnia, R., Barr, F. A., Flanagan, J. J., Barlowe, C., and Munro, S. (2007) The yeast orthologue of GRASP65 forms a complex with a coiled-coil protein that contributes to ER to Golgi traffic, *Journal of Cell Biology 176*, 255-261.

[24] Wang, Y., Satoh, A., and Warren, G. (2005) Mapping the functional domains of the Golgi stacking factor GRASP65, *J Biol Chem 280*, 4921-4928.

[25] Struck, N. S., Herrmann, S., Langer, C., Krueger, A., Foth, B. J., Engelberg, K., Cabrera, A. L., Haase, S., Treeck, M., Marti, M., Cowman, A. F., Spielmann, T., and Gilberger, T. W. (2008) Plasmodium falciparum possesses two GRASP proteins that are differentially targeted to the Golgi complex via a higher- and lower-eukaryote-like mechanism, *J Cell Sci 121*, 2123-2129.

[26] Fanning, A. S., and Anderson, J. M. (1996) Protein-protein interactions: PDZ domain networks, *Curr Biol 6*, 1385-1388.

[27] Vinke, F. P., Grieve, A. G., and Rabouille, C. (2011) The multiple facets of the Golgi reassembly stacking proteins, *Biochem J 433*, 423-433.

[28] Truschel, S. T., Sengupta, D., Foote, A., Heroux, A., Macbeth, M. R., and Linstedt, A. D. (2011) Structure of the membrane-tethering GRASP domain reveals a unique PDZ ligand interaction that mediates Golgi biogenesis, *J Biol Chem 286*, 20125-20129.

[29] Feng, Y., Yu, W., Li, X., Lin, S., Zhou, Y., Hu, J., and Liu, X. (2013) Structural insight into Golgi membrane stacking by GRASP65 and GRASP55 proteins, *J Biol Chem 288*, 28418-28427.

[30] Wang, Z. H., Rabouille, C., and Geisbrecht, E. R. (2015) Loss of a Clueless-dGRASP complex results in ER stress and blocks Integrin exit from the perinuclear endoplasmic reticulum in Drosophila larval muscle, *Biol Open 4*, 636-648.

[31] Lane, J. D., Lucocq, J., Pryde, J., Barr, F. A., Woodman, P. G., Allan, V. J., and Lowe, M. (2002) Caspase-mediated cleavage of the stacking protein GRASP65 is required for Golgi fragmentation during apoptosis, *J Cell Biol 156*, 495-509.

[32] Bisel, B., Wang, Y., Wei, J. H., Xiang, Y., Tang, D., Miron-Mendoza, M., Yoshimura, S., Nakamura, N., and Seemann, J. (2008) ERK regulates Golgi and centrosome orientation towards the leading edge through GRASP65, *J Cell Biol 182*, 837-843.

[33] Uversky, V. N. (2013) Unusual biophysics of intrinsically disordered proteins, *Biochim Biophys Acta 1834*, 932-951.

[34] Mendes, L. F., Garcia, A. F., Kumagai, P. S., de Morais, F. R., Melo, F. A., Kmetzsch, L., Vainstein, M. H., Rodrigues, M. L., and Costa-Filho, A. J. (2016) New structural

insights into Golgi Reassembly and Stacking Protein (GRASP) in solution, *Sci Rep 6*, 29976.

[35] Schuldiner, M., Collins, S. R., Thompson, N. J., Denic, V., Bhamidipati, A., Punna, T., Ihmels, J., Andrews, B., Boone, C., Greenblatt, J. F., Weissman, J. S., and Krogan, N. J. (2005) Exploration of the function and organization of the yeast early secretory pathway through an epistatic miniarray profile, *Cell 123*, 507-519.

[36] Klumperman, J. (2000) Transport between ER and Golgi, *Curr Opin Cell Biol 12*, 445-449.

[37] D'Angelo, G., Prencipe, L., Iodice, L., Beznoussenko, G., Savarese, M., Marra, P., Di Tullio, G., Martire, G., De Matteis, M. A., and Bonatti, S. (2009) GRASP65 and GRASP55 sequentially promote the transport of C-terminal valine-bearing cargos to and through the Golgi complex, *J Biol Chem 284*, 34849-34860.

[38] Kooy, J., Toh, B. H., Pettitt, J. M., Erlich, R., and Gleeson, P. A. (1992) Human autoantibodies as reagents to conserved Golgi components. Characterization of a peripheral, 230-kDa compartment-specific Golgi protein, *J Biol Chem 267*, 20255-20263.

[39] Fritzler, M. J., Hamel, J. C., Ochs, R. L., and Chan, E. K. (1993) Molecular characterization of two human autoantigens: unique cDNAs encoding 95- and 160-kD proteins of a putative family in the Golgi complex, *J Exp Med 178*, 49-62.

[40] Seelig, H. P., Schranz, P., Schröter, H., Wiemann, C., and Renz, M. (1994) Macrogolgin--a new 376 kD Golgi complex outer membrane protein as target of antibodies in patients with rheumatic diseases and HIV infections, *J Autoimmun 7*, 67-91.

[41] Nakamura, N., Rabouille, C., Watson, R., Nilsson, T., Hui, N., Slusarewicz, P., Kreis, T. E., and Warren, G. (1995) Characterization of a cis-Golgi matrix protein, GM130, *J Cell Biol 131*, 1715-1726.

[42] Waters, M. G., and Pfeffer, S. R. (1999) Membrane tethering in intracellular transport, *Curr Opin Cell Biol 11*, 453-459.

[43] Gillingham, A. K., and Munro, S. (2003) Long coiled-coil proteins and membrane traffic, *Biochim Biophys Acta 1641*, 71-85.

[44] Rabouille, C. (2017) Pathways of Unconventional Protein Secretion, *Trends Cell Biol 27*, 230-240.

[45] Rabouille, C., Malhotra, V., and Nickel, W. (2012) Diversity in unconventional protein secretion, *J Cell Sci 125*, 5251-5255.

[46] McGrath, J. P., and Varshavsky, A. (1989) The yeast STE6 gene encodes a homologue of the mammalian multidrug resistance P-glycoprotein, *Nature 340*, 400-404.

[47] Kim, J., Gee, H. Y., and Lee, M. G. (2018) Unconventional protein secretion - new insights into the pathogenesis and therapeutic targets of human diseases, *J Cell Sci 131*.

[48] Giuliani, F., Grieve, A., and Rabouille, C. (2011) Unconventional secretion: a stress on GRASP, *Curr Opin Cell Biol 23*, 498-504.

[49] Kim, J., Gee, H. Y., and Lee, M. G. (2018) Unconventional protein secretion - new insights into the pathogenesis and therapeutic targets of human diseases, *Journal of Cell Science 131*.

[50] MJ, C., WJ, C., and PN, L. (2020) Through the back door: Unconventional protein secretion., *Cell Surface 6:100045*

[51] Xu, X., Zhao, Y., Kirkman, E., and Lin, X. (2016) Secreted Acb1 Contributes to the Yeast-to-Hypha Transition in Cryptococcus neoformans, *Appl Environ Microbiol 82*, 1069-1079.

[52] Anjard, C., and Loomis, W. F. (2005) Peptide signaling during terminal differentiation of Dictyostelium, *Proceedings of the National Academy of Sciences of the United States of America 102*, 7607-7611.

[53] Orij, R., Postmus, J., Ter Beek, A., Brul, S., and Smits, G. J. (2009) In vivo measurement of cytosolic and mitochondrial pH using a pH-sensitive GFP derivative in Saccharomyces cerevisiae reveals a relation between intracellular pH and growth, *Microbiology (Reading) 155*, 268-278.

[54] Bruns, C., McCaffery, J. M., Curwin, A. J., Duran, J. M., and Malhotra, V. (2011) Biogenesis of a novel compartment for autophagosome-mediated unconventional protein secretion, *J Cell Biol 195*, 979-992.

[55] Duran, J. M., Anjard, C., Stefan, C., Loomis, W. F., and Malhotra, V. (2010) Unconventional secretion of Acb1 is mediated by autophagosomes, *J Cell Biol 188*, 527-536.

[56] Cruz-Garcia, D., Curwin, A. J., Popoff, J. F., Bruns, C., Duran, J. M., and Malhotra, V. (2014) Remodeling of secretory compartments creates CUPS during nutrient starvation, *J Cell Biol 207*, 695-703.

[57] Curwin, A. J., Brouwers, N., Alonso Y Adell, M., Teis, D., Turacchio, G., Parashuraman, S., Ronchi, P., and Malhotra, V. (2016) ESCRT-III drives the final stages of CUPS maturation for unconventional protein secretion, *Elife 5*.

[58] Chiritoiu, M., Brouwers, N., Turacchio, G., Pirozzi, M., and Malhotra, V. (2019) GRASP55 and UPR Control Interleukin-1β Aggregation and Secretion, *Dev Cell 49*, 145-155.e144.

[59] New, J., and Thomas, S. M. (2019) Autophagy-dependent secretion: mechanism, factors secreted, and disease implications, *Autophagy 15*, 1682-1693.

[60] Schotman, H., Karhinen, L., and Rabouille, C. (2008) dGRASP-mediated noncanonical integrin secretion is required for Drosophila epithelial remodeling, *Dev Cell 14*, 171-182.

[61] Schotman, H., Karhinen, L., and Rabouille, C. (2009) Integrins mediate their unconventional, mechanical-stress-induced secretion via RhoA and PINCH in Drosophila, *J Cell Sci 122*, 2662-2672.

[62] Giuliani, G., Giuliani, F., Volk, T., and Rabouille, C. (2014) The Drosophila RNA-binding protein HOW controls the stability of dgrasp mRNA in the follicular epithelium, *Nucleic Acids Res 42*, 1970-1986.

[63] Gee, H. Y., Noh, S. H., Tang, B. L., Kim, K. H., and Lee, M. G. (2011) Rescue of ΔF508-CFTR trafficking via a GRASP-dependent unconventional secretion pathway, *Cell 146*, 746-760.

[64] Rebane, A. A., Ziltener, P., LaMonica, L. C., Bauer, A. H., Zheng, H., López-Montero, I., Pincet, F., Rothman, J. E., and Ernst, A. M. (2020) Liquid-liquid phase separation of the Golgi matrix protein GM130, *FEBS Lett 594*, 1132-1144.

[65] Ziltener, P., Rebane, A. A., Graham, M., Ernst, A. M., and Rothman, J. E. (2020) The golgin family exhibits a propensity to form condensates in living cells, *FEBS Lett 594*, 3086-3094.

[66] Rothman, J. E. (2019) Jim's View: Is the Golgi stack a phase-separated liquid crystal?, *FEBS Lett 593*, 2701-2705.

[67] Flory, P. J. (1941) Thermodynamics of High Polymer Solutions, *The Journal of Chemical Physics 9*.

[68] Huggins, M. L. (1942) Some properties of solutions of long-chain compounds, *Journal of Physical Chemistry 43*, 151-158.

[69] Brangwynne, C. P., Eckmann, C. R., Courson, D. S., Rybarska, A., Hoege, C., Gharakhani, J., Jülicher, F., and Hyman, A. A. (2009) Germline P granules are liquid droplets that localize by controlled dissolution/condensation, *Science 324*, 1729-1732.

[70] Brangwynne, C. P., Mitchison, T. J., and Hyman, A. A. (2011) Active liquid-like behavior of nucleoli determines their size and shape in Xenopus laevis oocytes, *Proc Natl Acad Sci U S A 108*, 4334-4339.

[71] Boeynaems, S., Alberti, S., Fawzi, N. L., Mittag, T., Polymenidou, M., Rousseau, F., Schymkowitz, J., Shorter, J., Wolozin, B., Van Den Bosch, L., Tompa, P., and Fuxreiter, M. (2018) Protein Phase Separation: A New Phase in Cell Biology, *Trends Cell Biol 28*, 420-435.

[72] Alberti, S., Gladfelter, A., and Mittag, T. (2019) Considerations and Challenges in Studying Liquid-Liquid Phase Separation and Biomolecular Condensates, *Cell 176*, 419-434.

[73] Shin, Y., and Brangwynne, C. P. (2017) Liquid phase condensation in cell physiology and disease, *Science 357*.

[74] Sanders, D. W., Kedersha, N., Lee, D. S. W., Strom, A. R., Drake, V., Riback, J. A., Bracha, D., Eeftens, J. M., Iwanicki, A., Wang, A., Wei, M. T., Whitney, G., Lyons, S. M., Anderson, P., Jacobs, W. M., Ivanov, P., and Brangwynne, C. P. (2020) Competing Protein-RNA Interaction Networks Control Multiphase Intracellular Organization, *Cell 181*, 306-324.e328.

[75] Brangwynne, C. P., Tompa, P., and Pappu, R. V. (2015) Polymer physics of intracellular phase transitions, *Nature Physics 11*, 899–904.

[76] Turoverov, K. K., Kuznetsova, I. M., Fonin, A. V., Darling, A. L., Zaslavsky, B. Y., and Uversky, V. N. (2019) Stochasticity of Biological Soft Matter: Emerging Concepts in Intrinsically Disordered Proteins and Biological Phase Separation, *Trends Biochem Sci 44*, 716-728.

[77] Fonin, A. V., Darling, A. L., Kuznetsova, I. M., Turoverov, K. K., and Uversky, V. N. (2018) Intrinsically disordered proteins in crowded milieu: when chaos prevails within the cellular gumbo, *Cell Mol Life Sci 75*, 3907-3929.

[78] Conicella, A. E., Zerze, G. H., Mittal, J., and Fawzi, N. L. (2016) ALS Mutations Disrupt Phase Separation Mediated by α-Helical Structure in the TDP-43 Low-Complexity C-Terminal Domain, *Structure 24*, 1537-1549.

[79] Zbinden, A., Pérez-Berlanga, M., De Rossi, P., and Polymenidou, M. (2020) Phase Separation and Neurodegenerative Diseases: A Disturbance in the Force, *Dev Cell 55*, 45-68.

[80] Rambourg, A., Clermont, Y., and Hermo, L. (1981) Three-dimensional structure of the Golgi apparatus, *Methods Cell Biol 23*, 155-166.

[81] Rambourg, A., and Clermont, Y. (1990) Three-dimensional electron microscopy: structure of the Golgi apparatus, *Eur J Cell Biol 51*, 189-200.

[82] Bachert, C., and Linstedt, A. D. (2010) Dual anchoring of the GRASP membrane tether promotes trans pairing, *J Biol Chem 285*, 16294-16301.

[83] Heinrich, F., Nanda, H., Goh, H. Z., Bachert, C., Lösche, M., and Linstedt, A. D. (2014) Myristoylation restricts orientation of the GRASP domain on membranes and promotes membrane tethering, *J Biol Chem 289*, 9683-9691.

[84] Levi, S. K., Bhattacharyya, D., Strack, R. L., Austin, J. R., and Glick, B. S. (2010) The yeast GRASP Grh1 colocalizes with COPII and is dispensable for organizing the secretory pathway, *Traffic 11*, 1168-1179.

[85] Dunker, A. K., Lawson, J. D., Brown, C. J., Williams, R. M., Romero, P., Oh, J. S., Oldfield, C. J., Campen, A. M., Ratliff, C. M., Hipps, K. W., Ausio, J., Nissen, M. S., Reeves, R., Kang, C., Kissinger, C. R., Bailey, R. W., Griswold, M. D., Chiu, W.,

Garner, E. C., and Obradovic, Z. (2001) Intrinsically disordered protein, *J Mol Graph Model 19*, 26-59.

[86] Dunker, A. K., Silman, I., Uversky, V. N., and Sussman, J. L. (2008) Function and structure of inherently disordered proteins, *Curr Opin Struct Biol 18*, 756-764.

[87] Permyakov, S. E., Bakunts, A. G., Denesyuk, A. I., Knyazeva, E. L., Uversky, V. N., and Permyakov, E. A. (2008) Apo-parvalbumin as an intrinsically disordered protein, *Proteins 72*, 822-836.

[88] Uversky, V. N. (2009) Intrinsically disordered proteins and their environment: effects of strong denaturants, temperature, pH, counter ions, membranes, binding partners, osmolytes, and macromolecular crowding, *Protein J 28*, 305-325.

[89] Perticaroli, S., Nickels, J. D., Ehlers, G., Mamontov, E., and Sokolov, A. P. (2014) Dynamics and rigidity in an intrinsically disordered protein, β-casein, *J Phys Chem B 118*, 7317-7326.

[90] Conchillo-Solé, O., de Groot, N. S., Avilés, F. X., Vendrell, J., Daura, X., and Ventura, S. (2007) AGGRESCAN: a server for the prediction and evaluation of "hot spots" of aggregation in polypeptides, *BMC Bioinformatics 8*, 65.

[91] Iakoucheva, L. M., and Dunker, A. K. (2003) Order, disorder, and flexibility: prediction from protein sequence, *Structure 11*, 1316-1317.

[92] Xue, B., Dunbrack, R. L., Williams, R. W., Dunker, A. K., and Uversky, V. N. (2010) PONDR-FIT: a meta-predictor of intrinsically disordered amino acids, *Biochim Biophys Acta 1804*, 996-1010.

[93] Lees, J. G., Smith, B. R., Wien, F., Miles, A. J., and Wallace, B. A. (2004) CDtool-an integrated software package for circular dichroism spectroscopic data processing, analysis, and archiving, *Anal Biochem 332*, 285-289.

[94] Sreerama, N., and Woody, R. W. (2000) Estimation of protein secondary structure from circular dichroism spectra: comparison of CONTIN, SELCON, and CDSSTR methods with an expanded reference set, *Anal Biochem 287*, 252-260.

[95] van Stokkum, I. H., Spoelder, H. J., Bloemendal, M., van Grondelle, R., and Groen, F. C. (1990) Estimation of protein secondary structure and error analysis from circular dichroism spectra, *Anal Biochem 191*, 110-118.

[96] Whitmore, L., and Wallace, B. A. (2004) DICHROWEB, an online server for protein secondary structure analyses from circular dichroism spectroscopic data, *Nucleic Acids Res 32*, W668-673.

[97] Whitmore, L., and Wallace, B. A. (2008) Protein secondary structure analyses from circular dichroism spectroscopy: methods and reference databases, *Biopolymers 89*, 392-400.

[98] Nilsson, M. R. (2004) Techniques to study amyloid fibril formation in vitro, *Methods 34*, 151-160.

[99] Finn, R. D., Bateman, A., Clements, J., Coggill, P., Eberhardt, R. Y., Eddy, S. R., Heger, A., Hetherington, K., Holm, L., Mistry, J., Sonnhammer, E. L., Tate, J., and Punta, M. (2014) Pfam: the protein families database, *Nucleic Acids Res 42*, D222-230.

[100] Theillet, F. X., Kalmar, L., Tompa, P., Han, K. H., Selenko, P., Dunker, A. K., Daughdrill, G. W., and Uversky, V. N. (2013) The alphabet of intrinsic disorder: I. Act like a Pro: On the abundance and roles of proline residues in intrinsically disordered proteins, *Intrinsically Disord Proteins 1*, e24360.

[101] Chakrabortee, S., Tripathi, R., Watson, M., Schierle, G. S., Kurniawan, D. P., Kaminski, C. F., Wise, M. J., and Tunnacliffe, A. (2012) Intrinsically disordered proteins as molecular shields, *Mol Biosyst 8*, 210-219.

[102] Woody, R. W. (2009) Circular dichroism spectrum of peptides in the poly(Pro)II conformation, *J Am Chem Soc 131*, 8234-8245.

[103] Kazakov, A. S., Markov, D. I., Gusev, N. B., and Levitsky, D. I. (2009) Thermally induced structural changes of intrinsically disordered small heat shock protein Hsp22, *Biophys Chem 145*, 79-85.

[104] Mendes, L. F. S., Basso, L. G. M., Kumagai, P. S., Fonseca-Maldonado, R., and Costa, A. J. (2018) Disorder-to-order transitions in the molten globule-like Golgi Reassembly and Stacking Protein, *Biochimica Et Biophysica Acta-General Subjects 1862*, 855-865.

[105] Bychkova, V. E., Basova, L. V., and Balobanov, V. A. (2014) How membrane surface affects protein structure, *Biochemistry (Mosc) 79*, 1483-1514.

[106] Cherepanov, D. A., Feniouk, B. A., Junge, W., and Mulkidjanian, A. Y. (2003) Low dielectric permittivity of water at the membrane interface: effect on the energy coupling mechanism in biological membranes, *Biophys J 85*, 1307-1316.

[107] Andrade, M. A., Chacón, P., Merelo, J. J., and Morán, F. (1993) Evaluation of secondary structure of proteins from UV circular dichroism spectra using an unsupervised learning neural network, *Protein Eng 6*, 383-390.

[108] Khechinashvili, N. N., Kabanov, A. V., Kondratyev, M. S., and Polozov, R. V. (2018) Thermodynamics of globular proteins, *J Biomol Struct Dyn 36*, 701-710.

[109] Lopes, J. L., Orcia, D., Araujo, A. P., DeMarco, R., and Wallace, B. A. (2013) Folding factors and partners for the intrinsically disordered protein micro-exon gene 14 (MEG-14), *Biophys J 104*, 2512-2520.

[110] Wu, H., and Fuxreiter, M. (2016) The Structure and Dynamics of Higher-Order Assemblies: Amyloids, Signalosomes, and Granules, *Cell 165*, 1055-1066.

[111] Bolognesi, B., Kumita, J. R., Barros, T. P., Esbjorner, E. K., Luheshi, L. M., Crowther, D. C., Wilson, M. R., Dobson, C. M., Favrin, G., and Yerbury, J. J. (2010) ANS binding reveals common features of cytotoxic amyloid species, *ACS Chem Biol 5*, 735-740.

[112] Morris, A. M., Watzky, M. A., and Finke, R. G. (2009) Protein aggregation kinetics, mechanism, and curve-fitting: a review of the literature, *Biochim Biophys Acta 1794*, 375-397.

[113] Gillam, J. E., and MacPhee, C. E. (2013) Modelling amyloid fibril formation kinetics: mechanisms of nucleation and growth, *J Phys Condens Matter 25*, 373101.

[114] Hawe, A., Sutter, M., and Jiskoot, W. (2008) Extrinsic fluorescent dyes as tools for protein characterization, *Pharm Res 25*, 1487-1499.

[115] Groenning, M., Olsen, L., van de Weert, M., Flink, J. M., Frokjaer, S., and Jørgensen, F. S. (2007) Study on the binding of Thioflavin T to beta-sheet-rich and non-beta-sheet cavities, *J Struct Biol 158*, 358-369.

[116] Klunk, W. E., Jacob, R. F., and Mason, R. P. (1999) Quantifying amyloid by congo red spectral shift assay, *Methods Enzymol 309*, 285-305.

[117] Chan, F. T. S., Pinotsi, D., S., K.-S. G., and Kaminski, C. F. (2014) Structure-Specific Intrinsic Fluorescence of Protein Amyloids Used to Study their Kinetics of Aggregation, *Protein Misfolding & Aggregation.*, 147–155.

[118] Pinotsi, D., Buell, A. K., Dobson, C. M., Kaminski Schierle, G. S., and Kaminski, C. F. (2013) A label-free, quantitative assay of amyloid fibril growth based on intrinsic fluorescence, *Chembiochem 14*, 846-850.

[119] Kumar, E. K., Haque, N., and Prabhu, N. P. (2017) Kinetics of protein fibril formation: Methods and mechanisms, *Int J Biol Macromol 100*, 3-10.

[120] Gejyo, F., Yamada, T., Odani, S., Nakagawa, Y., Arakawa, M., Kunitomo, T., Kataoka, H., Suzuki, M., Hirasawa, Y., and Shirahama, T. (1985) A new form of amyloid protein associated with chronic hemodialysis was identified as beta 2-microglobulin, *Biochem Biophys Res Commun 129*, 701-706.

[121] Galvagnion, C., Buell, A. K., Meisl, G., Michaels, T. C., Vendruscolo, M., Knowles, T. P., and Dobson, C. M. (2015) Lipid vesicles trigger α-synuclein aggregation by stimulating primary nucleation, *Nat Chem Biol 11*, 229-234.

[122] O'Rourke, T. W., and Reines, D. (2016) Determinants of Amyloid Formation for the Yeast Termination Factor Nab3, *PLoS One 11*, e0150865.

[123] Fowler, D. M., Koulov, A. V., Balch, W. E., and Kelly, J. W. (2007) Functional amyloid--from bacteria to humans, *Trends Biochem Sci 32*, 217-224.

[124] Dominguez, A., Varona, R. M., Villanueva, J. R., and Sentandreu, R. (1982) Mutants of Saccharomyces cerevisiae cell division cycle defective in cytokinesis. Biosynthesis of the cell wall and morphology, *Antonie Van Leeuwenhoek 48*, 145-157.

[125] Koo, E. H., Lansbury, P. T., and Kelly, J. W. (1999) Amyloid diseases: Abnormal protein aggregation in neurodegeneration, *Proceedings of the National Academy of Sciences of the United States of America 96*, 9989-9990.

[126] Cereghetti, G., Saad, S., Dechant, R., and Peter, M. (2018) Reversible, functional amyloids: towards an understanding of their regulation in yeast and humans, *Cell Cycle 17*, 1545-1558.

[127] Iadanza, M. G., Jackson, M. P., Hewitt, E. W., Ranson, N. A., and Radford, S. E. (2018) A new era for understanding amyloid structures and disease, *Nature Reviews Molecular Cell Biology 19*, 755-773.

[128] Almeida, Z. L., and Brito, R. M. M. (2020) Structure and Aggregation Mechanisms in Amyloids, *Molecules 25*.

[129] Alberti, S., Halfmann, R., and Lindquist, S. (2010) BIOCHEMICAL, CELL BIOLOGICAL, AND GENETIC ASSAYS TO ANALYZE AMYLOID AND PRION AGGREGATION IN YEAST, *Methods in Enzymology, Vol 470: Guide to Yeast Genetics:: Functional Genomics, Proteomics, and Other Systems Analysis, 2nd Edition 470*, 709-734.

[130] Elghetany, M. T., and Saleem, A. (1988) METHODS FOR STAINING AMYLOID IN TISSUES - A REVIEW, *Stain Technology 63*, 201-212.

[131] Reiman, E. M., and Jagust, W. J. (2012) Brain imaging in the study of Alzheimer's disease, *Neuroimage 61*, 505-516.

[132] Chan, F. T. S., Schierle, G. S. K., Kumita, J. R., Bertoncini, C. W., Dobson, C. M., and Kaminski, C. F. (2013) Protein amyloids develop an intrinsic fluorescence signature during aggregation, *Analyst 138*, 2156-2162.

[133] Esbjorner, E. K., Chan, F., Rees, E., Erdelyi, M., Luheshi, L. M., Bertoncini, C. W., Kaminski, C. F., Dobson, C. M., and Schierle, G. S. K. (2014) Direct Observations of Amyloid beta Self-Assembly in Live Cells Provide Insights into Differences in the Kinetics of A beta(1-40) and A beta(1-42) Aggregation, *Chemistry & Biology 21*, 732-742.

[134] Schierle, G. S. K., Bertoncini, C. W., Chan, F. T. S., van der Goot, A. T., Schwedler, S., Skepper, J., Schlachter, S., van Ham, T., Esposito, A., Kumita, J. R., Nollen, E. A. A., Dobson, C. M., and Kaminski, C. F. (2011) A FRET Sensor for Non-Invasive Imaging of Amyloid Formation in Vivo, *Chemphyschem 12*, 673-680.

[135] Viotti, C. (2016) ER to Golgi-Dependent Protein Secretion: The Conventional Pathway, *Methods Mol Biol 1459*, 3-29.

[136] Rabouille, C., Malhotra, V., and Nickel, W. (2012) Diversity in unconventional protein secretion, *Journal of Cell Science 125*, 5251-5255.

[137] Nickel, W., and Rabouille, C. (2009) Mechanisms of regulated unconventional protein secretion, *Nature Reviews Molecular Cell Biology 10*, 148-155.

[138] Brough, D., Pelegrin, P., and Nickel, W. (2017) An emerging case for membrane pore formation as a common mechanism for the unconventional secretion of FGF2 and IL-1 beta, *Journal of Cell Science 130*, 3197-3202.

[139] Malhotra, V. (2013) Unconventional protein secretion: an evolving mechanism, *Embo Journal 32*, 1660-1664.

[140] Cruz-Garcia, D., Malhotra, V., and Curwin, A. J. (2018) Unconventional protein secretion triggered by nutrient starvation, *Seminars in Cell & Developmental Biology 83*, 22-28.

[141] Fontana, N. A., Fonseca-Maldonado, R., Mendes, L. F. S., Meleiro, L. P., and Costa, A. J. (2018) The yeast GRASP Grh1 displays a high polypeptide backbone mobility along with an amyloidogenic behavior, *Scientific Reports 8*.

[142] Reddy, S. T., Uversky, V. N., and Costa-Filho, A. J. (2020) Biophysical characterization of intrinsically disordered human Golgi matrix protein GRASP65, *Int J Biol Macromol 162*, 1982-1993.

[143] Mendes, L. F. S., Fontana, N. A., Oliveira, C. G., Freire, M., Lopes, J. L. S., Melo, F. A., and Costa-Filho, A. J. (2019) The GRASP domain in golgi reassembly and stacking proteins: differences and similarities between lower and higher Eukaryotes, *Febs Journal 286*, 3340-3358.

[144] Mendes, L. F. S., Batista, M. R. B., Judge, P. J., Watts, A., Redfield, C., and Costa, A. J. (2020) Conformational flexibility of GRASPs and their constituent PDZ subdomains reveals structural basis of their promiscuous interactome, *Febs Journal 287*, 3255-3272.

[145] Reddy, S. T., Mendes, L. F. S., Fontana, N. A., and Costa, A. J. (2019) Exploring structural aspects of the human Golgi matrix protein GRASP55 in solution, *International Journal of Biological Macromolecules 135*, 481-489.

[146] Reddy, S. T., Uversky, V. N., and Costa-Filho, A. J. (2020) Nucleation-dependent amyloid fibrillation of human GRASP55 in aqueous solution, *European Biophysics Journal with Biophysics Letters 49*, 133-143.

[147] Cruz-Garcia, D., Curwin, A. J., Popoff, J. F., Bruns, C., Duran, J. M., and Malhotra, V. (2014) Remodeling of secretory compartments creates CUPS during nutrient starvation, *Journal of Cell Biology 207*, 695-703.

[148] Lindquist, S. (1986) THE HEAT-SHOCK RESPONSE, *Annual Review of Biochemistry 55*, 1151-1191.

[149] Rueden, C. T., Schindelin, J., Hiner, M. C., DeZonia, B. E., Walter, A. E., Arena, E. T., and Eliceiri, K. W. (2017) ImageJ2: ImageJ for the next generation of scientific image data, *BMC Bioinformatics 18*, 529.

[150] Wilks, J. C., and Slonczewski, J. L. (2007) pH of the cytoplasm and periplasm of Escherichia coli: rapid measurement by green fluorescent protein fluorimetry, *J Bacteriol 189*, 5601-5607.

[151] Jain, A., Blum, C., and Subramaniam, V. (2009) Fluorescence Lifetime Spectroscopy and Imaging of Visible Fluorescent Proteins, In *Advances in Biomedical Engineering* (Elsevier, Ed.), pp 147-176.

[152] Venters, B. J., Wachi, S., Mavrich, T. N., Andersen, B. E., Jena, P., Sinnamon, A. J., Jain, P., Rolleri, N. S., Jiang, C., Hemeryck-Walsh, C., and Pugh, B. F. (2011) A comprehensive genomic binding map of gene and chromatin regulatory proteins in Saccharomyces, *Mol Cell 41*, 480-492.

[153] Vernon, R. M., Chong, P. A., Tsang, B., Kim, T. H., Bah, A., Farber, P., Lin, H., and Forman-Kay, J. D. (2018) Pi-Pi contacts are an overlooked protein feature relevant to phase separation, *Elife 7*.

[154] Vernon, R. M., and Forman-Kay, J. D. (2019) First-generation predictors of biological protein phase separation, *Curr Opin Struct Biol 58*, 88-96.

[155] van Mierlo, G., Jansen, J. R. G., Wang, J., Poser, I., van Heeringen, S. J., and Vermeulen, M. (2021) Predicting protein condensate formation using machine learning, *Cell Rep 34*, 108705.

[156] Wang, Z., Zhang, G., and Zhang, H. (2018) Protocol for Analyzing Protein Liquid-liquid Phase SEparation, *Biophysics Reports 5*, 1-9.

[157] Ellis, R. J. (2001) Macromolecular crowding: obvious but underappreciated, *Trends Biochem Sci 26*, 597-604.

[158] Patel, A., Lee, H. O., Jawerth, L., Maharana, S., Jahnel, M., Hein, M. Y., Stoynov, S., Mahamid, J., Saha, S., Franzmann, T. M., Pozniakovski, A., Poser, I., Maghelli, N., Royer, L. A., Weigert, M., Myers, E. W., Grill, S., Drechsel, D., Hyman, A. A., and Alberti, S. (2015) A Liquid-to-Solid Phase Transition of the ALS Protein FUS Accelerated by Disease Mutation, *Cell 162*, 1066-1077.

[159] Wegmann, S., Eftekharzadeh, B., Tepper, K., Zoltowska, K. M., Bennett, R. E., Dujardin, S., Laskowski, P. R., MacKenzie, D., Kamath, T., Commins, C., Vanderburg, C., Roe, A. D., Fan, Z., Molliex, A. M., Hernandez-Vega, A., Muller, D., Hyman, A. A., Mandelkow, E., Taylor, J. P., and Hyman, B. T. (2018) Tau protein liquid-liquid phase separation can initiate tau aggregation, *EMBO J 37*.

[160] Babinchak, W. M., Haider, R., Dumm, B. K., Sarkar, P., Surewicz, K., Choi, J. K., and Surewicz, W. K. (2019) The role of liquid-liquid phase separation in aggregation of the TDP-43 low-complexity domain, *J Biol Chem 294*, 6306-6317.

[161] Orij, R., Brul, S., and Smits, G. J. (2011) Intracellular pH is a tightly controlled signal in yeast, *Biochim Biophys Acta 1810*, 933-944.

[162] Oates, M. E., Romero, P., Ishida, T., Ghalwash, M., Mizianty, M. J., Xue, B., Dosztányi, Z., Uversky, V. N., Obradovic, Z., Kurgan, L., Dunker, A. K., and Gough, J. (2013) D^2P^2: database of disordered protein predictions, *Nucleic Acids Res 41*, D508-516.

[163] Walsh, I., Martin, A. J., Di Domenico, T., and Tosatto, S. C. (2012) ESpritz: accurate and fast prediction of protein disorder, *Bioinformatics 28*, 503-509.

[164] Dosztányi, Z., Csizmók, V., Tompa, P., and Simon, I. (2005) The pairwise energy content estimated from amino acid composition discriminates between folded and intrinsically unstructured proteins, *J Mol Biol 347*, 827-839.

[165] Ghalwash, M. F., Dunker, A. K., and Obradović, Z. (2012) Uncertainty analysis in protein disorder prediction, *Mol Biosyst 8*, 381-391.

[166] Ishida, T., and Kinoshita, K. (2007) PrDOS: prediction of disordered protein regions from amino acid sequence, *Nucleic Acids Res 35*, W460-464.

[167] Peng, K., Radivojac, P., Vucetic, S., Dunker, A. K., and Obradovic, Z. (2006) Length-dependent prediction of protein intrinsic disorder, *BMC Bioinformatics 7*, 208.

[168] Romero, P., Obradovic, Z., Li, X., Garner, E. C., Brown, C. J., and Dunker, A. K. (2001) Sequence complexity of disordered protein, *Proteins 42*, 38-48.

[169] Simm, D., Hatje, K., and Kollmar, M. (2015) Waggawagga: comparative visualization of coiled-coil predictions and detection of stable single α-helices (SAH domains), *Bioinformatics 31*, 767-769.

[170] Fakhree, M. A. A., Blum, C., and Claessens, M. M. A. E. (2019) Shaping membranes with disordered proteins, *Arch Biochem Biophys 677*, 108163.

[171] Moutevelis, E., and Woolfson, D. N. (2009) A periodic table of coiled-coil protein structures, *J Mol Biol 385*, 726-732.

[172] Papanikou, E., and Glick, B. S. (2009) The yeast Golgi apparatus: insights and mysteries, *FEBS Lett 583*, 3746-3751.

[173] Singh, A., Upadhyay, V., Upadhyay, A. K., Singh, S. M., and Panda, A. K. (2015) Protein recovery from inclusion bodies of Escherichia coli using mild solubilization process, *Microb Cell Fact 14*, 41.

[174] Greenfield, N. J. (2006) Using circular dichroism spectra to estimate protein secondary structure, *Nat Protoc 1*, 2876-2890.

[175] Vivian, J. T., and Callis, P. R. (2001) Mechanisms of tryptophan fluorescence shifts in proteins, *Biophys J 80*, 2093-2109.

[176] Palade, G. (1975) INTRACELLULAR ASPECTS OF PROCESS OF PROTEIN-SYNTHESIS, *Science 189*, 347-358.

[177] Chalfie, M., Tu, Y., Euskirchen, G., Ward, W. W., and Prasher, D. C. (1994) Green fluorescent protein as a marker for gene expression, *Science 263*, 802-805.

[178] Misteli, T. (2001) The concept of self-organization in cellular architecture, *J Cell Biol 155*, 181-185.

[179] Rabouille, C., Misteli, T., Watson, R., and Warren, G. (1995) Reassembly of Golgi stacks from mitotic Golgi fragments in a cell-free system, *J Cell Biol 129*, 605-618.

[180] Lee, I., Tiwari, N., Dunlop, M. H., Graham, M., Liu, X. R., and Rothman, J. E. (2014) Membrane adhesion dictates Golgi stacking and cisternal morphology, *Proceedings*

of the National Academy of Sciences of the United States of America 111, 1849-1854.

[181] Rabouille, C., and Linstedt, A. (2016) GRASP: A Multitasking Tether, *Frontiers in Cell and Developmental Biology 4*.

[182] Zhang, X. Y., and Wang, Y. Z. (2016) GRASPs in Golgi Structure and Function, *Frontiers in Cell and Developmental Biology 3*.

[183] Wu, H., Li, T., and Zhao, J. (2020) GRASP55: A Multifunctional Protein, *Curr Protein Pept Sci 21*, 544-552.

[184] Short, B., Preisinger, C., Korner, R., Kopajtich, R., Byron, O., and Barr, F. A. (2001) A GRASP55-rab2 effector complex linking Golgi structure to membrane traffic, *Journal of Cell Biology 155*, 877-883.

[185] Kuo, A., Zhong, C. L., Lane, W. S., and Derynck, R. (2000) Transmembrane transforming growth factor-alpha tethers to the PDZ domain-containing, Golgi membrane-associated protein p59/GRASP55, *Embo Journal 19*, 6427-6439.

[186] Xiang, Y., and Wang, Y. Z. (2010) GRASP55 and GRASP65 play complementary and essential roles in Golgi cisternal stacking, *Journal of Cell Biology 188*, 237-251.

[187] Jarvela, T., and Linstedt, A. D. (2014) Isoform-specific tethering links the Golgi ribbon to maintain compartmentalization, *Molecular Biology of the Cell 25*, 133-144.

[188] Bekier, M. E., Wang, L. B., Li, J., Huang, H. R., Tang, D. M., Zhang, X. Y., and Wang, Y. Z. (2017) Knockout of the Golgi stacking proteins GRASP55 and GRASP65 impairs Golgi structure and function, *Molecular Biology of the Cell 28*, 2833-2842.

[189] Veenendaal, T., Jarvela, T., Grieve, A. G., van Es, J. H., Linstedt, A. D., and Rabouille, C. (2014) GRASP65 controls the cis Golgi integrity in vivo, *Biology Open 3*, 431-443.

[190] Barr, F. A., Preisinger, C., Kopajtich, R., and Korner, R. (2001) Golgi matrix proteins interact with p24 cargo receptors and aid their efficient retention in the Golgi apparatus, *Journal of Cell Biology 155*, 885-891.

[191] Xiang, Y., Zhang, X., Nix, D. B., Katoh, T., Aoki, K., Tiemeyer, M., and Wang, Y. (2013) Regulation of protein glycosylation and sorting by the Golgi matrix proteins GRASP55/65, *Nat Commun 4*, 1659.

[192] Cabral, M., Anjard, C., Malhotra, V., Loomis, W. F., and Kuspa, A. (2010) Unconventional Secretion of AcbA in Dictyostelium discoideum through a Vesicular Intermediate, *Eukaryotic Cell 9*, 1009-1017.

[193] Hwang, T. C., and Kirk, K. L. (2013) The CFTR ion channel: gating, regulation, and anion permeation, *Cold Spring Harb Perspect Med 3*, a009498.

[194] Gadsby, D. C., Vergani, P., and Csanády, L. (2006) The ABC protein turned chloride channel whose failure causes cystic fibrosis, *Nature 440*, 477-483.

[195] Gee, H. Y., Noh, S. H., Tang, B. L., Kim, K. H., and Lee, M. G. (2011) Rescue of Delta F508-CFTR Trafficking via a GRASP-Dependent Unconventional Secretion Pathway, *Cell 146*, 746-760.

[196] Schotman, H., Karhinen, L., and Rabouille, C. (2009) Integrins mediate their unconventional, mechanical-stress-induced secretion via RhoA and PINCH in Drosophila, *Journal of Cell Science 122*, 2662-2672.

[197] Ahat, E., Li, J., and Wang, Y. Z. (2019) New Insights Into the Golgi Stacking Proteins, *Frontiers in Cell and Developmental Biology 7*.

[198] Zhang, X. Y., and Wang, Y. Z. (2018) The Golgi stacking protein GORASP2/GRASP55 serves as an energy sensor to promote autophagosome maturation under glucose starvation, *Autophagy 14*, 1649-1651.

[199] Emebo, D., and Wang, Y. (2020) Cytosolic Ca2+ modulates Golgi structure through PKC α -mediated GRASP55 phosphorylation, *ISCIENCE*

[200] Szklarczyk, D., Gable, A. L., Lyon, D., Junge, A., Wyder, S., Huerta-Cepas, J., Simonovic, M., Doncheva, N. T., Morris, J. H., Bork, P., Jensen, L. J., and Mering, C. V. (2019) STRING v11: protein-protein association networks with increased coverage, supporting functional discovery in genome-wide experimental datasets, *Nucleic Acids Res 47*, D607-D613.

[201] Shorter, J., Watson, R., Giannakou, M. E., Clarke, M., Warren, G., and Barr, F. A. (1999) GRASP55, a second mammalian GRASP protein involved in the stacking of Golgi cisternae in a cell-free system, *Embo Journal 18*, 4949-4960.

[202] Tang, D., Yuan, H., and Wang, Y. (2010) The role of GRASP65 in Golgi cisternal stacking and cell cycle progression, *Traffic 11*, 827-842.

[203] Uversky, V. N., Gillespie, J. R., and Fink, A. L. (2000) Why are "natively unfolded" proteins unstructured under physiologic conditions?, *Proteins 41*, 415-427.

[204] Tompa, P. (2002) Intrinsically unstructured proteins, *Trends Biochem Sci 27*, 527-533.

[205] Peng, Z., Yan, J., Fan, X., Mizianty, M. J., Xue, B., Wang, K., Hu, G., Uversky, V. N., and Kurgan, L. (2015) Exceptionally abundant exceptions: comprehensive characterization of intrinsic disorder in all domains of life, *Cell Mol Life Sci 72*, 137-151.

[206] Dunker, A. K., Brown, C. J., and Obradovic, Z. (2002) Identification and functions of usefully disordered proteins, *Adv Protein Chem 62*, 25-49.

[207] Dunker, A. K., Brown, C. J., Lawson, J. D., Iakoucheva, L. M., and Obradović, Z. (2002) Intrinsic disorder and protein function, *Biochemistry 41*, 6573-6582.

[208] Wright, P. E., and Dyson, H. J. (2015) Intrinsically disordered proteins in cellular signalling and regulation, *Nat Rev Mol Cell Biol 16*, 18-29.

[209] Uversky, V. N. (2013) Intrinsic disorder-based protein interactions and their modulators, *Curr Pharm Des 19*, 4191-4213.

[210] Coelho-Cerqueira, E., Carmo-Gonçalves, P., Pinheiro, A. S., Cortines, J., and Follmer, C. (2013) α-Synuclein as an intrinsically disordered monomer--fact or artefact?, *FEBS J 280*, 4915-4927.

[211] Redwan, E. M., Xue, B., Almehdar, H. A., and Uversky, V. N. (2015) Disorder in milk proteins: caseins, intrinsically disordered colloids, *Curr Protein Pept Sci 16*, 228-242.

[212] Sieber, T., Scholz, R., Spoerner, M., Schumann, F., Kalbitzer, H. R., and Dobner, T. (2011) Intrinsic disorder in the common N-terminus of human adenovirus 5 E1B-55K and its related E1BN proteins indicated by studies on E1B-93R, *Virology 418*, 133-143.

[213] Hamdi, K., Salladini, E., O'Brien, D. P., Brier, S., Chenal, A., Yacoubi, I., and Longhi, S. (2017) Structural disorder and induced folding within two cereal, ABA stress and ripening (ASR) proteins, *Sci Rep 7*, 15544.

[214] Zhang, X., Wang, L., Ireland, S. C., Ahat, E., Li, J., Bekier, M. E., Zhang, Z., and Wang, Y. (2019) GORASP2/GRASP55 collaborates with the PtdIns3K UVRAG complex to facilitate autophagosome-lysosome fusion, *Autophagy 15*, 1787-1800.

[215] Sipe, J. D., and Cohen, A. S. (2000) Review: history of the amyloid fibril, *J Struct Biol 130*, 88-98.

[216] Chiti, F., and Dobson, C. M. (2006) Protein misfolding, functional amyloid, and human disease, *Annu Rev Biochem 75*, 333-366.

[217] Munder, M. C., Midtvedt, D., Franzmann, T., Nüske, E., Otto, O., Herbig, M., Ulbricht, E., Müller, P., Taubenberger, A., Maharana, S., Malinovska, L., Richter, D., Guck, J., Zaburdaev, V., and Alberti, S. (2016) A pH-driven transition of the cytoplasm from a fluid- to a solid-like state promotes entry into dormancy, *Elife 5*.

[218] Lee, H. J., and Zheng, J. J. (2010) PDZ domains and their binding partners: structure, specificity, and modification, *Cell Commun Signal 8*, 8.

[219] Liu, X., and Fuentes, E. J. (2019) Emerging Themes in PDZ Domain Signaling: Structure, Function, and Inhibition, *Int Rev Cell Mol Biol 343*, 129-218.

[220] Chi, C. N., Bach, A., Strømgaard, K., Gianni, S., and Jemth, P. (2012) Ligand binding by PDZ domains, *Biofactors 38*, 338-348.

[221] Truschel, S. T., Zhang, M., Bachert, C., Macbeth, M. R., and Linstedt, A. D. (2012) Allosteric regulation of GRASP protein-dependent Golgi membrane tethering by mitotic phosphorylation, *J Biol Chem 287*, 19870-19875.

[222] Hu, F., Shi, X., Li, B., Huang, X., Morelli, X., and Shi, N. (2015) Structural basis for the interaction between the Golgi reassembly-stacking protein GRASP65 and the Golgi matrix protein GM130, *J Biol Chem 290*, 26373-26382.

[223] Barr, F. A., Nakamura, N., and Warren, G. (1998) Mapping the interaction between GRASP65 and GM130, components of a protein complex involved in the stacking of Golgi cisternae, *EMBO J 17*, 3258-3268.

[224] Zhao, J., Li, B., Huang, X., Morelli, X., and Shi, N. (2017) Structural Basis for the Interaction between Golgi Reassembly-stacking Protein GRASP55 and Golgin45, *J Biol Chem 292*, 2956-2965.

[225] Sengupta, D., Truschel, S., Bachert, C., and Linstedt, A. D. (2009) Organelle tethering by a homotypic PDZ interaction underlies formation of the Golgi membrane network, *J Cell Biol 186*, 41-55.

[226] Resh, M. D. (1999) Fatty acylation of proteins: new insights into membrane targeting of myristoylated and palmitoylated proteins, *Biochim Biophys Acta 1451*, 1-16.

[227] Kim, J., Noh, S. H., Piao, H., Kim, D. H., Kim, K., Cha, J. S., Chung, W. Y., Cho, H. S., Kim, J. Y., and Lee, M. G. (2016) Monomerization and ER Relocalization of GRASP Is a Requisite for Unconventional Secretion of CFTR, *Traffic 17*, 733-753.

[228] Sutterlin, C., Polishchuk, R., Pecot, M., and Malhotra, V. (2005) The Golgi-associated protein GRASP65 regulates spindle dynamics and is essential for cell division, *Molecular Biology of the Cell 16*, 3211-3222.

[229] Sengupta, D., and Linstedt, A. D. (2010) Mitotic inhibition of GRASP65 organelle tethering involves Polo-like kinase 1 (PLK1) phosphorylation proximate to an internal PDZ ligand, *J Biol Chem 285*, 39994-40003.

[230] Zhang, X., Wang, L., Lak, B., Li, J., Jokitalo, E., and Wang, Y. (2018) GRASP55 Senses Glucose Deprivation through O-GlcNAcylation to Promote Autophagosome-Lysosome Fusion, *Dev Cell 45*, 245-261.e246.

[231] Tang, D., Zhang, X., Huang, S., Yuan, H., Li, J., and Wang, Y. (2016) Mena-GRASP65 interaction couples actin polymerization to Golgi ribbon linking, *Mol Biol Cell 27*, 137-152.

[232] Cheng, J. P., Betin, V. M., Weir, H., Shelmani, G. M., Moss, D. K., and Lane, J. D. (2010) Caspase cleavage of the Golgi stacking factor GRASP65 is required for Fas/CD95-mediated apoptosis, *Cell Death Dis 1*, e82.

[233] Ayala, I., Crispino, R., and Colanzi, A. (2019) GRASP65 controls Golgi position and structure during G2/M transition by regulating the stability of microtubules, *Traffic 20*, 785-802.

[234] Barlow, L. D., Nývltová, E., Aguilar, M., Tachezy, J., and Dacks, J. B. (2018) A sophisticated, differentiated Golgi in the ancestor of eukaryotes, *BMC Biol 16*, 27.

[235] Jurk, C. M., Roske, Y., and Heinemann, U. (2018) Crystal Structures of the Single PDZ Domains from GRASP65 and their Interaction with the Golgin GM130, *Croat. Chem. Acta 91(2)*, 255–264.

[236] Dementieva, I. S., Tereshko, V., McCrossan, Z. A., Solomaha, E., Araki, D., Xu, C., Grigorieff, N., and Goldstein, S. A. (2009) Pentameric assembly of potassium channel tetramerization domain-containing protein 5, *J Mol Biol 387*, 175-191.

[237] Piao, H., Kim, J., Noh, S. H., Kweon, H. S., Kim, J. Y., and Lee, M. G. (2017) Sec16A is critical for both conventional and unconventional secretion of CFTR, *Sci Rep 7*, 39887.

[238] Cartier-Michaud, A., Bailly, A. L., Betzi, S., Shi, X., Lissitzky, J. C., Zarubica, A., Sergé, A., Roche, P., Lugari, A., Hamon, V., Bardin, F., Derviaux, C., Lembo, F., Audebert, S., Marchetto, S., Durand, B., Borg, J. P., Shi, N., Morelli, X., and Aurrand-Lions, M. (2017) Genetic, structural, and chemical insights into the dual function of GRASP55 in germ cell Golgi remodeling and JAM-C polarized localization during spermatogenesis, *PLoS Genet 13*, e1006803.

[239] Roghi, C., Jones, L., Gratian, M., English, W. R., and Murphy, G. (2010) Golgi reassembly stacking protein 55 interacts with membrane-type (MT) 1-matrix metalloprotease (MMP) and furin and plays a role in the activation of the MT1-MMP zymogen, *FEBS J 277*, 3158-3175.

[240] Li, J., Tang, D., Ireland, S. C., and Wang, Y. (2019) DjA1 maintains Golgi integrity via interaction with GRASP65, *Mol Biol Cell 30*, 478-490.

[241] RM, W., Z, O., V, M., W, B., EC, G., J, Y., S, T., CJ, B., and AK, D. (2001) The protein folding problem: amino acid determinants of intrinsic order and disorder, *Pac Symp Biocomput.* , 89-100.

[242] Radivojac, P., Iakoucheva, L. M., Oldfield, C. J., Obradovic, Z., Uversky, V. N., and Dunker, A. K. (2007) Intrinsic disorder and functional proteomics, *Biophys J 92*, 1439-1456.

[243] Vacic, V., Uversky, V. N., Dunker, A. K., and Lonardi, S. (2007) Composition Profiler: a tool for discovery and visualization of amino acid composition differences, *BMC Bioinformatics 8*, 211.

[244] Obradovic, Z., Peng, K., Vucetic, S., Radivojac, P., and Dunker, A. K. (2005) Exploiting heterogeneous sequence properties improves prediction of protein disorder, *Proteins 61 Suppl 7*, 176-182.

[245] Dosztányi, Z., Csizmok, V., Tompa, P., and Simon, I. (2005) IUPred: web server for the prediction of intrinsically unstructured regions of proteins based on estimated energy content, *Bioinformatics 21*, 3433-3434.

[246] Mészáros, B., Erdos, G., and Dosztányi, Z. (2018) IUPred2A: context-dependent prediction of protein disorder as a function of redox state and protein binding, *Nucleic Acids Res 46*, W329-W337.

[247] Oldfield, C. J., Cheng, Y., Cortese, M. S., Romero, P., Uversky, V. N., and Dunker, A. K. (2005) Coupled folding and binding with alpha-helix-forming molecular recognition elements, *Biochemistry 44*, 12454-12470.

[248] Cheng, Y., Oldfield, C. J., Meng, J., Romero, P., Uversky, V. N., and Dunker, A. K. (2007) Mining alpha-helix-forming molecular recognition features with cross species sequence alignments, *Biochemistry 46*, 13468-13477.

[249] Mészáros, B., Simon, I., and Dosztányi, Z. (2009) Prediction of protein binding regions in disordered proteins, *PLoS Comput Biol 5*, e1000376.

[250] Dosztányi, Z., Mészáros, B., and Simon, I. (2009) ANCHOR: web server for predicting protein binding regions in disordered proteins, *Bioinformatics 25*, 2745-2746.

Appendix

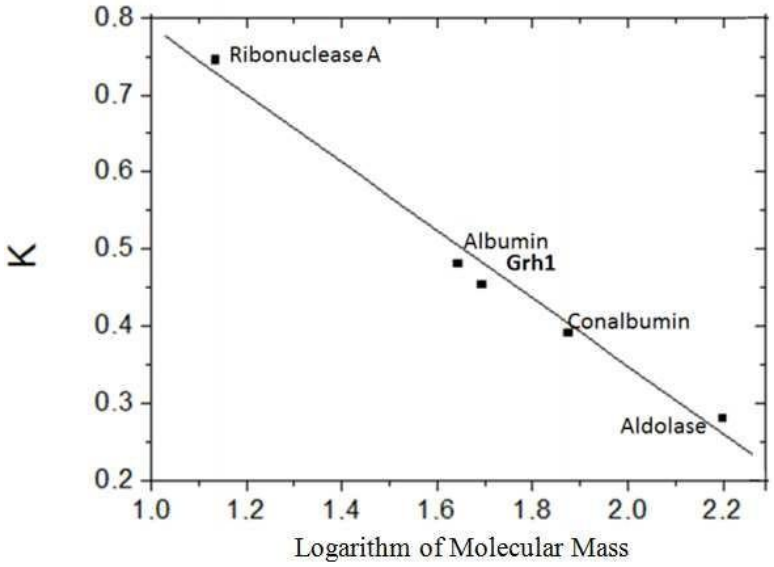

Supplementary Figure 1: Relationship between the partition coefficient (K) and the logarithm of Molecular Mass

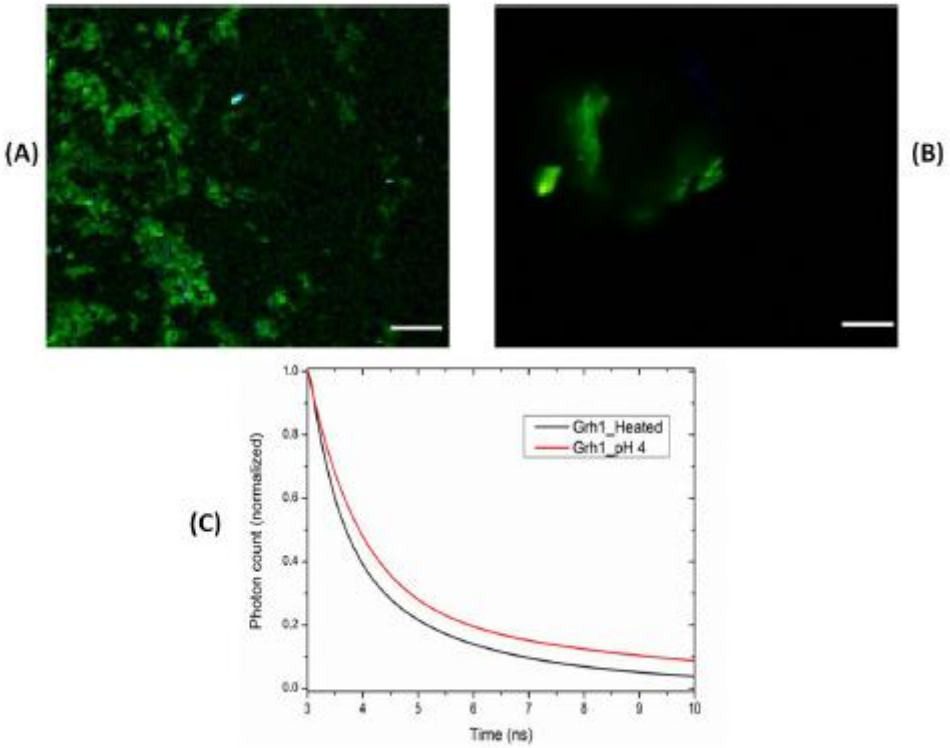

Supplementary Figure 2: Grh1 fibrillates *in vitro* in different conditions. FLIM images of purified Grh1 excited at 375 nm. **(A)** Heated to 37°C. **(B)** At pH 4. **(C)** Time decays of fluorescence for heated Grh1 (black) and at pH 4 (red). Scale bar: 10 µm

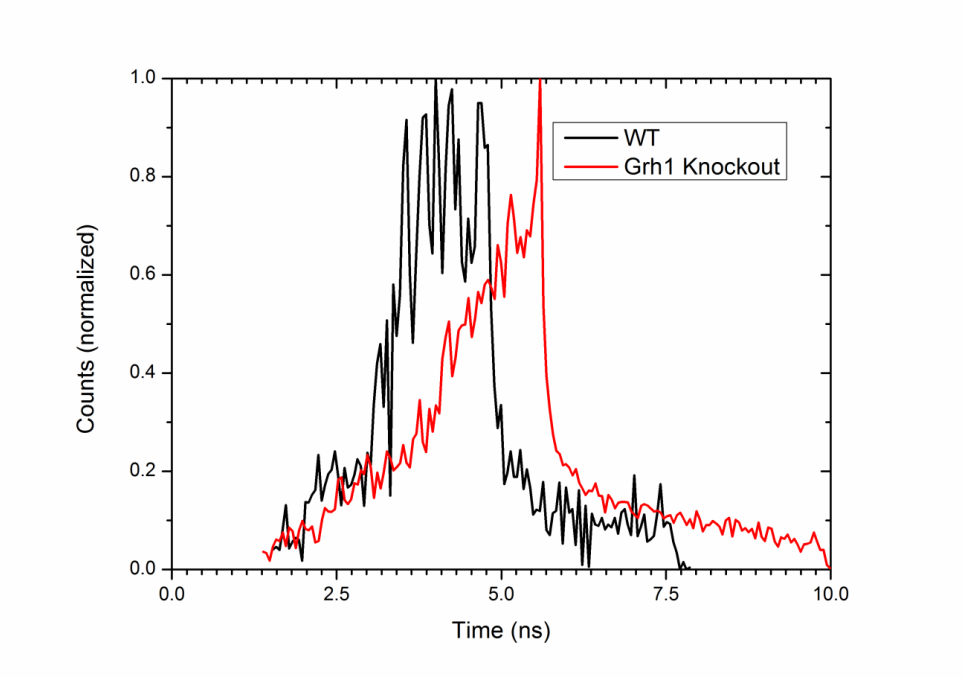

Supplementary Figure 3: Histograms of lifetime values obtained from WT (black) and Grh1-knockout (red) yeast cells subjected to starvation and excited at 375 nm.

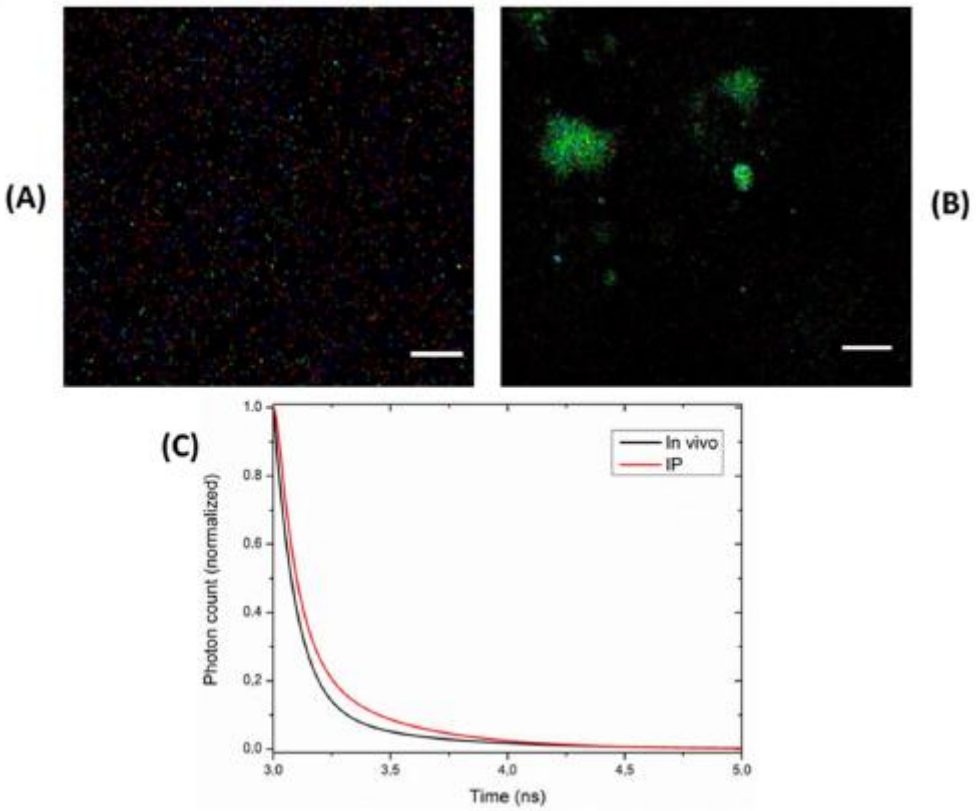

Supplementary Figure 4: Results of the experiments with GFP-tagged Grh1: (A) FLIM image of the control sample, (B) FLIM image of the fibrils immunoprecipitated from cells submitted to starvation, and (C) time decays of fluorescence from the cells in starvation (black) and from the immunoprecipitated sample (IP - red). Scale bar: 10 µm.

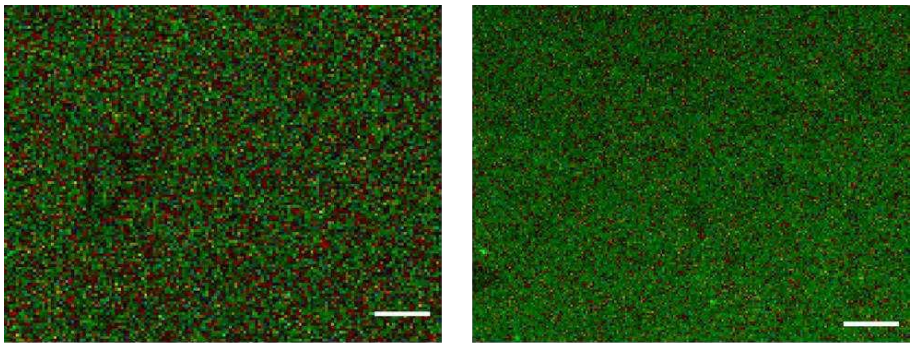

Supplementary Figure 5: Reversibility experiments. FLIM images of cells submitted to (A) starvation, and (B) heat-shock and cycled back to non-stress conditions. Scale bar: 10 µm.

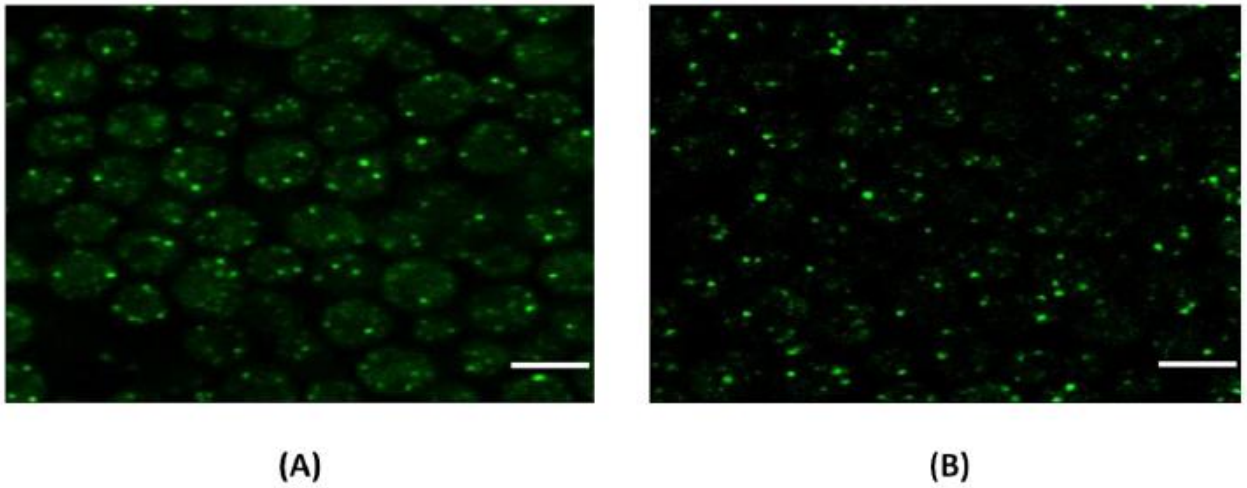

Supplementary Figure 6: Images from multiphoton microscopy of GFP-tagged Grh1 cells excited at 880 nm: (A) control; (B) heated at 37°C. Scale bar: 5 µm